

**CONFORMATIONALLY IMMOBILE CALIX[6]ARENES AS  
NEGATIVE RESISTS IN ELECTRON BEAM LITHOGRAPHY**

**THESIS**

**Presented to the Graduate Council of  
Southwest Texas State University  
In Partial Fulfillment of  
the Requirements**

**For the Degree  
Master of SCIENCE**

**By**

**Gabriel H. Monreal, B.A.**

**San Marcos, Texas  
August 2003**

## **DEDICATION**

This work is dedicated with much love and adoration to my mother, Berta Hernandez, who has never failed to be a source of strength and encouragement for me. I also dedicate this work to my children, Andrew Emmanuel and Rebecca Renee Monreal, who have blessed me with abundant inspiration, joy, and the gift of fatherhood.

## **ACKNOWLEDGEMENTS**

I would like to thank all of the members in the Chemistry and Physics Departments who were involved in the tremendous amount of collaboration for this project. I especially thank Dr. Carlos Gutierrez for his encouragement and advice throughout my graduate career.

I want to expressively thank Dr. Spencer and Dr. Geerts for their patience, availability, and willingness to contribute into research efforts. Both men spent countless hours designing and performing experiments with me. They have been a source of inspiration and strength, and it is certain that without their insight and hard work, this project would not have been possible.

I want to give the most heartfelt expression of gratitude to my advisor, Dr. Blanda. Words cannot express how much his understanding, patience, and wisdom have meant to me for this project. His allowance for me to think and perform independently gave me the strength that was necessary to complete this interdisciplinary endeavor.

This thesis was submitted on July 25, 2003.

## TABLE OF CONTENTS

LIST OF TABLES.....	x
LIST OF FIGURES.....	xii
ABSTRACT.....	xvii
1.0 INTRODUCTION.....	1
1.1 IntegratedCircuits.....	1
1.2 Microchip Fabrication.....	2
1.3 Photolithography Overview.....	2
1.4 The Role of Photoresist in Lithography.....	7
1.5 Negative Resists.....	10
1.6 Positive Resists.....	13
1.7 Limitations of Photolithography.....	18
1.8 Electron Beam Lithography.....	20
1.9 Limitations of Electron Beam Lithography.....	22
1.10 Electron Beam Resists.....	25
1.11 Calixarenes as Electron Beam Resists.....	27
1.12 <u>Thesis Proposal</u> : Conformationally Rigid Calix[6]arenes as High Resolution Negative Resists in Electron Beam Lithography.....	35
2.0 SYNTHETIC STRATEGY.....	38
2.1 Overview.....	38
2.2 Calix[6]arene Numbering.....	38
2.3 Conformational Mobility of Calixarenes.....	39
2.4 Conformational Immobilization.....	40
2.5 Effects of Allyl Substituents on Sensitivity.....	42
2.6 Electron Beam-Induced Polymerization Mechanism of <b>1</b> and <b>2</b> .....	43
2.7 <u>STEP 1</u> : Synthesis of <i>p-tert-butylcalix[6]arene</i> , compound A (5, 11, 17, 23, 29 35-hexa- <i>p-tert-butyl</i> -37, 38, 39, 40, 41, 42- hexahydroxycalix[6]arene).....	45
2.8 <u>STEP 2</u> : Synthesis of Dealkylated Calix[6]arene, compound B (37, 38, 39, 40, 41 ,52-hexahydroxycalix[6]arene.....	47

2.9	<u>STEP 3: Synthesis of Diallyloxytetrahydroxycalix[6]arene (37, 40-Diallyloxy-38, 39, 41, 42-tetrahydroxycalix[6]arene)</u> .....	48
2.10	<u>STEP 4: Stereo-Selective Synthesis of 2 Conformers of Diallyloxy-bis-<i>m</i>-xylenyloxy calix[6]arene (37,40-Diallyloxy-(38-42),(39-40)-bis-<i>m</i>-xylenyloxy-calix[6]arene)</u> .....	49
3.0	EXPERIMENTAL.....	52
3.1	Materials.....	52
3.2	Semiconductor Processing and Characterization Tools.....	53
3.3	Calix[6]arene Synthesis.....	54
3.3.1	Preparation of Compound A.....	54
3.3.2	Preparation of Compound B.....	55
3.3.3	Preparation of Compound C.....	56
3.3.4	Preparation of Diallyloxy-bis- <i>m</i> -xylenyloxy-calix[6]arene (1,2,3- Alternate Isomer, 1).....	57
3.3.5	Preparation of Diallyloxy-bis- <i>m</i> -xylenyloxy-calix[6]arene (Cone Isomer, 2).....	58
3.4	Formulation of Calixarene Resists.....	59
3.4.1	General Formulation Protocol.....	59
3.4.2	Calculation of Formulation Masses.....	59
3.4.3	Formulation of Resists containing BPO.....	60
3.5	Spin-Coating the Calixarene Resists.....	60
3.5.1	Processing Cleanliness.....	60
3.5.2	Spin-Coating Protocol and Soft Bake Parameters.....	61
3.5.3	Dynamic Dispense Procedure.....	61
3.6	Characterization of Optical Parameters of 1 and 2 Using 3-Angle Null Ellipsometry.....	62
3.6.1	Determination of Exact Ellipsometric Measurement Angles.....	62
3.6.2	Determination of the Native SiO <sub>2</sub> Thickness of an Uncoated Wafer.....	63
3.6.3	Determination of Indices of Refraction and Extinction Coefficients of 1 and 2.....	63
3.6.4	Determination of Resist Film Thickness and Uniformity.....	64
3.6.5	Stylus Profilometry.....	64
3.6.6	Data Acquisition for Spin Speed Curves.....	64
3.6.7	Remeasurement of Film Thickness of 1.....	65
3.7	Electron Beam Exposure of the Resists.....	66
3.7.1	Sample Preparation.....	66
3.7.2	Sensitivity/Contrast Exposures.....	67
3.7.3	High Resolution Exposure and Beam Current Measurement.....	69
3.7.4	Develop and Pattern Inspection.....	70

3.8	Characterization of Resist Sensitivity and Contrast using the AFM...	70
3.8.1	Atomic Force Microscopy.....	70
3.8.2	Determination of Post-Exposure Resist Thickness.....	70
3.8.3	Measurement of High Resolution Linewidths.....	71
3.8.4	Sample Visualization with the SEM.....	71
4.0	RESULTS.....	72
4.1	Ellipsometric and Profilometric Characterization of Calix[6]arene Thin Films.....	72
4.1.1	Determination of the Native SiO <sub>2</sub> Thickness of an Uncoated Wafer.....	72
4.1.2	Ellipsometric Determination of $n$ and $k$ of <b>1</b> ( $n_1$ and $k_1$ ).....	73
4.1.3	Comparative Thickness Measurement Using Stylus Profilometry.....	74
4.1.4	Measurement on Wt% Series of Films for <b>1</b> .....	74
4.1.5	Comparative Analysis of Thickness by Profilometry.....	77
4.1.6	Analysis of Film Thickness Variation for Cal-1.5 by Profilometry.....	78
4.2	Creation of Spin Speed Curves of <b>1</b> (at 0.5 and 1.0 wt%).....	80
4.2.1	Preparation and Ellipsometric Measurement of Samples (0.5 wt% <b>1</b> ).....	80
4.2.2	Results and Spin Speed Curve for 0.5 wt% <b>1</b> (from 1000-6000 rpm).....	81
4.2.3	Preparation and Ellipsometric Measurement of Samples (1.0 wt% <b>1</b> ).....	83
4.2.4	Results and Spin Speed Curve for 1.0 wt% <b>1</b> (from 1000-6000 rpm).....	84
4.2.5	Summary of Spin Speed Curves for <b>1</b> .....	86
4.3	Ellipsometric Determination of $n$ and $k$ of <b>2</b> ( $n_2$ and $k_2$ ).....	87
4.3.1	Sample Preparation and Raw Data for determination of $n_2$ and $k_2$ .....	87
4.3.2	Determination of $n_2$ and $k_2$ .....	87
4.4	Creation of Spin Speed Curves for <b>2</b> (at 0.5 and 1.0 wt%).....	88
4.4.1	Preparation and Ellipsometric Measurement of Samples (0.5 wt% <b>2</b> ).....	88
4.4.2	Results and Spin Speed Curve for 0.5 wt% <b>2</b> (from 1000-6000 rpm).....	90
4.4.3	Preparation and Ellipsometric Measurement of Samples (1.0 wt% <b>2</b> ).....	91
4.4.4	Results and Spin Speed Curve for 1.0 wt% <b>2</b> (from 1000-6000 rpm).....	92
4.5	Remeasurement of Film Thickness of <b>1</b> (0.5 and 1.0 wt%).....	94
4.5.1	Ellipsometric Data.....	94
4.5.2	Results and Spin Curves of Remeasured Films.....	95

4.6 Initial Measurement of Calixarene Line Widths	
Using Atomic Force Microscopy.....	97
4.6.1 Examination of Preliminary Samples of <b>1</b> and <b>2</b> .....	97
4.6.2 Changes in Line Width as a Result of Exposure Dosage.....	98
4.6.3 Determination of the Width	
of the Highest Resolution Line.....	101
4.7 Examination of Line Widths of Calixarene <b>1</b> and <b>2</b> Formulations	
With BPO Using the Scanning Electron Microscope (SEM).....	102
4.8 AFM Analysis of Box Features.....	103
4.8.1 Dose-Dependant Appearance of Boxes.....	103
4.8.2 Measurement of Box dimensions.....	104
4.9 Creation of a Contrast Curve for <b>1</b> .....	105
4.9.1 Resist Sensitivity and Contrast.....	105
4.9.2 Gel Dose ( $D_g$ ) and Insolubilization Dose ( $D_i$ ).....	105
4.9.3 Attenuation of the Beam Current.....	106
4.9.4 Data for the Contrast Curve of <b>1</b> .....	106
4.9.5 Contrast Curve for <b>1</b> .....	107
4.9.6 Determination of the Contrast of <b>1</b>	
Using an Extrapolated Line.....	108
5.0 DISCUSSION.....	110
5.1 Overview.....	110
5.2 Considerations for the Spin Coating Process.....	111
5.2.1 Non-Uniform Calixarene Thin Films.....	111
5.2.2 Creation of Uniform Films.....	112
5.2.3 Uniformity Problems attributed to Humidity.....	113
5.2.4 Possible Reasons for Thickness Variation of Resist	
Across the Wafer.....	113
5.3 Considerations Concerning Ellipsometric Measurements	
of <b>1</b> and <b>2</b> .....	114
5.3.1 Determination of the Native SiO <sub>2</sub> Thickness	
Of an Uncoated Wafer.....	114
5.3.2 Ellipsometric Conditioning of $k_1$ and $k_2$ .....	115
5.3.3 Reasons for Discrepancies Between Ellipsometric	
and Profilometric Thickness Values.....	116
5.4 Non-Ideal Spin Curves.....	118
5.4.1 The Necessity For Identical Spin Conditions	
During Processing.....	119
5.4.2 Importance of Precision in Resist Application.....	120
5.4.3 Shelf Life of Resist Coats.....	121
5.5 Exposure Considerations.....	122
5.5.1 Creation of the Grid.....	122
5.5.2 Use of a Thicker Calixarene Resist Film For	
SEM Visualization.....	123
5.5.3 Charging Effect of Thick Films During Exposure.....	124

5.5.4 Importance of Well-defined Side Walls of Submicron Lines.....	124
5.5.5 Consistent AFM Measurement Points For Step Height.....	126
5.6 Comparison of Resolution, Sensitivity, and Contrast of <b>1</b> and <b>2</b> With Calixarenes From the Literature.....	127
6.0 CONCLUSION.....	130
6.1 Summary of Results.....	130
6.2 Future Experiments.....	131
REFERENCES.....	133
APPENDIX.....	138

## LIST OF TABLES

<b>Table 4.1.1.1</b> Raw data for the determination of native oxide thickness.....	72
<b>Table 4.1.1.2</b> Native oxide thickness for three different positions.....	73
<b>Table 4.1.2.1</b> Raw Ellipsometric Data for the determination of $n$ and $k$ of <b>1</b> .....	73
<b>Table 4.1.2.2</b> Optical constants of <b>1</b> (assuming 2.05 nm thick native oxide layer).....	74
<b>Table 4.1.4.1</b> Samples of <b>1</b> for weight percent.....	75
<b>Table 4.1.4.2</b> Cal-0.5 (0.5 wt % <b>1</b> ) raw data.....	75
<b>Table 4.1.4.3</b> Cal-1.0 (1.0 wt % <b>1</b> ) raw data.....	75
<b>Table 4.1.4.4</b> Cal-1.5 (1.5 wt %) raw data.....	76
<b>Table 4.1.4.5</b> Cal-5.0 (5.0 wt %) raw data.....	76
<b>Table 4.1.4.6</b> Summary of Ellipsometric Thicknesses of Various Wt% of <b>1</b> .....	76
<b>Table 4.1.5</b> Thickness ranges for 3 samples of <b>1</b> determined by profilometry....	78
<b>Table 4.1.6</b> Profilometer Results for Resist Thickness Across Cal-1.5 [From wafer edge (1) to wafer center (10)].....	78
<b>Table 4.2.1</b> Raw Ellipsometric Data for Spin Curve Series of 0.5 wt% <b>1</b> .....	80-81
<b>Table 4.2.2</b> Calculated average thicknesses for 0.5 wt% <b>1</b> at 6 spin speeds.....	82
<b>Table 4.2.3</b> Raw Ellipsometric Data for Spin Curve Series of 1.0 wt% <b>1</b> .....	83-84
<b>Table 4.2.4</b> Calculated average thicknesses for 1.0 wt% <b>1</b> at 6 spin speeds.....	85
<b>Table 4.3.1</b> Raw Ellipsometric Data for the determination of $n$ and $k$ of <b>1</b> .....	87

<b>Table 4.3.2</b> Optical Constants of <b>2</b> (assuming 2.05 nm thick native oxide layer).....	88
<b>Table 4.4.1</b> Raw Ellipsometric Data for Spin Curve Series of <i>0.5 wt% 2</i> .....	89
<b>Table 4.4.2</b> Calculated average thicknesses for <i>0.5 wt% 2</i> at 6 spin speeds.....	90
<b>Table 4.4.3</b> Raw Ellipsometric Data for Spin Curve Series of <i>1.0 wt% 2</i> .....	91-92
<b>Table 4.4.4</b> Calculated average thicknesses for <i>1.0 wt% 2</i> at 6 spin speeds.....	93
<b>Table 4.5.1</b> Raw data for remeasurement of film thickness of <b>1</b> after one month.....	94-95
<b>Table 4.5.2</b> Thickness Growth of Calixarene Films over 1 month.....	95-96
<b>Table 4.6.3</b> Measurements of a line created at 45 pA (2 s, 20 kV) exposure...	101
<b>Table 4.9.4</b> Data collected for the determination of sensitivity and contrast of <b>1</b> .....	106
<b>Table 5.6</b> Comparison table for literature calixarenes with <b>1</b> and <b>2</b> .....	128

## LIST OF FIGURES

<b>Figure 1.3.1</b>	Photolithography in the IC Manufacturing Scheme.....	3
<b>Figure 1.3.2</b>	Overview of the Photolithography Process.....	4
<b>Figure 1.3.3</b>	Output Spectrum of the Hg-Arc Lamp.....	6
<b>Figure 1.4.1</b>	Comparison of Lithography using Positive and Negative Resist.....	8
<b>Figure 1.5.1</b>	Synthesis of Cyclicized Rubber For Negative Resist.....	11
<b>Figure 1.5.2</b>	Photoreaction of a Bis(arylazide) to form a Reactive Nitrene.....	12
<b>Figure 1.5.3</b>	Various Reaction Modes of the Reactive Nitrene.....	12
<b>Figure 1.5.4</b>	Crosslinking of the Rubber Matrix by Addition of the Nitrene.....	13
<b>Figure 1.6.1</b>	Hexamethyldisilazane and Synthesis of the Novolac Resin.....	14
<b>Figure 1.6.2</b>	Reactions of the Diazonaphthoquinone PAC Upon Exposure.....	15
<b>Figure 1.6.3</b>	Mechanism of DNQ/Novolac Positive Resist.....	16
<b>Figure 1.6.4</b>	Dissolution Rates of unexposed and fully exposed mixtures of DNQ-novolac resists as a function of DNQ loading.....	17
<b>Figure 1.7.2</b>	Diffraction Problem in Optical Lithography (Note how image size is distorted as $\lambda$ approaches mask feature of size $d$ ).....	18
<b>Figure 1.8.1</b>	Schematic of an Electron Beam Exposure System.....	21
<b>Figure 1.9.1</b>	Schematic of Electron Forward and Back Scattering in electron resist exposure at 20 and 50 kV.....	23
<b>Figure 1.9.2</b>	Exposure distribution and Monte Carlo simulations of a 100 point-source electrons in a target of 1 $\mu\text{m}$ -thick resist on an infinitely thick silicon substrate at accelerating voltages of (a)10, (b) 25, and (c) 50 kV.....	24

<b>Figure 1.9.3</b> Micrograph of swollen images in an experimental negative resist.....	25
<b>Figure 1.10.1</b> Polystyrene-Based Negative Electron Beam Resists.....	26
<b>Figure 1.10.2</b> Electron beam-induced cleavage of the insoluble PMMA matrix into soluble by-products. The post-develop result is a positive-tone image.....	26
<b>Figure 1.11.1</b> Synthesis of <i>p</i> - <i>tert</i> -butylcalix[ <i>n</i> ]arene ( <i>n</i> = 4 to 8).....	27
<b>Figure 1.11.2</b> Various depictions of the Calix[4]arene.....	28
<b>Figure 1.11.3</b> Synthesis of <i>p</i> -methylcalix[6]arene hexaacetate, a prototype resist (5,11,17,23,29,35- hexamethyl- 37,38,39,40,41,42-hexaacetoxycalix[6]arene).....	29
<b>Figure 1.11.4</b> (a) Comparison of etch rates between calixarene and PMMA resists.(b) 7 nm features on Ge fabricated using calixarene prototype resist.....	30
<b>Figure 1.11.5</b> Synthesis of a chloromethylated calix[6]arene derivative (5,11,17,23,29,35-hexachloromethyl-37,38,39,40,41,42-hexamethoxycalix[6]arene) for electron beam lithography.....	32
<b>Figure 1.11.6</b> Sensitivity to electron dose for calix[ <i>n</i> ]arenes (CMC[ <i>n</i> ]AOMe, <i>n</i> = 5,6,7) and prototype calix[6]arene (MC[6]AOAc.....	33
<b>Figure 1.12.1</b> 2 Conformers of Diallyloxy Bis- <i>m</i> -Xylenyloxy Calix[6]arene (1,2,3-alternate and Cone).....	35
<b>Figure 2.2.1</b> Nomenclature system of calix[6]arene (36,37,38,39,40,41,42-hexol).....	39
<b>Figure 2.3.1</b> Pathways for conformational Inversions of calix[ <i>n</i> ]arene.....	39
<b>Figure 2.4.1</b> $\alpha,\alpha'$ -dibromo- <i>m</i> -xylene, linker to induce conformational Immobility.....	41
<b>Figure 2.4.2</b> Two conformers of Diallyloxy Bis- <i>m</i> -Xylenyloxy Calix[6]arene (1 and 2).....	41
<b>Figure 2.5.1</b> Contrast curves comparing the sensitivity of allyl-functionalized calix[4]arene versus unsubstituted calix[4]arene.....	42

<b>Figure 2.6.1</b> A possible mechanism of the free-radical polymerization of the allyl groups in adjacent calixarenes upon electron beam exposure.....	43
<b>Figure 2.7.1</b> Synthesis of <i>p-tert</i> -butylcalix[6]arene, compound A (5, 11, 17, 23, 29 35-hexa- <i>p-tert</i> -butyl-37, 38, 39, 40, 41, 42-hexahydroxycalix[6]arene).....	45
<b>Figure 2.8.1</b> Synthesis of Dealkylated Calix[6]arene (37, 38, 39, 40, 41 ,52-hexahydroxycalix[6]arene).....	47
<b>Figure 2.9.1</b> Synthesis of Diallyloxytetrahydroxycalix[6]arene, compound C (37, 40-Diallyloxy-38, 39, 41, 42-tetrahydroxycalix[6]arene).....	48
<b>Figure 2.10.1</b> Stereo-selective synthesis of <b>1</b> and <b>2</b> .....	49
<b>Figure 3.7.1.1</b> Sample preparation of a 4" coated wafer (along sample back)...	66
<b>Figure 3.7.1.2</b> Creation of grid on the front of a 1"x1" resist-covered wafer.....	67
<b>Figure 3.7.2</b> Exposure Features (boxes and lines) at their corresponding times.....	68
<b>Figure 3.7.3</b> Experimental setup for the creation of high resolution lines.....	69
<b>Figure 4.1.4</b> Snapshot of Cal-5.0, showing the coloration (film thickness variation) of an 81 nm thick film of <b>1</b> .....	77
<b>Figure 4.1.6</b> Profilometric Cross-section of Resist Step Height for the edge of the wafer to the wafer center.....	79
<b>Figure 4.2.2</b> Spin Speed Curve of 0.5 wt% Calixarene ( <b>1</b> ) Resist.....	82
<b>Figure 4.2.4</b> Spin Speed Curve of 1.0 wt% Calixarene ( <b>1</b> ) Resist.....	85
<b>Figure 4.2.5</b> Combined Spin Speed Curves of <b>1</b> at 0.5 and 1.0 wt%.....	86
<b>Figure 4.4.2</b> Spin speed curve of 0.5 wt% calixarene ( <b>2</b> ) resist.....	91
<b>Figure 4.4.4</b> Spin Speed Curve of 1.0 wt% Calixarene ( <b>2</b> ) Resist.....	93
<b>Figure 4.5.2</b> Spin curve showing film growth of a thin film of 1.0 wt% <b>1</b> over time.....	96
<b>Figure 4.5.3</b> Spin curve showing film growth of a thin film of 0.5 wt% <b>1</b> over time.....	97

<b>Figure 4.6.1</b> AFM scans of (a) <b>2</b> at beam current of 107 pA and (b) <b>2</b> at 84 pA. <i>Note the visual differences in line widths at different beam currents (dosages)</i> .....	98
<b>Figure 4.6.2.1</b> Line width of <b>2</b> as a result of exposure time (dose). Line width of this <i>overexposed</i> feature is 8.7 $\mu\text{m}$ (100 s exposure)—compare with Figure 4.6.2.2.....	99
<b>Figure 4.6.2.2</b> Line width <b>2</b> as a result of exposure time (dose). Line width of this feature is 0.8 $\mu\text{m}$ (2 s exposure).....	100
<b>Figure 4.6.3</b> Highest Resolution Line, created at 20kV acceleration voltage with a beam current of 45 pA (2 s exposure).....	101
<b>Figure 4.7</b> SEM micrographs of: (a) <b>1</b> with 1% BPO and (b) <b>2</b> with 1% BPO exposed by using a 20 kV electron beam at an average beam current of 1.2 nA.....	102
<b>Figure 4.8.1</b> AFM scan of a 100 second box made from <b>2</b> .....	103
<b>Figure 4.8.2</b> 3-Dimensional scan of the 40X30 $\mu\text{m}$ (100 s) box made from <b>2</b> ..	104
<b>Figure 4.9.4</b> Calculation for the Dosage of the 55 s contrast curve box.....	107
<b>Figure 4.9.5</b> Contrast curve for <b>1</b> .....	108
<b>Figure 4.9.6</b> Determination of the contrast of <b>1</b> using an extrapolated line.....	109
<b>Figure 5.2.1</b> Non-uniform film observed on a wafer coated with <b>1</b> .....	111
<b>Figure 5.3.1</b> Three layer “sandwich” used to create modeling and fit of the optical constants of <b>1</b> and <b>2</b> .....	115
<b>Figure 5.3.3.1</b> Estimation of true film thickness with the lowest RMSE.....	116
<b>Figure 5.3.3.2</b> Microscopic view of scattered light from a contamination-free ellipsometric measurement point of a sample.....	117
<b>Figure 5.4.1</b> Non-ideal spin curve of 0.5 wt% <b>2</b> .....	119
<b>Figure 5.4.2</b> Non-Ideal spin curve for 1.0 wt% <b>1</b> .....	121
<b>Figure 5.5.1</b> Microscope picture of the grid with patterned features inside.....	123

**Figure 5.5.4** Bridging between lines of **2** during a pitch experiment.....125

**Figure 5.5.5** Consistent measurement point of step height of a box  
with AFM.....126

## **ABSTRACT**

### **CONFORMATIONALLY IMMOBILE CALIX[6]ARENES AS NEGATIVE RESISTS IN ELECTRON BEAM LITHOGRAPHY**

**By**

**Gabriel H. Monreal, B.A.**

**Southwest Texas State University**

**August 2003**

**SUPERVISING PROFESSOR: Dr. Michael T. Blanda**

The challenge of creating smaller integrated circuits drives a necessity for novel semiconductor fabrication materials which will facilitate the processing of nanometer-scale features. Literature reports that calixarenes have the potential to meet this challenge, due to their ultrahigh resolution and their process robustness. For this study, the “1,2,3-alternate” and “cone” conformers of Diallyloxy-Bis-*m*-Xylenyloxycalix[6]arene were synthesized via a pre-elaborated

pathway, purified, and then formulated into negative electron beam resists. The index of refraction (at 632.8 nm) was determined for both compounds. Spin speed curves of various concentrations (w/w) of these compounds were also created. Both compounds were found to form thin, robust films up to 5.0 wt%.

These calixarene resists were then exposed using a scanning electron microscope (SEM). All formulations gave qualitative results, as patterns were observed under an optical microscope after development. The sensitivity of the 1,2,3-alternate conformer was found to be relatively good with respect to known literature calix[6]arenes, as well as PMMA. A high contrast of 4.0 was determined for this conformer by constructing a contrast curve. The gel and insolubilization dosages were also determined.

Pictures and scans of the features created using these calix[6]arenes were taken using an atomic force microscope (AFM) and the SEM. The width of the highest resolution line was 0.474  $\mu\text{m}$ , as measured by AFM. Formulations involving the use of a radical initiator (benzoyl peroxide) were exposed for both conformers, and no significant change in pattern quality or sensitivity from non-initiator formulations was observed. The exposure characteristics of the conformationally immobile calix[6]arenes in the electron beam resists described herein were comparable to literature calixarene resist characteristics. Both conformers also show the promise of ultrahigh resolution.

## **1.0 INTRODUCTION**

### **1.1 Integrated Circuits**

The development of new materials, as well as mature and robust processes that facilitate microchip fabrication, is a major theme in the manufacturing of solid-state semiconductor devices. Since the invention of the integrated circuit by Jack Kilby and Robert Noyce<sup>1</sup> in 1959, there has been a preponderance of research and development devoted to making the microchip able to process more information in less time and with minimal power consumption. To achieve this end, one of the major challenges in semiconductor device fabrication has been the miniaturization of microchips, including their components.

Miniaturization has led to successive generations of smaller, more efficient solid-state electronics that are capable of operating at faster speeds while consuming less power.<sup>2</sup> Each generation of microchips has been created and developed by utilizing principles of chemistry, physics, materials science, and engineering. Despite such innovations, there is a continual need and demand for smaller semiconductor devices.

## **1.2 Microchip Fabrication**

It is important to realize that the fabrication of functional and dependable integrated circuits is achieved through a sequential, layer-by-layer method, selectively processing an active area while leaving other areas intact. From blank wafer to the completed integrated circuit (IC), there can be literally hundreds of steps, each with their own processes, constraints, and requirements.<sup>3</sup>

These processes include oxidation, diffusion, chemical vapor deposition (CVD), physical vapor deposition (PVD or sputter), photolithography, etch, and ion implantation. In order to obtain high process yields, as well as functional and reliable submicron devices, all processes must be conducted under “cleanroom” conditions, while observing the respective set of criteria and specifications that must be met in each layer. One of the most critical and demanding processes that is used during the fabrication of microchips is photolithography.

### **1.3 Photolithography Overview**

Unlike other semiconductor manufacturing processes that may be used exclusively near the beginning or the end of microchip fabrication, photolithography plays a pivotal role in that it is employed at nearly all levels of microchip fabrication. In addition, it is the lithography process that defines the “critical dimension,” or smallest feature size within an integrated circuit.<sup>4</sup> Figure 1.3.1 is a simplified illustration of how photolithography fits into the integrated circuit manufacturing scheme.

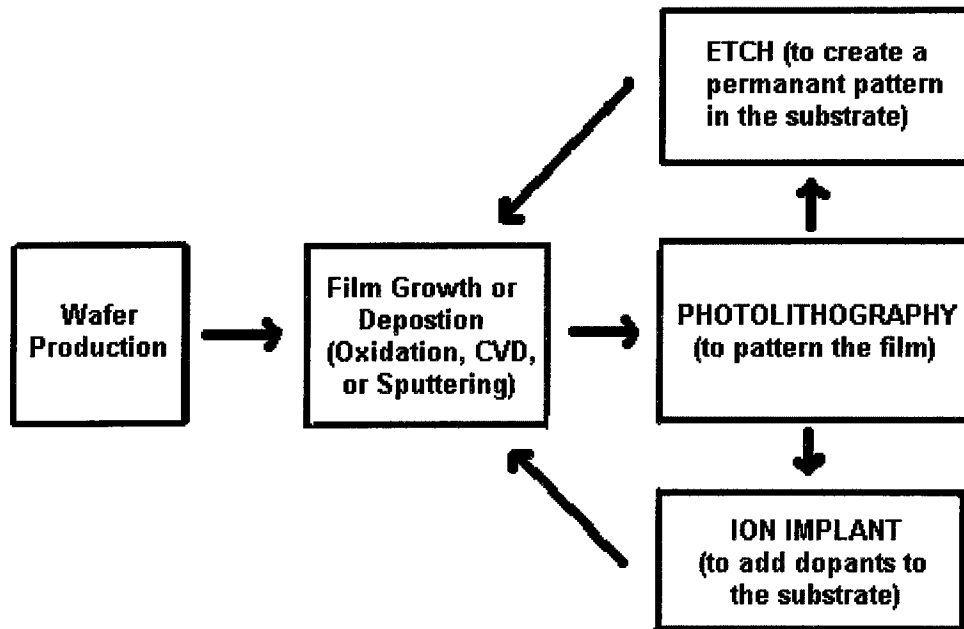


**Figure 1.3.1** Photolithography in the IC Manufacturing Scheme

Using photolithography, a pattern is transferred onto a substrate in a series of four major steps. A depiction of this process is shown in Figure 1.3.2. During the *coating* stage, the surface of the substrate is cleaned to rid it of contaminants and then it is uniformly coated with a photoactive substance called “photoresist” (or simply “resist”) in preparation for exposure. The substrate itself may be single crystal silicon, polycrystalline silicon (polysilicon or simply “poly”), SiO<sub>2</sub>, metal, or any of the other various materials that are grown or deposited on the wafer surface and require patterning.

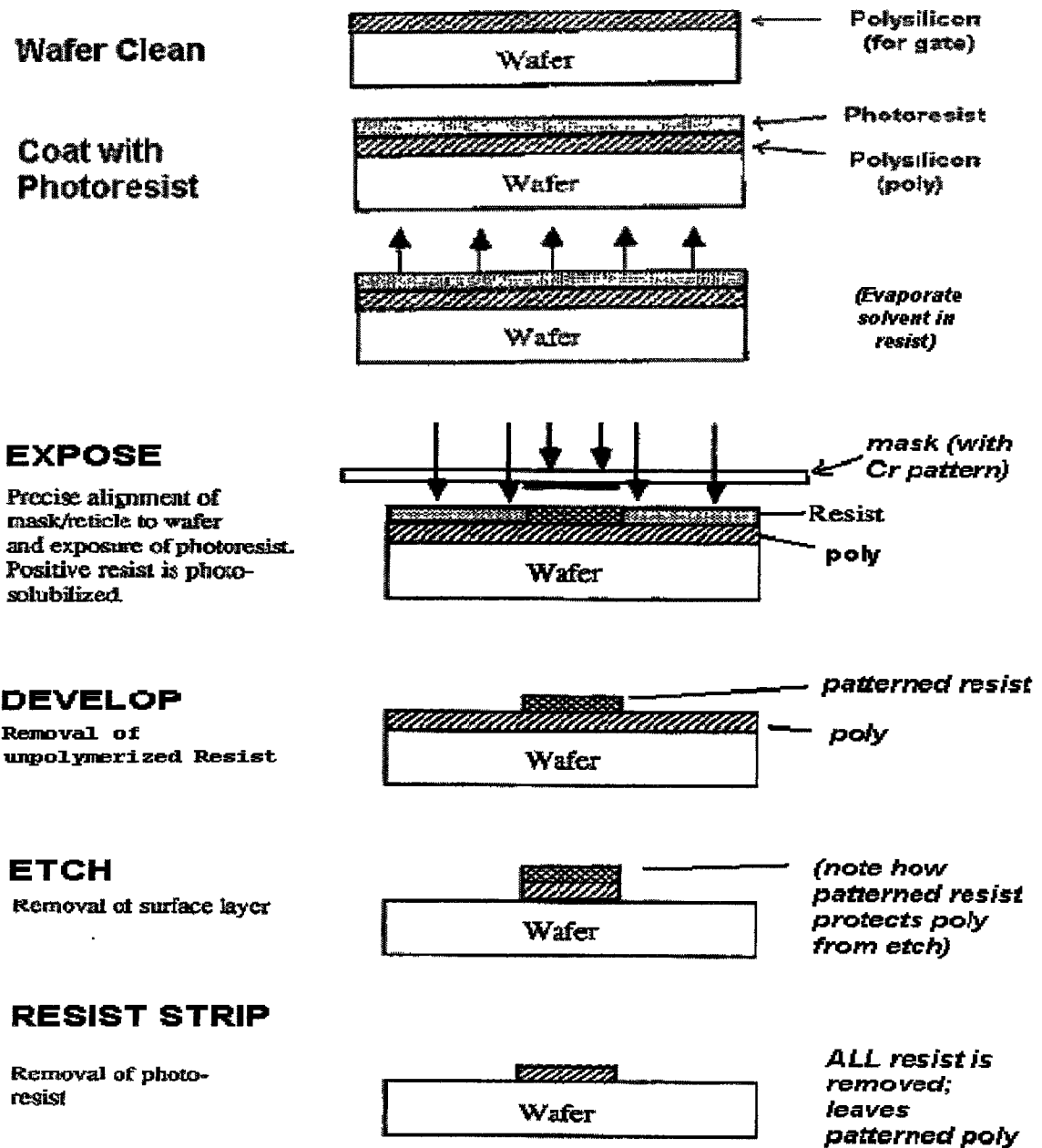


Figure 1.3.2 Overview of the Photolithography Process<sup>3</sup>

The *Exposure* process takes place in a tool commonly called a “stepper”. During exposure, the surface is covered with a template that contains the pattern to be processed at that particular level called a “photomask” or “reticle.” The wafer is then exposed with some appropriate light source, which causes a

photochemical reaction to occur within the areas of the photoresist that has been impinged upon by the exposure source.

The wafer is then *developed* in a solvent or solution that will wash away either the exposed or unexposed portions of the resist away (depending on the chemistry of the photoresist), leaving a positive or negative image of the photomask on the wafer.<sup>5</sup> The integrity of the developed pattern and the pattern alignment relative to previous layers is then inspected using an optical microscope or metrology tools. If the wafer passes inspection, it is then generally subjected to one of two modes of fabrication: the etch process or the ion implantation process.

In the etch process, the wafer is subjected to a plasma or liquid that will selectively attack and etch the areas of the wafer that are not protected by photoresist. Once the surface has been etched, the resist is removed and a relief of the original photomask is left upon the wafer.

During the ion implantation process, alignment is less critical, as the critical dimensions of the areas to be processed are much larger than those of the etch process. The resist-patterned wafer is bombarded with Group III or Group V dopants that will enter the areas of the wafer substrate that are not protected by the patterned resist, and alter the electrical properties of the substrate. The resist is removed, and the wafer is sent on for further processing.

Exposure sources in commercial stepper systems of recent generations have been Hg-arc lamps, which produces a reliable, high intensity exposure output. The spectrum of such a lamp is seen in Figure 1.3.3. Using filters, the

stepper will select a specific wavelength of the spectra, which is necessary to avoid image degradation that would otherwise be caused by chromatic aberration.<sup>5</sup>

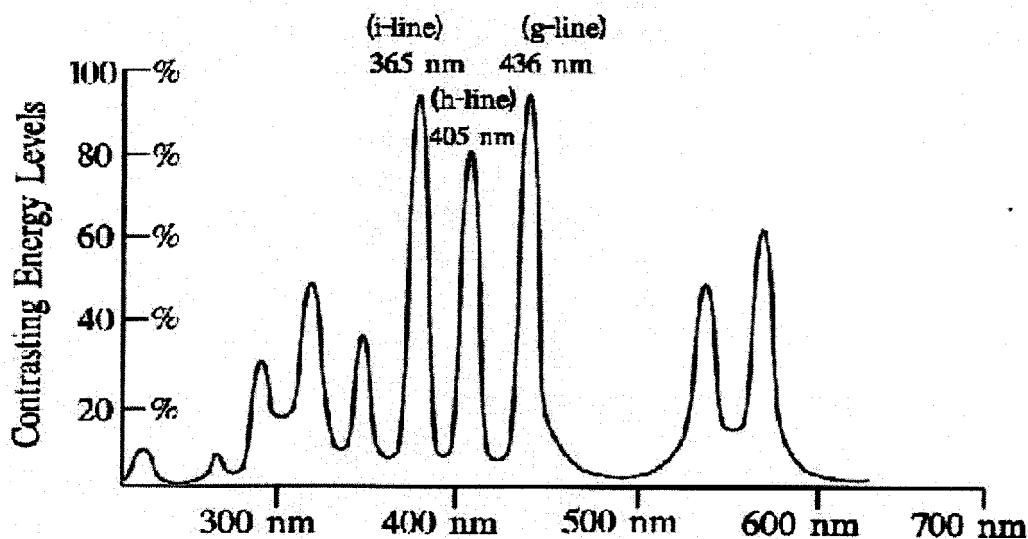


**Figure 1.3.3** Output Spectrum of the Hg-Arc Lamp

The terms *G-line*, *H-line*, and *I-line* refer to the stepper systems that have been designed to operate at the 436, 405, and 365-nm Hg lines respectively. In the interest of creating smaller devices, generations of IC manufacturing have progressed from G-line, to the shorter I-line, and are currently using alternate sources that depend upon excimer laser systems such as the ArF laser, which has a wavelength of 193 nm.

There are indeed variations to this lithographic scheme that depend on the type of materials, processes, and hardware that are used.<sup>3</sup> Nevertheless, the key point is that once the photoresist has served its purpose during etch or implant (by allowing for processing of selected areas of the wafer), it is then

completely removed. Hence, the penultimate goal of lithography is to faithfully reproduce the mask image onto the resist-covered wafer with the best possible degree of resolution.<sup>3</sup> In addition, the resist image must also be precisely aligned to previous layers so that all critical interconnections can be established after etch. There are many factors that influence successful lithography; invariably, two of the most critical are the lithography system and the photoresist itself.

#### 1.4 The Role of Photoresist in Lithography

The photoresist has been described as the heart of the masking process.<sup>6</sup> As such, all photolithography and etch processes are engineered to accommodate a particular resist formulation to achieve the formation of well resolved profiles in the substrate. Photoresists, or simply resists, are tailored to respond to specific wavelengths of light from the exposure source. Furthermore, each of the different masking processes in the fabrication of ICs may use a resist that is formulated of different components and component concentrations.

Regardless of specific formulation, most resists contain the same basic substituents: *monomers (or polymers)*, *photoactive compounds* (also known as *sensitizer* or *PAC*), and some type of *solvent*. The purpose of the solvent is merely to suspend the solid components so that they may be laid upon the substrate surface in an even and uniform manner by spin coating.<sup>4</sup> The nature of the monomeric (or polymeric) material and PAC depends on the type of resist to be employed.

The terms “positive resist” and “negative resist” are used to describe the type of image that the resist will leave on the substrate upon exposure. Figure 1.4.1 compares how positive and negative resists will respond to exposure to leave an image on the substrate. Note how the pattern left by the positive resist after exposure and develop is of the same tone as the chrome pattern on the photomask, while that of the negative resist is opposite. The etch process will then leave a permanent image in the substrate that is of the same tone as the resist.

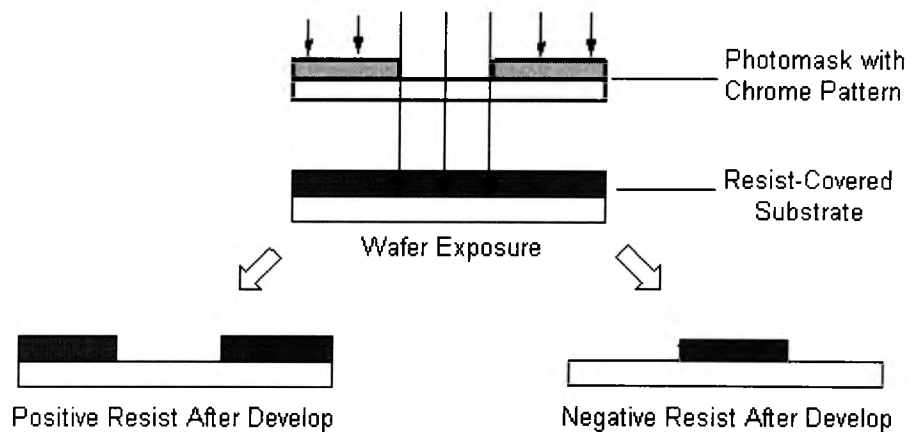


**Figure 1.4.1** Comparison of Lithography using Positive and Negative Resist<sup>5</sup>

Because it plays such a pivotal role in IC manufacturing, the resist is stringently evaluated under a number of performance criteria.<sup>5</sup> *Sensitivity and contrast* refer to the ability of a resist to react to the exposure source with an acceptable reaction rate to result in a pattern of high integrity. That is, the portion of the resist that is exposed must react while leaving the unexposed resist unreacted. Resist sensitivity is defined by convention as the incident input

energy per unit area that is necessary to achieve the appropriate chemical response in the resist.<sup>7</sup> This is expressed mathematically in Formula 1.

$$D = \frac{E}{A} \quad (1)$$

Here, D is the dose, E is the incident energy in appropriate units, and A is the exposure area. The *lithographically useful sensitivity* has been termed as dose per unit area that results in dimensional equality of clear and opaque features that are nominally equal in pattern design.<sup>7</sup>

Resist sensitivity is dependant upon the properties of its constituent polymeric materials and the PAC sensitizer. Polymer properties that affect sensitivity include molecular weight, dispersity, glass transition temperature ( $T_g$ ), density, and quantum efficiency.<sup>4</sup> Indeed, a resist must exhibit a sensitivity that is compatible with the exposure parameters of the exposure tool in order to not limit the amount of product that the tool processes. The sensitivity of the resist must also confer reproducible results.

*Resolution* is another performance factor and refers to the ability of a resist to create a pattern of specific dimensions and with good cross-sectional profiles on the substrate. The smaller the pattern a resist can faithfully and reproducibly image, the better its resolution.<sup>3</sup> The resolution capabilities of any lithographic process are determined by hardware, processing, and material considerations.<sup>5</sup> All other conditions being optimal, the resist itself must be able to create images with the highest degree of resolution for the creation of submicron features.

Two other performance criteria are *adhesion* and *etch resistance*.

Obviously the resist must be able to adhere to the substrate during the photolithography and etch process; likewise the resist must also be removed completely once it has served its purpose. Finally, the resist protect the underlying substrate during the harsh etch conditions so that pattern transfer is facilitated. Because dry-etching techniques use plasma-induced gaseous reactions in an environment with a high radio frequency flux, the polymer material in the resist must exhibit high thermal and radio frequency stability.<sup>6</sup>

### 1.5 Negative Resists

Historically, optical negative resists have often been described as the first “workhorses” of the semiconductor industry. Billions of dollars worth of microelectronics have been fabricated using these materials.<sup>5</sup> In general, negative resists offer good etch protection and excellent adhesion to the substrate. However, because they were incapable of resolving features smaller than 2  $\mu\text{m}$ , they were replaced by positive resists in the mid 1970s to facilitate the creation of fine submicron patterns.<sup>4</sup>

The primary components in binary negative resists is a matrix resin made of poly (*cis*-isoprene), a synthetic rubber that is obtained by the Ziegler-Natta catalyzed polymerization of isoprene,<sup>16,17</sup> and a sensitizer which will facilitate crosslinking.<sup>4,5</sup> In order to create a material with a higher  $T_g$  and toughness, the poly(*cis*-isoprene) is then treated with acidic reagents under proprietary conditions to result in a partially cyclized product,<sup>5</sup> as seen in Figure 1.5.1.

These cyclized rubber materials are quite soluble in nonpolar, organic solvents to make solutions that can be spin-coated to yield uniform thin films which adhere strongly to a wide range of substrate materials.<sup>6</sup>

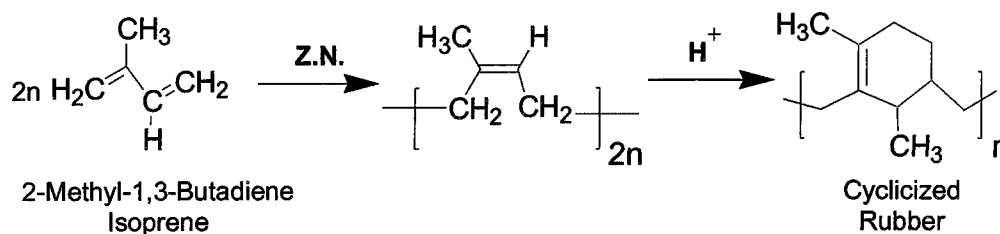


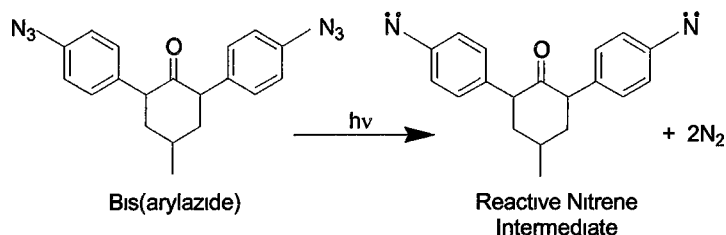
**Figure 1.5.1** Synthesis of Cyclized Rubber For Negative Resist

It is important to note that negative resists will generally undergo a “photopolymerization” reaction, in which the elastomeric material becomes crosslinked upon exposure with the aid of a sensitizer. This crosslinking yields a matrix that is insoluble in the developer and thereby leaves a negative pattern.

Unfortunately, negative resists suffer from the “swelling” phenomenon, in which the solvent will absorb into and distort the 3-dimensional matrix.<sup>5,8</sup> Without a good develop process, the result can be poorly resolved features, hence the resolution limitation of optical negative resists.

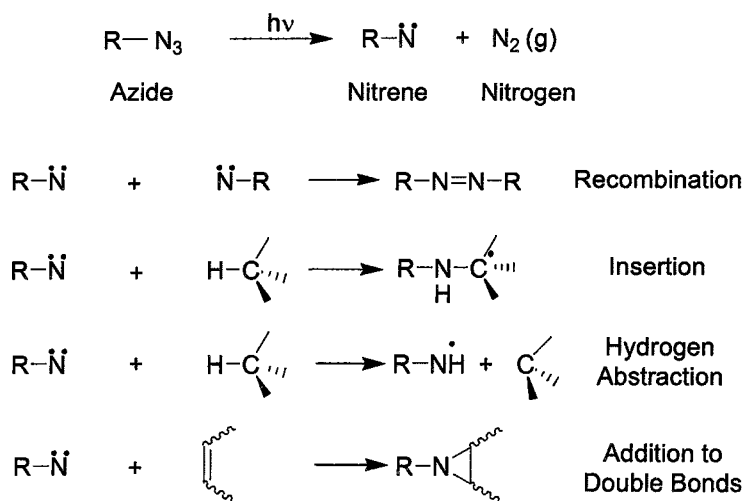
The sensitizer for these synthetic rubbers are a class of molecules that are generically termed the *bis(arylazides)*. These PACs are synthesized by the condensation of 2 molecules of *p*-azidobenzaldehyde with a substituted cyclohexanone.<sup>4</sup> The resultant bis(arylazide) molecule has a strong absorption at about 360 nm, but is almost transparent above 420 nm. Thus, the PAC would be lithographically useful at the I-line (365 nm), but not at the G-line (436 nm).<sup>5</sup>

Figure 1.5.2 shows the reaction of a bis(arylazide) under light to create a reactive nitrene intermediate, which will then form crosslinks in the rubber matrix.



**Figure 1.5.2** Photoreaction of a Bis(arylazide) to form a Reactive Nitrene

Upon exposure, there are a number of photochemical transformations that are associated with the creation of a 3-dimensional, crosslinked matrix. The excited state of the azide results in the evolution of nitrogen gas and the nitrene intermediate, depicted in Figure 1.5.3. The nitrene may then undergo various modes of radical reactions to create more stable structures, but eventually result in intermolecular polymer-polymer crosslinks to form the insoluble matrix.



**Figure 1.5.3** Various Reaction Modes of the Reactive Nitrene

These reactions of the intermediate include recombination to form azodyes, abstraction of hydrogen to create secondary radicals that may undergo coupling reactions, and the insertion of the nitrene into the double bond of the rubber polymer to create three-membered, heterocyclic aziridine linkages,<sup>5</sup> shown in Figure 1.5.4.

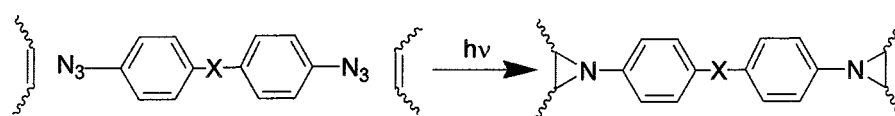


**Figure 1.5.4** Crosslinking of the Rubber Matrix by Addition of the Nitrene

## 1.6 Positive Resists

By 1972, positive resist systems had completely supplanted negative resists for higher-end applications.<sup>4</sup> This was because positive-tone resists generally offer higher contrast and better resolution due to the absence of swelling during the development phase. Other characteristics that have made positive resists an enduring success are their high thermal stability and an environmentally friendly developer (aqueous basic solution, as opposed to the solvent-based developer of negative resist).

Furthermore, positive resist also offers a better dry etch resistance, which is important since plasma etching processes have become necessary in IC fabrication to etch smaller features.<sup>6</sup> However, unlike the negative resists, positive resists have poor adhesion to polar substrates such as SiO<sub>2</sub> and require

priming of the substrate with an adhesion promoter, typically hexamethyldisilazane (HMDS).

Classical positive resist is a two-component system comprised of novolac resin and a diazonaphthoquinone sensitizer. Novolac is a term derived from the Swedish word “lak” which means laquer or resin, and was originally used as such.<sup>9</sup> Novolac, seen in Figure 1.6.1, is the product of the acid-induced copolymerization of *m*- or *p*-cresol and formaldehyde and serves as the *binder* or *matrix* in a positive resist.

These resins are soluble in common organic solvents and can be coated from solution to form high quality isotropic, glassy thin films.<sup>5</sup> Incidentally, novolac is also moderately soluble in aqueous base due to their phenolic functional group. Novolac resins used in resist formulations have a broad dispersity, with molecular weights ( $M_n$ ) that range from 1000-3000, which corresponds to molecules that contain 8 to 20 repeating phenolic units.<sup>4</sup>

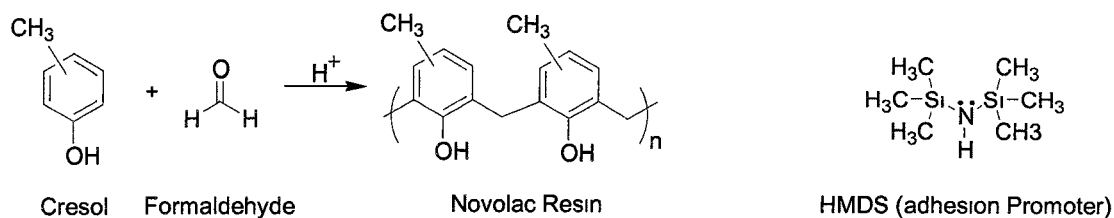


**Figure 1.6.1** Hexamethyldisilazane and Synthesis of the Novolac Resin

Diazonaphthoquinones (DNQ) are the photoactive components in positive resists, and can be seen in Figure 1.6.2. The substituent R in DNQ is generally an arylsulfonate (-OSO<sub>3</sub>Ph), which serves as a “ballast” group to moderate

solubility and alter the absorption characteristics of the sensitizer. DNQ sulfonates are soluble in organic solvents but not in aqueous basic solutions. However, upon exposure the DNQ sensitizer is converted via a series of reactions to give a base-soluble indenecarboxylic acid, seen in Figure 1.6.2.

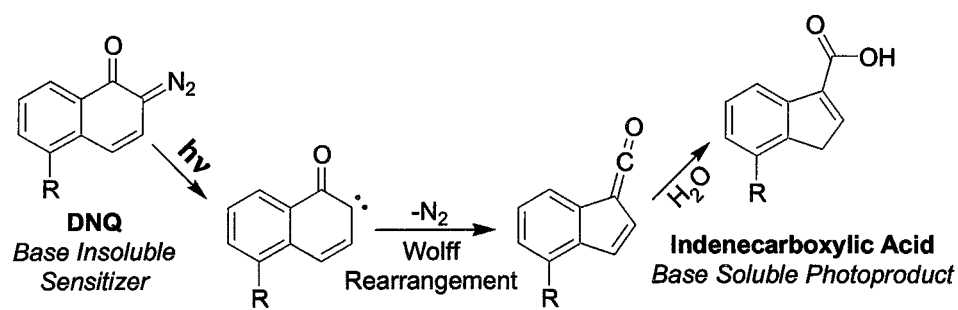


**Figure 1.6.2** Reactions of the Diazonaphthoquinone PAC Upon Exposure

Figure 1.6.3 depicts the mechanism of pattern generation for DNQ-novolac positive resists. The DNQ photoproduct is extremely soluble in aqueous base due to its acid functionality, and increases the rate of dissolution of the exposed area.<sup>6</sup> This rationale is the basis of the “photosolubilization” of the irradiated area, and leaves the high contrast positive-tone relief image of the photomask in the resist.

The exact mechanism of DNQ-novolac interactions has been studied extensively but are still poorly understood.<sup>4-6</sup> DNQ sensitizers typically comprise about 20% of the total solid mass in positive resist.<sup>3</sup> The photolytic generation of the base-soluble sensitizer leads to a marked solubility increase in the already moderately soluble novolac matrix. Factors that determine how the novolac structure affects the lithographic performance of DNQ-novolac positive resists

are the molecular weight ( $M_n$ ) and polydispersity of the resin, methylene linkage position, and the ratio of *m*- to *p*-cresol precursors.<sup>10,11</sup>

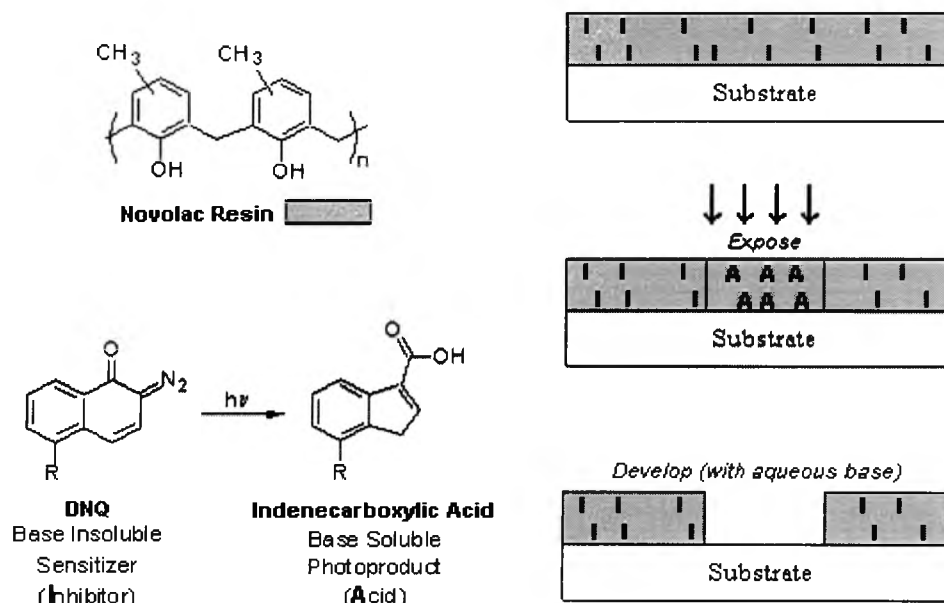


**Figure 1.6.3** Mechanism of DNQ/Novolac Positive Resist<sup>5</sup>

Nevertheless, it is necessary to recognize that the mechanism of DNQ-novolac systems is based on *kinetic* reasons.<sup>4</sup> Figure 1.6.4. depicts how dissolution rates for exposed *and* unexposed resist are dependant upon *the amount of DNQ* in the resist. The addition of DNQ dissolution inhibitor to novolac resins actually results in a decrease in the dissolution rate of *unexposed* resist, This is the reason why DNQ is known as a “dissolution inhibitor.”<sup>4-6</sup> As the concentration of DNQ is increased in a given formulation, the dissolution rate of the unexposed resist is further decreased, due to DNQ-novolac interactions.

However, upon exposure, the DNQ-novolac mixture demonstrates a dissolution rate that is greater in the *exposed* area of the resist than that of pure novolac resin alone. This modulation in dissolution behavior via DNQ loading

and selective (photomasked) exposure is the fundamental basis of the generation of positive-tone images in DNQ-novolac resists.

This behavior is notably different from the cyclicized rubber/ bis(arylazide)-based negative resists, in which image generation is based upon thermodynamically determined differences in solubility.<sup>4</sup> Note that for negative resist, fully exposed areas of resist will not dissolve even under unlimited develop times.

This variance in dissolution rates for DNQ-novolac based resists is a fundamental reason why much time is invested in the photolithographic process engineering of functional and dependable ICs. For positive resist systems, the identification and maintenance of optimal exposure and development process times during the lithographic process is a key challenge within the semiconductor manufacturing industry.

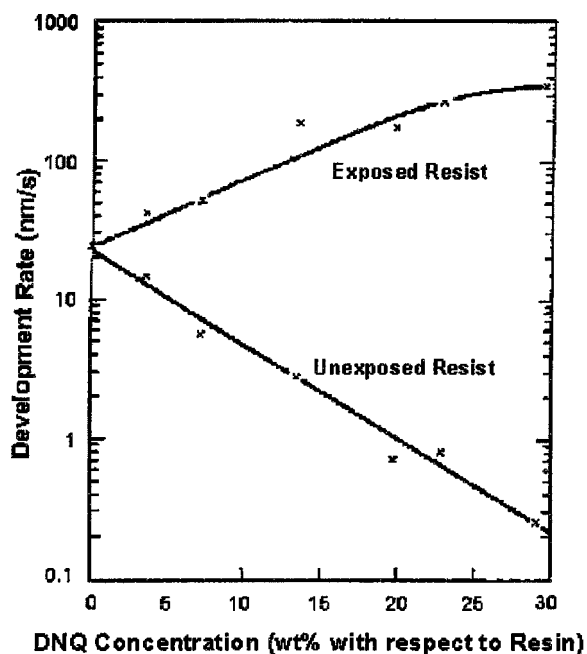


**Figure 1.6.4** Dissolution Rates of unexposed and fully exposed mixtures of DNQ-novolac resists as a function of DNQ loading<sup>4</sup>

## 1.7 Limitations of Photolithography

Although the evolution of lithography systems has allowed for high-quality lenses and exposure systems, the resolution capability of conventional optical photolithography is quickly approaching its physical limits.<sup>4,6,18</sup> The primary problem in photolithography is diffraction, where there is a change in the directions and intensities of a group of waves after passing by an obstacle or through an aperture whose size is approximately the same as the wavelength of the waves.

There is no resolution problem if the features on the photomask are substantially larger than the wavelength. However, diffraction effects begin to be prominent as the wavelength of the light source approaches the dimensions of the photomask.<sup>4,5</sup> This is because the diffracted rays will substantially increase the intended size of the image, as well as distort image quality (as seen in Figure 1.7.2).

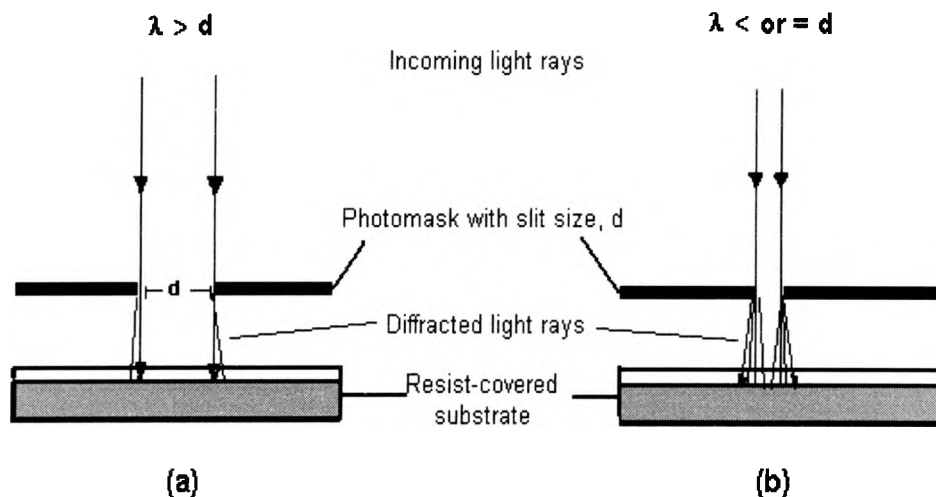


**Figure 1.7.2** Diffraction Problem in Optical Lithography  
(Note how image size is distorted as  $\lambda$  approaches mask feature of size  $d$ )

In general, the resolution capability of a photolithographic system is given by equation 2. Here, it is possible to increase resolution (R) by reducing the exposure wavelength ( $\lambda$ ), increasing the numerical aperture (NA--a measure of the ability of the lens system to compensate for diffraction errors), or by improving the process-dependant parameters (k) such as photoresist sensitivity.<sup>5</sup>

$$R = \frac{k\lambda}{NA} \quad (2)$$

In addition to diffraction, the stepper lens system also has a limitation in the level of focus at which all features can be nominally printed. There is a functional relationship between the critical dimensions of a given feature and the focus and exposure of a given process. It is important to note here that all features to be printed on a wafer must be on a flat or near flat surface, so that features will be within the focal budget of the lens system. A convenient formula for determining the focal budget of an optical lens system is given by equation 3, the depth of focus (DOF) of the lens system.<sup>5</sup>

$$DOF = \frac{\lambda}{2(NA)^2} \quad (3)$$

In this formula, the depth of focus or focal latitude is clearly dependant on the wavelength of light used to expose and the numerical aperture of the system. The better a system is able to compensate for image aberrations due to diffraction, the higher the numerical aperture. It is desirable for the latent image produced in the resist by the stepper to keep the image in focus *throughout* the thickness of the resist. Note that the lens NA and DOF are inversely

proportional, making an unfortunate tradeoff in valuable parameters. This constraint makes the DOF and NA optimization of the lithographic system a crucial and challenging parameter in photolithography.

Invariably, focal errors may be introduced by lens aberrations and non-planar wafer topographies that are unavoidable in the process. These diffraction-related problems are serious limitations to pattern resolution that make conventional photolithography a supreme challenge. Consequently, aside from certain cases where extreme ultraviolet (EUV) lithography is being investigated, photolithography is usually not used industrially when there is a need to pattern very small features (<100 nm).

Diffraction-related limitations also preclude the use of photolithography in the fabrication of photomasks, whose features are much too fine and require the precise, high resolution capabilities of electron beam lithography to pattern. Consequently, electron beam lithography has become the method of choice for creating the photomasks and reticles that are used in photolithography.<sup>2</sup>

## **1.8 Electron Beam Lithography**

Electron beam Lithography (EBL) is a mature technology that has been used in the fabrication of integrated circuits since the 1970s. This is because of the inherent ability of a scanning electron microscope (SEM) to accurately deflect a finely focused beam of electrons over a surface. In the same manner as that of conventional photolithography, the substrate surface in EBL can be coated with a radiation-sensitive layer of resist. If the resist is capable of high resolution, the

EBL system can write patterns upon the substrate with a degree of accuracy and precision that far surpasses that of photolithography. A schematic of such a system is show in Figure 1.8.1.

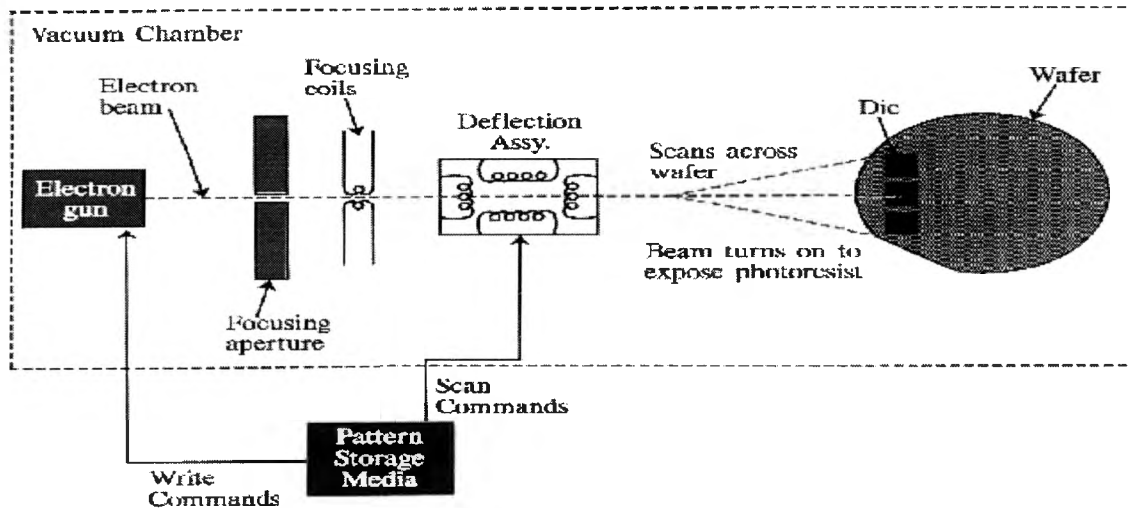


**Figure 1.8.1** Schematic of an Electron Beam Exposure System

Here an electron gun is used as the source, and the electron beam is controlled by a computerized lithography system, which precisely guides the beam over the wafer by the use of deflection and focus coils. The wafer itself is on a mechanical stage, which can be moved with respect to the beam. In theory, assuming the limitations imposed by the hardware are in check, the resolution for such a system is dependant on the spot size of the beam itself (which can be less than 1 nm in width).<sup>12</sup> Unfortunately, the spot size of the beam alone *does not* dictate linewidth and resolution, as there are key factors that limit these properties in electron beam lithography.

## 1.9 Limitations of Electron Beam Lithography

It is important to compare the advantages and disadvantages that such a system will have over conventional photolithography. Obviously, since pattern generation is not diffraction limited, the system is easily capable of defining very small features with a high degree of resolution. In addition, the pattern overlay and reproducibility is excellent since the beam is computer controlled. Finally, a computer controlled system eliminates the need for expensive and fragile photomasks, which also eliminates the possibility of mask-generated imaging errors in the lithography process.

On the other hand, the throughput is much slower for EBL; it takes more time to scan the beam precisely over the wafer than it does to flash expose a wafer. The tradeoff for high resolution is longer processing time. This slow throughput is the primary reason why EBL is not used on a mass scale to produce small technologies. The other two main disadvantages are electron scattering and resist swelling. These factors limit how small images can be fabricated and must be addressed when considering the ultrahigh resolution capabilities of EBL.

Electrons, the exposure source in EBL, are fundamental particles whose properties are well established in quantum physics and physical chemistry.<sup>13,14</sup> They exhibit no comparable diffraction with the substrate because their wavelength can be 4 to 5 times shorter than that of the UV light sources used in photolithography.<sup>5</sup> Electrons are known to scatter strongly with a given substrate, due to interactions between the impinging electron beam and the

nuclei of the sample. The result of this behavior leads to “forward” and “backscattering” of electrons, a primary resolution limitation of EBL.

Upon entering a solid material, the electrons in the beam lose energy by way of elastic and inelastic collisions with the atoms in the material. These collisions result in the scattering process that broadens the beam, normal to the incident beam direction<sup>15</sup>. Two types of scattering are seen—forward scattering in the resist and backscattering from the substrate, seen in Figure 1.9.1.

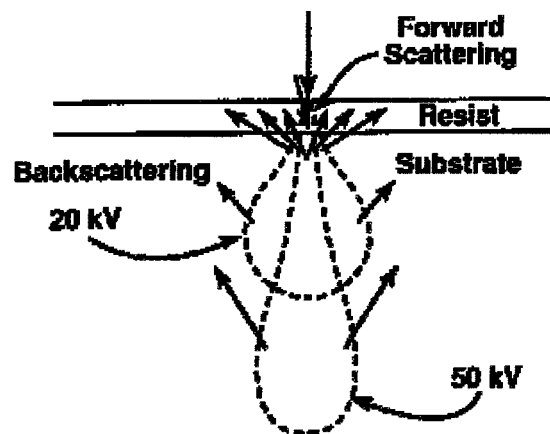


**Figure 1.9.1** Schematic of Electron Forward and Back Scattering in electron resist exposure at 20 and 50 kV<sup>5</sup>

Figure 1.9.2 illustrates these effects at different electron accelerating voltages schematically and with Monte Carlo modeling, which is a computer-aided method that is useful in predicting simulated electron trajectories. Noteworthy is the particle-like behavior of the electrons, as a greater accelerating voltage will decrease the amount of forward scattering in the resist but increase the amount of backscattering from the substrate.

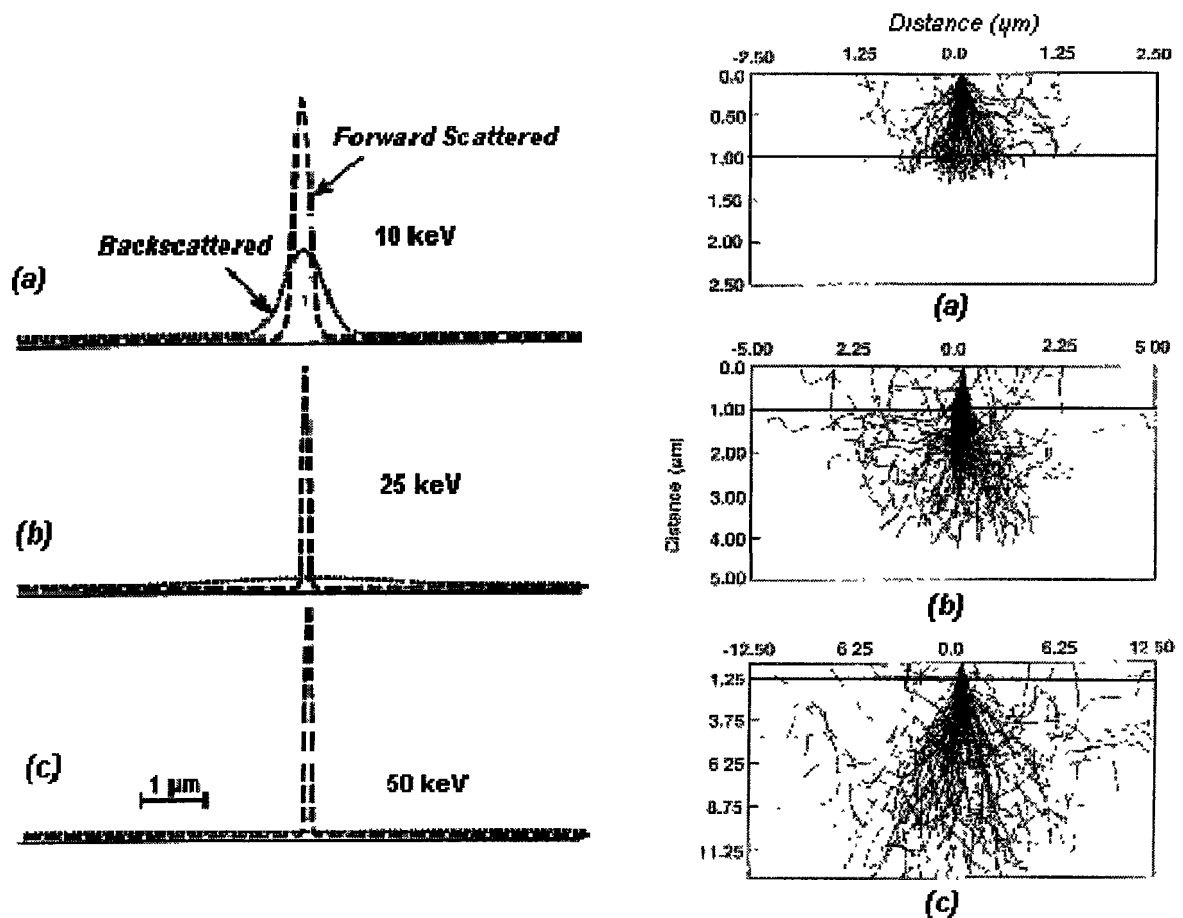


**Figure 1.9.2** Exposure distribution and Monte Carlo simulations<sup>6,7</sup> of a 100 point-source electrons in a target of 1 μm-thick resist on an infinitely thick silicon substrate at accelerating voltages of (a) 10, (b) 25, and (c) 50 kV.

Deformation of the pattern due to swelling of the resist during the development process is another consideration. Although high contrast resists are capable of resolving features with well-defined sidewall profiles, these images may be distorted by swelling.<sup>6</sup> This is because the cross-linked area of the resist tends to absorb a large amount of solvent during the development stage, thereby increasing the dimensions of the pattern. This effect can be quite problematic for situations in which the features are within close proximity of each

other--the patterns may swell so much that adjacent features may bridge and thus limit the generation of small features that are closely spaced.

Another problem caused by resist swelling is the formation of snake-like distortions in fine, narrow images. This “snaking” effect is due to the fact that the resist will expand not only in the horizontal (x) direction, but also within the z-plane of the resist matrix. Since the resist is well adhered to the substrate and cannot increase the length of the resist pattern, the top of the resist must relieve the compressional stress in matrix plane by expanding outwardly. The resultant snaking can be seen in Figure 1.9.3.

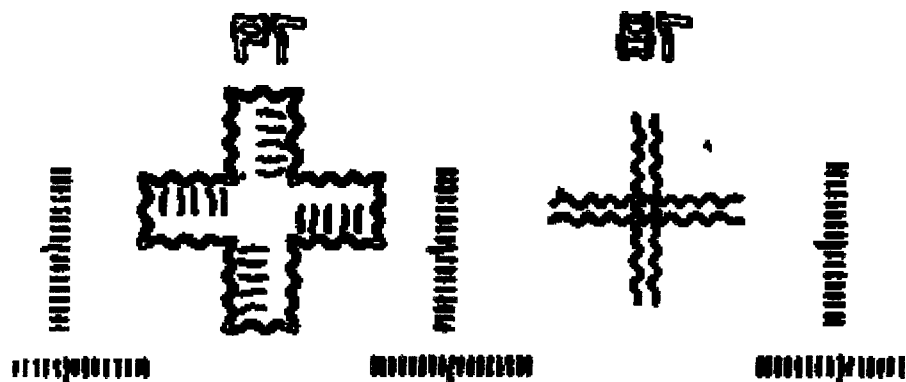


**Figure 1.9.3** Micrograph of swollen images in an experimental negative resist<sup>5</sup>

### 1.10 Electron Beam Resists

Electron beam lithography, like photolithography, also uses positive and negative-tone resists. Negative electron beam resists include the styrene family, seen in Figure 1.10.1. Unsubstituted polystyrene is weakly sensitive, but substitution of the aryl group with chloromethyl or halogen groups results in a marked increase in sensitivity.<sup>5,36</sup>

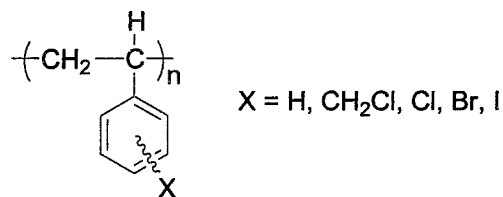


**Figure 1.10.1** Polystyrene-Based Negative Electron Beam Resists

Poly(methyl methacrylate) (PMMA) is a well-established positive e-beam resist and offers the advantages of high resolution, ease of handling, good film-forming characteristics, and wide processing latitude.<sup>5</sup> Figure 1.10.2 shows the reaction scheme in which insoluble PMMA polymer is cleaved upon e-beam exposure and forms soluble by-products to leave the positive-tone image upon develop.

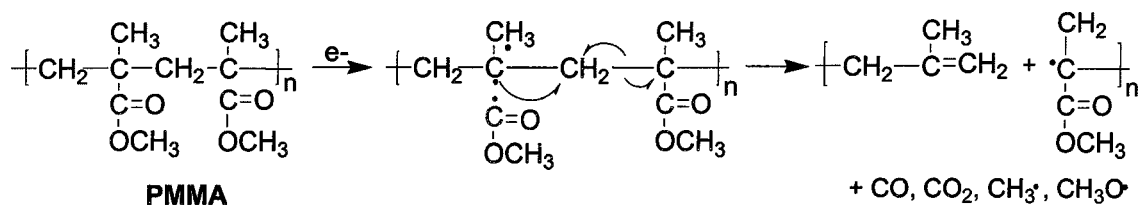


**Figure 1.10.2** Electron beam-induced cleavage of the insoluble PMMA matrix into soluble by-products. The post-develop result is a positive-tone image.

Nevertheless, PMMA resists are relatively insensitive (requiring 100  $\mu\text{C}/\text{cm}^2$  at a 20 kV exposure dose), a factor that limits throughput in EBL.<sup>6</sup> In addition, these resists offer comparatively poor dry etching characteristics compared to resists that have aromatic functionalities, such as novolac.<sup>5</sup> There is therefore a constant search for new materials that will offer good sensitivity

and etch resistance, while offering the high resolution that is necessary to pattern the ultra-small features of cutting-edge micro and nanoelectronics.

### 1.11 Calixarenes as Electron Beam Resists

In the search for high resolution electron beam resists, a family of organic compounds known as calix[*n*]arenes has been found to be promising materials for nanolithography.<sup>19-21</sup> Calix[*n*]arenes are cyclicized, oligomeric products of the base-induced condensation of *p*-*tert*-butylphenol and formaldehyde (Figure 1.11.1), where *n* indicates the number of repeating phenolic/methylene units in the molecule.<sup>22,23</sup> The size of the calixarene annulus depends upon a templating effect during their synthesis between the cation of the base and the forming ring. In general, the larger the cation, the larger number of repeating phenolic units in the macrocyclic calixarene product.<sup>22,24</sup>

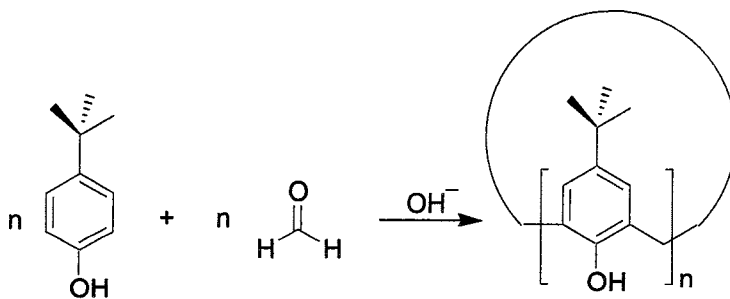


**Figure 1.11.1** Synthesis of *p*-*tert*-butylcalix[*n*]arene (*n* = 4 to 8)

Calix[4]arenes, the most extensively studied of these molecules, were originally named by Gutsche from the Latin word “calix” (vase) which describes the cup-like structure the molecule assumes when all of the phenolic moieties point in the same direction.<sup>22</sup> Calixarenes can be depicted in various ways, as

seen in figure 1.11.2, but a three-dimensional drawing is convenient to show the spatial orientation of the phenolic members and the methylene linkers, which are conformationally mobile.<sup>22,23</sup>

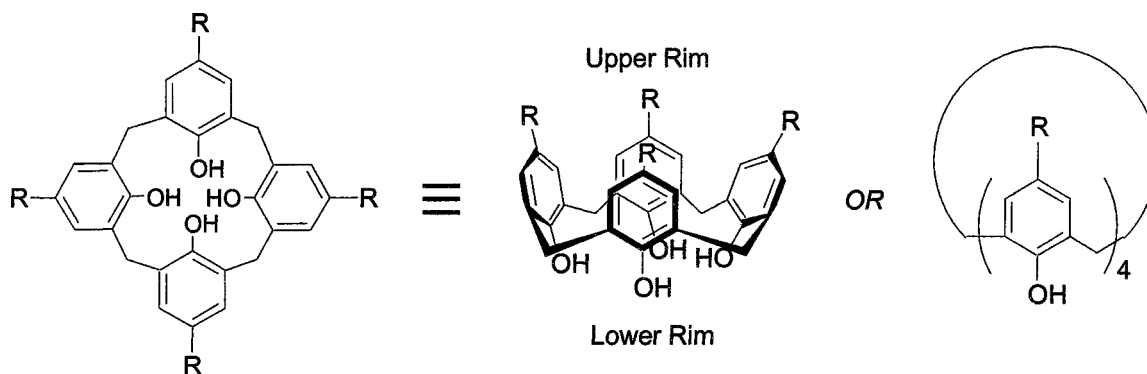


**Figure 1.11.2** Various depictions of the Calix[4]arene

The three-dimensional depiction also shows the *upper and lower rim* of the calixarene molecule, both of which can be functionalized with various groups. As such, the calixarene has been described as a “molecular scaffold” upon which different functional groups can be appended to make a vast number of derivatives. Indeed, the synthetic versatility of calixarenes has led to a staggering array of studies that feature the applications of the calixarene family in supramolecular chemistry.<sup>22-25</sup>

---

In 1992, Wamme and Ohnishi reported the first use of calixarene derivatives as resists, reporting high chemical and thermal stability of the calixarene material, as well as its good film-forming characteristics by spin coating.<sup>26</sup> The derivative in this prototype calixarene resist was a hexaacetate of

*p*-methylcalix[6]arene (MC6AOAc), a conformationally mobile calixarene that demonstrated no flow or softening upon the lithography process. The synthesis of this molecule is shown in Figure 1.11.3.

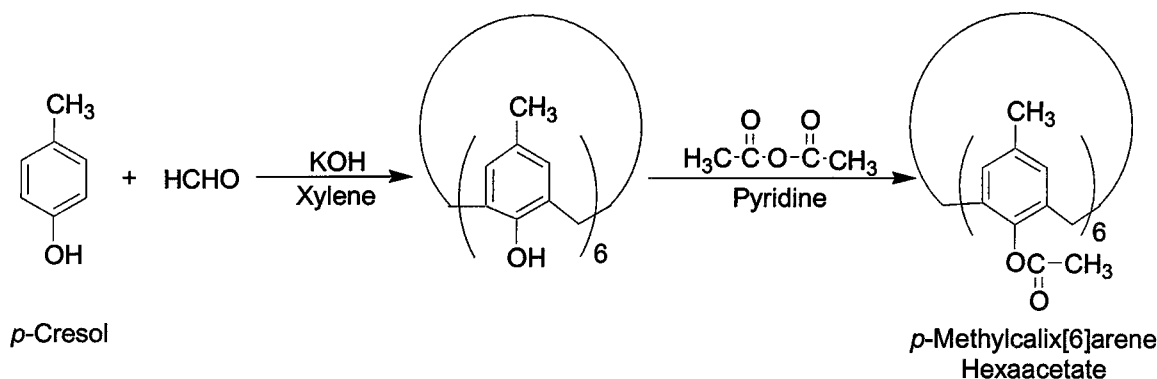


**Figure 1.11.3** Synthesis of *p*-methylcalix[6]arene hexaacetate, a prototype resist (5,11,17,23,29,35-hexamethyl-37,38,39,40,41,42-hexaacetoxycalix[6]arene)

Along with a high heat resistivity, this derivative also demonstrated good adhesion to a semiconductor (germanium) substrate, with spin-coated films that held good integrity up to 800 nm thick, but could be spun as thin as 10 nm. This is a marked contrast from related polymers do not easily form very thin films.<sup>26</sup> In addition, the films spun from these calixarenes demonstrated inactivity to light, but the ability to react under high energy beams, such as electron or ion beams. Using this resist and a focused ion-beam direct writing system, negative patterns with linewidths of 100 nm were reproducibly delineated.

In another study, the aforementioned calixarene derivative (MC6AOAc) was discovered to have *ultrahigh resolution capabilities* as negative electron beam resist, as features with uniform widths of 7 nm were patterned into semiconductor substrates<sup>27</sup> (Figure 1.11.4.b).

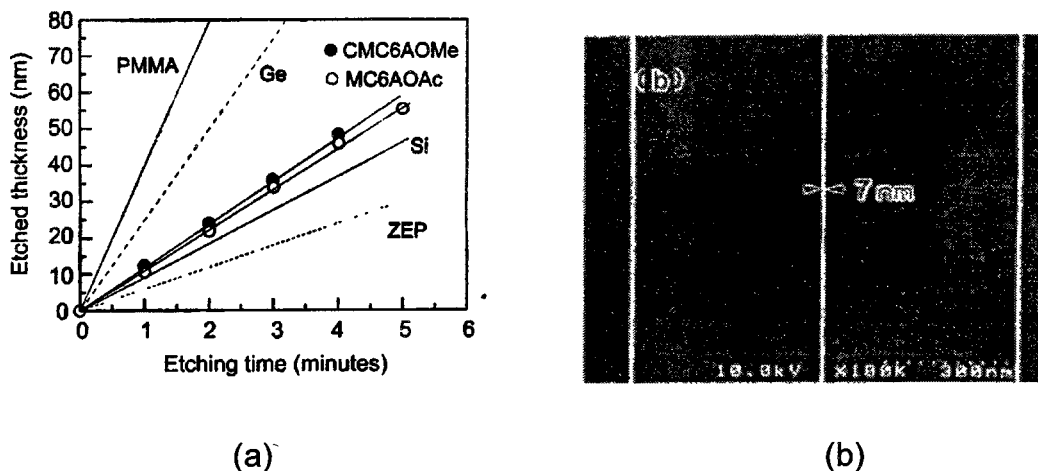


**Figure 1.11.4** (a) Comparison of etch rates between calixarene and PMMA resists. (b) 7 nm features on Ge fabricated using calixarene prototype resist<sup>27</sup>

There are some useful comparisons that can be made with novolac resins here, first of which is *etch resistance*. It has been reasoned that industrially established resists such as SAL (a negative electron beam resist from Shipley), ZEP (a positive e-beam resist from Nippon Zeon), and AZ (novolac-based photoresist from Hoechst) all have a high degree of dry etch resistance due to their structurally similar monomeric functional group, the phenolic moiety.<sup>33</sup>

Indeed, it is recognized that non-aromatic resists such as PMMA offer far less efficient dry-etch resistance than resists (such as calixarene) that have aromatic functionalities.<sup>28,33,5</sup> Such effects are also demonstrated graphically in Figure 1.11.4 (a), demonstrating how the prototype calixarene resist offers an etch rate four times less than PMMA, and thus an appreciable protection to the substrate during the dry-etch (plasma) process.

Despite their monomeric similarities, the *physical properties* of calixarenes and novolacs are also remarkably different. Novolacs are able to form cyclic or

hemicyclic intramolecular hydrogen bonds within the same molecule, while intermolecular H-bonds are few.<sup>4</sup> These supramolecular interactions are known to be dependant upon variances in novolac chain lengths (dispersity) and the constitution of *o*-, *p*-, or *m*-cresol used in their synthesis, and result in a high degree of disorder in thin films when compared to calixarene.

Calixarenes, on the other hand, have a crystal organization in the solid phase that is highly regular, and can therefore orient themselves to maximize the intermolecular interactions between the hydroxylic and hydrophilic moieties of neighboring molecules in thin films. As a result, the high lattice energy of calixarenes confers an insolubility in most common organic solvents but extremely high melting points compared to other organic compounds<sup>4</sup> (e.g., 411°C for *p-tert*-butylcalix[8]arene as compared to a 140°C *T<sub>g</sub>* for novolac<sup>4,37</sup>). A high melting point gives calixarenes a reasonable degree of thermal stability, an obvious advantage when the molecules are to be subjected to the harsh processing conditions of the semiconductor fabrication arena.

In addition, calixarenes have exhibited the ability to be patterned with *ultrahigh resolution* (10 nm), owing to their nanometer scale size. One calixarene molecule is approximately 1 nm in width<sup>28,30</sup> as compared to the much larger, more randomly sized molecules in novolac resins. Presumably, the more orderly packing of calixarenes may lead to sharper cross-sectional sidewalls in the resist, since a 10 nm wide pattern implies a film that is 9 to 10 calixarene molecules wide. Ultimate resolution is then thought to be limited by the size of the resist

molecule itself. This gives the calixarene a resolution capability that related novolac chain polymers cannot achieve.<sup>30,31</sup>

The sensitivity of calixarenes is a subject of many studies in the literature and merits discussion. In general, calixarenes are reported to have a sensitivity that is 10 to 20 times less than PMMA. Synthesis of a calixarene derivative with a chloromethylated group in the para position (shown in Figure 1.11.5) *doubles* the sensitivity of the derivative as compared to the prototype calixarene resist.<sup>31</sup>

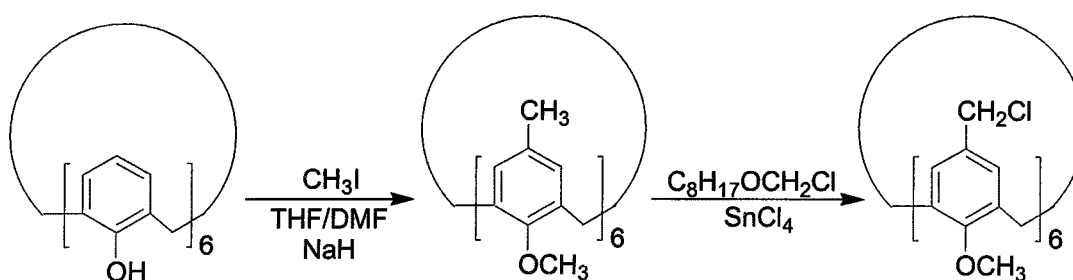


**Figure 1.11.5** Synthesis of a chloromethylated calix[6]arene derivative (5,11,17,23,29,35-hexachloromethyl-37,38,39,40,41,42-hexamethoxycalix[6]arene) for electron beam lithography

This chloromethylated derivative was first reported by Ungaro,<sup>32</sup> and is thought to be more lithographically sensitive because the bonding energy of the C-Cl bond is less than that of the C-H bond and also because the chlorine atom has a larger capture cross section for irradiated electrons.<sup>33</sup> Increasing the sensitivity of the calixarene by changing the functional groups of the upper or lower rim demonstrates the flexibility that calixarenes inherently offer to the science and art of resist technology.

Although the sensitivity of calixarenes is less than that of other electron beam resists, their resolution is comparatively superior. Traditionally, the trend has been to increase resist sensitivity. However a high sensitivity can

compromise resolution, as studies have shown that the width of dot features is dependant on sensitivity.<sup>5,33</sup> This means that the more sensitive a resist, the larger the dot size, presumably since the irradiating electrons will cause those molecules immediately adjacent to the exposed area to crosslink. Because calixarene resists have a contrast comparable or better than common electron beam resists, their relatively low sensitivity can be an advantage in the fabrication of nanoscopic devices because they will crosslink only in those areas that are exposed.<sup>33</sup>

Finally, the number of phenolic residues in the calixarene has impact on resist sensitivity. Increasing the number of arenes in the molecule has a corresponding effect on resist sensitivity.<sup>33,29</sup> Studies on analogously functionalized calixarenes of different ring sizes (four to seven phenolic moieties) have demonstrated that the larger calixarenes have higher sensitivity and contrast<sup>33</sup> at varying exposure dosages, seen in Figure 1.11.6.

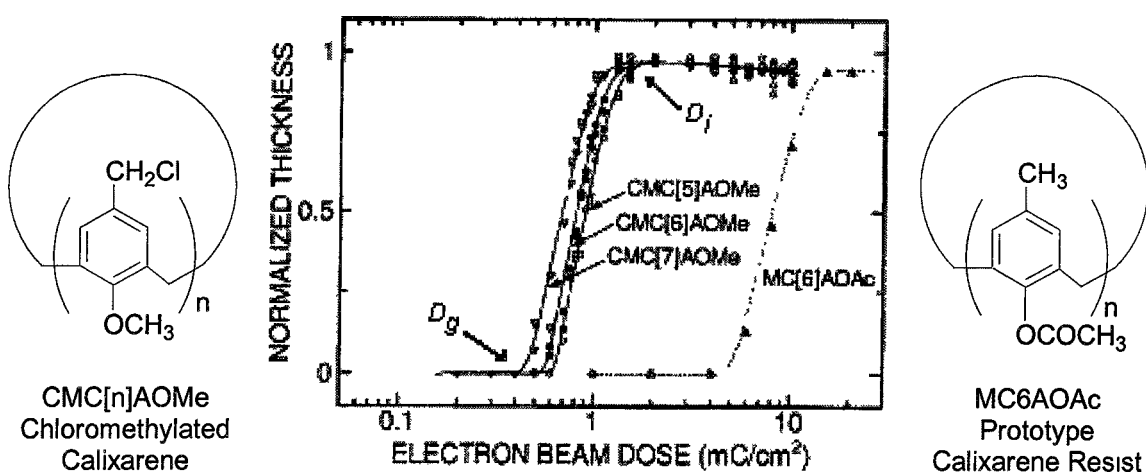


**Figure 1.11.6** Sensitivity to electron dose for calix[n]arenes (CMC[n]AOMe,  $n = 5,6,7$ ) and prototype calix[6]arene (MC[6]AOAc)<sup>33</sup>

This figure is known as a “contrast curve”, which is a commonly used and essential plot for evaluating and comparing the sensitivity and contrast of different resists. To obtain such a plot, a nominally thick film of resist is applied to a wafer, exposed to a range of doses, and developed. The normalized thickness of the remaining resist is measured and then plotted versus the log of the exposure dose.<sup>4,5</sup>

$D_g$  (gel dose) is the minimum dose necessary to create an insoluble residue, while  $D_i$  (insolubilization dose) is the minimum dose required to give a patterned film thickness equal to the original, unexposed resist thickness. The contrast ( $\gamma$ ) of the resist is then given by equation 4, and is the slope of the extrapolated line in the crossover region for that set of data and can be useful to compare resist contrasts if all experimental conditions are provided.

$$\gamma = \frac{1}{\log \frac{D_i}{D_g}} \quad (4)$$

Note that the chloromethylated calixarenes in Figure 1.11.6 require a lower electron dose and are thus more sensitive than the prototype resist, but share the same contrast.

In summary, calixarenes offer many advantages that can be useful for the fabrication of nanometer-scale devices. These include ultrahigh resolution, high thermal stability, synthetic versatility, excellent adhesion, and good protection to the substrate during the etch process. They are synthesized from relatively inexpensive reagents and are approximately 1 nm in width, a property that makes them appropriate in patterning very small features. Indeed, functional

nanometer-scale devices with critical dimensions of 30 nm have already been successfully fabricated using calixarene-based resist.<sup>38</sup> Thus, when coupled with high-resolution electron beam lithography, calixarenes have the potential to realize the miniaturization of future generations of semiconductor devices, and therefore merit research and development.

### 1.12 **Thesis Proposal: Conformationally Rigid Calix[6]arenes as High Resolution Negative Resists in Electron Beam Lithography**

Recently, the synthesis of two semi-rigid Bis-bridged calixarene conformers has been elaborated in two independent multistep, high-yield processes.<sup>34,35</sup> The structures of these two conformers (shown in Figure 1.12.1) are elegant and offer a high degree of structural regularity, due to the lack of conformational interconversions that are typical for non-bridged calix[6]arenes.<sup>22,24</sup>

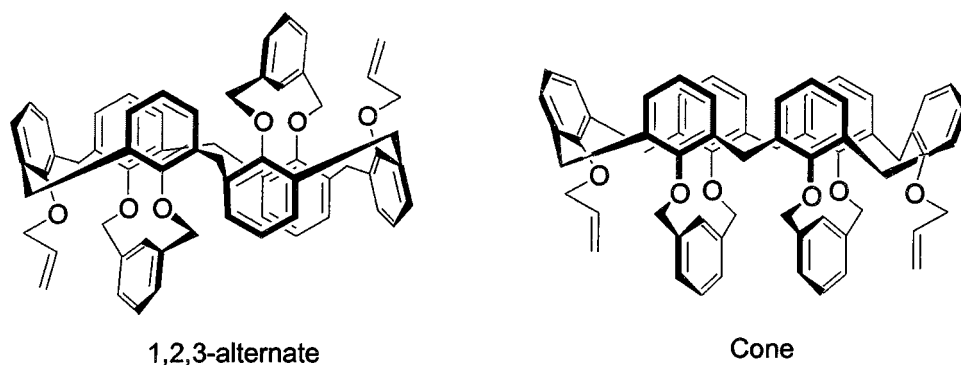


**Figure 1.12.1** 2 Conformers of Diallyloxy Bis-*m*-Xylenyloxy Calix[6]arene (1,2,3-alternate and Cone)

Because the effects that structurally semirigid compounds may have on resist performance has not been reported in the literature, there is a need for the evaluation of conformationally immobile calixarenes as electron beam resists. In addition, calixarenes that are functionalized with radically polymerizable allyl groups *on the upper or lower calix rim of each phenolic residue* are also under investigation for calix[4]arenes,<sup>36</sup> but no such study exists for selectively functionalized calix[6]arenes. Therefore, studies of calix[6]arenes with *strategically functionalized* photopolymerizable groups such as the allyl group may offer new insight to the mechanism and lithographic capabilities of the calixarene resist family.

We have investigated the physical and lithographic properties of two novel conformers of selectively functionalized diallyloxy Bis-*m*-xylenyloxy calix[6]arene (1,2,3-alternate and Cone conformers) as negative electron beam resists. In separate experiments, resist films using either conformer have been spin-coated on 4", p-type silicon wafers with various resist thicknesses in order to characterize their index of refraction and obtain spin speed curves. The films were then subjected to electron beam exposure at various doses and plotted in order to determine resist sensitivity and contrast. The resolution capability of both conformers was also investigated and scanning electron micrographs and atomic force microscope (AFM) images of patterned films were obtained.

In addition, the effects of benzoyl peroxide as a free-radical initiator (sensitizer) for both conformers was evaluated in separate resist formulations. All experiments were performed in such a way as to create a comparison

between these structurally unique compounds with the aforementioned calixarene resist prototypes in order to evaluate the usefulness of these novel compounds as materials in electron beam lithography.

## 2.0 SYNTHETIC STRATEGY

### 2.1 Overview

Two conformers of diallyloxy bis-*m*-xylenyloxycalix[6]arene (**1**=1,2,3-alternate conformer; **2**=cone conformer) both come from common precursors in a four step, selectively functionalized synthesis that is detailed here.

In this section, the rationale behind each functionalization step of diallyloxy-bis-*m*-xylenyloxycalix[6]arene is presented in a manner which highlights the unique chemical qualities that may render this molecule lithographically useful. A comparative approach is taken to establish differences between this structurally unique molecule and the calixarenes of other reported electron beam resists. Comparison will justify how the study of the lithographic properties of these particular molecules may help unravel new details in calixarene resist technology.

### 2.2 Calix[6]arene Numbering

It is useful to give the numbering system of the unsubstituted version of the calix[6]arene in order to specifically identify which parts of the basic calix[6]arene skeleton are functionalized to create the molecular conformers used in this study. The structure of dealkylated calix[6]arene is provided in Figure

2.2.1 which also designates the lettering of the constituent aryl groups for future reference.

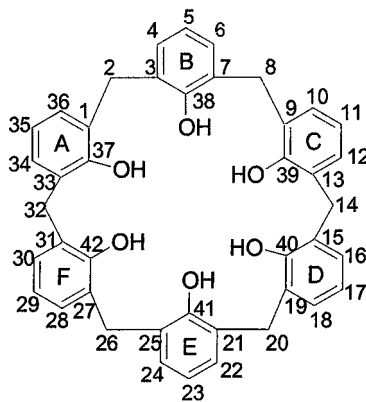


**Figure 2.2.1** Nomenclature system of calix[6]arene (36,37,38,39,40,41,42-hexol)

### 2.3 Conformational Mobility of Calixarenes

Calixarenes are highly flexible molecules, capable of bending at the linker methylene groups, as well as complete ring inversions of the aryl groups through the annulus of the molecule.<sup>22</sup> These effects lead to a high degree of conformational mobility, where the phenolic residues may rotate through the annulus of the macrocycle, as shown in Figure 2.3.1

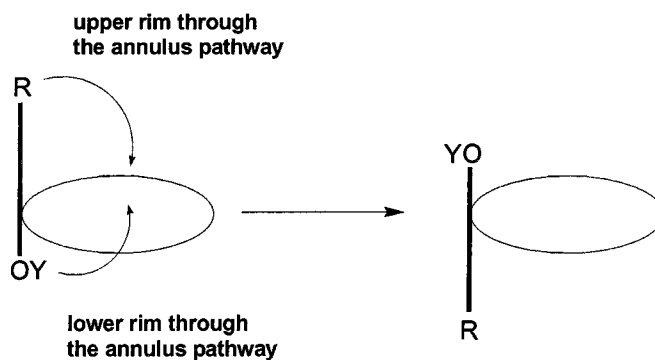


**Figure 2.3.1** Pathways for conformational Inversions of calix[n]arene<sup>22</sup>

This conformational flexibility increases proportionally with  $n$  (the number of phenolic residues) in calix[ $n$ ]arenes, and may allow for the complete inversion of the functional groups of the upper or lower calix rim.<sup>24</sup> Structural mobility in calix[6]arene allows for eight different molecular conformations,<sup>22</sup> as even the bulky *p-tert*-butyl group on the upper rim of *p-tert*-butylcalix[6]arene has the freedom to pass through the annulus.<sup>22</sup>

## 2.4 Conformational Immobilization

Currently, there is no report in the literature that demonstrates the use of conformationally immobile calix[6]arenes as electron beam resists. As such, the study of conformationally immobile calix[6]arenes has the potential to add a new level of insight to the chemical and physical dynamics by which calixarenes serve as e-beam resists. In addition, the study of conformationally immobile calix[6]arenes as electron beam resists can provide a comparison to established calixarene resists in order to evaluate the effects of immobilization on the performance of calixarenes as ultrahigh resolution electron beam resists.

The synthesis of conformationally immobile calixarenes can be achieved by using bridging reagents that link the intramolecular hydroxyl groups of lower rim of the molecule to create semirigid compounds.<sup>22,25,34</sup> Various linkers that enable immobilization of the members in the calix annulus have been reported for synthetic and supramolecular purposes,<sup>22,25</sup> but we have chosen to use  $\alpha,\alpha'$ -dibromo-*m*-xylene (Figure 2.4.1) in a pre-established synthesis<sup>34,35</sup> to create the

two conformers of calix[6]arene that are used as electron beam resist materials for this study.

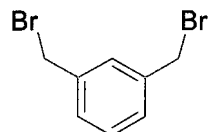


**Figure 2.4.1**  $\alpha,\alpha'$ -dibromo-*m*-xylene, linker to induce conformational immobility

The synthetic protocol that leads to the two individual conformers (seen in Figure 2.4.2) has been established from previous work.<sup>34,35</sup> The inclusion of additional substituents that contain aromatic functionalities (such as the *m*-xylene linkers) may prove to be useful for the fabrication of semiconductors, since resist materials with aryl groups tend to confer a higher degree of protection to the substrate during the dry-etch process<sup>5</sup>.

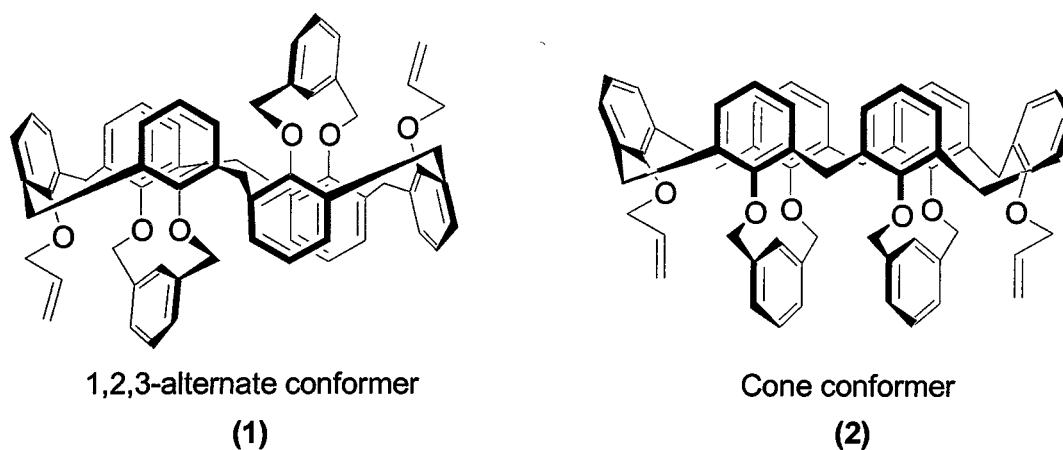


**Figure 2.4.2** Two conformers of Diallyloxy Bis-*m*-Xylenyloxy Calix[6]arene (1 and 2)

The four step synthesis of these calix[6]arene conformers is outlined in sections 2.7 through 2.10. For the sake of brevity, the 1,2,3-alternate and cone conformers of diallyloxy-bis-*m*-xylenylxoycalix[6]arene will be referred to hereinafter as 1 and 2.

## 2.5 Effects of Allyl Substituents on Sensitivity

Recent studies have indicated that calixarene resist sensitivity can be increased by an order of magnitude with the introduction of allyl groups into the upper or lower rim of the molecule, while still maintaining a high degree of etch resistance.<sup>41</sup> Figure 2.5.1, for example, illustrates how the sensitivity of a calix[4]arene-based resist is increased when fully functionalized with allyl groups.

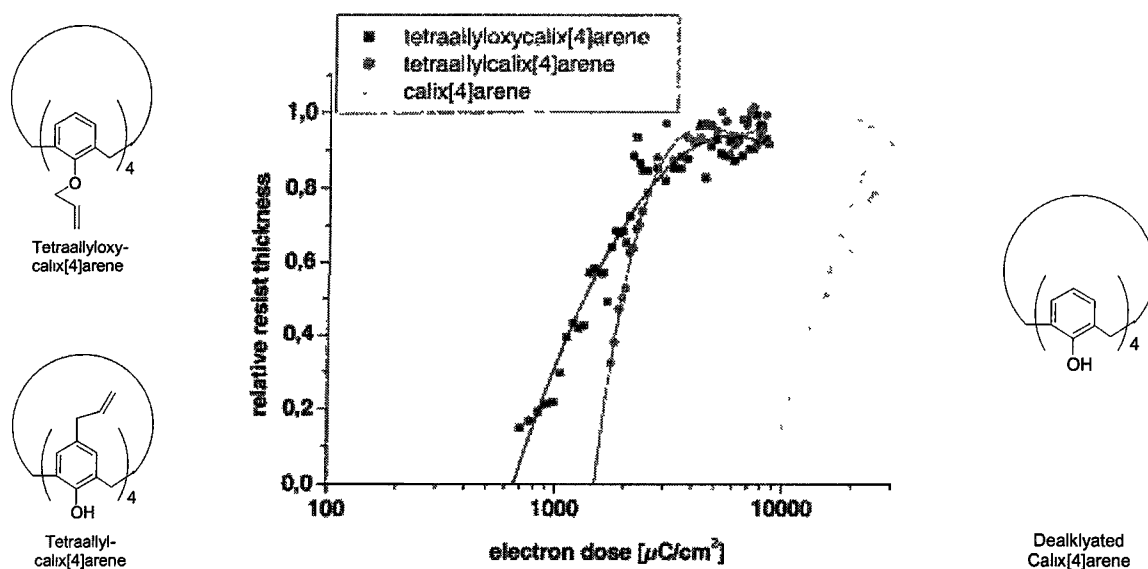


**Figure 2.5.1** Contrast curves comparing the sensitivity of allyl-functionalized calix[4]arene versus unsubstituted calix[4]arene<sup>41</sup>

Tetraallyxocalix[4]arene and tetraallylcalix[4]arene both demonstrated an increase in sensitivity over dealkylated calix[4]arene, while the position of the allyl group was reported to not have a strong influence on resist behavior.<sup>41</sup> In addition, the allyl group added better solubility and film quality to the molecules, properties that can presumably be carried over into **1** and **2**.

## 2.6 Electron Beam-Induced Polymerization Mechanism of **1** and **2**

The exact polymerization mechanism which enables other reported calixarenes to create high-resolution, negative tone images *has not* been established in the literature. Because of its well-known crosslinking properties in polymer science,<sup>16</sup> the *allyl group* has been strategically selected as the key functional group that will cause the polymerization of **1** and **2** upon electron beam exposure. Figure 2.5.1 is one route that could potentially begin to create an insoluble calixarene matrix via high energy electron beam exposure of **1** and **2**.

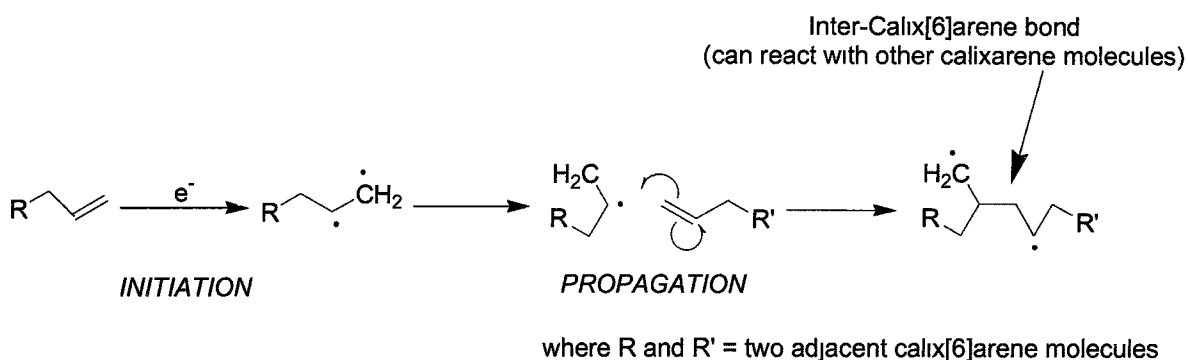


**Figure 2.6.1** A possible mechanism of the free-radical polymerization of the allyl groups in adjacent calixarenes upon electron beam exposure

The free-radical initiation of monomers in the solid state by exposure to electromagnetic energy or high energy particles is a well established mechanism.<sup>16,42, 43</sup> The radicals that are created by electron beam exposure in this particular mechanism may then undergo various modes of propagation, hydrogen-abstraction, and ultimately insertion into nearby allyl groups to *terminate* the reaction and thereby create the three-dimensional, high-molecular weight calixarene matrix. This matrix is insoluble in the developer and is therefore the basis of the negative patterns in **1** and **2**.

In addition, **1** and **2** offer strategically-positioned allyl groups on opposite sides of the calix (A and D ring). This is a stark contrast to previously reported calixarenes, whose upper or lower rims are *completely* functionalized (such as the tetraallyl-functionalized calix[4]arenes in Figure 2.5.1). Presumably, the selectively functionalized allyl groups in **1** and **2** render them more susceptible to *intermolecular polymerization reactions* between the allyl groups of adjacent calixarene molecules in the resist film.

Separate studies have been conducted to determine how benzoyl peroxide (BPO), a common radical initiator, may affect the crosslinking and resolution capabilities of **1** and **2**. This has been attempted by introducing recrystallized BPO into separate **1** and **2** resist formulations, and then processing them to characterize their effect on developed features.

**2.7 STEP 1: Synthesis of *p*-*tert*-butylcalix[6]arene, compound A (5, 11, 17, 23, 29 35-hexa-*p*-*tert*-butyl-37, 38, 39, 40, 41, 42-hexahydroxycalix[6]arene)**

The steps to the selective functionalization with allyl groups and the conformational immobilization of **1** and **2** are outlined below. The first synthesis step entails the creation of *p*-*tert*-butylcalix[6]arene (Figure 2.7.1), a common starting calix[6]arene precursor with a well-established synthesis and a high yield.<sup>22</sup> The synthesis is convenient, as it involves the use of relatively cheap reactants in a “one-pot” method.

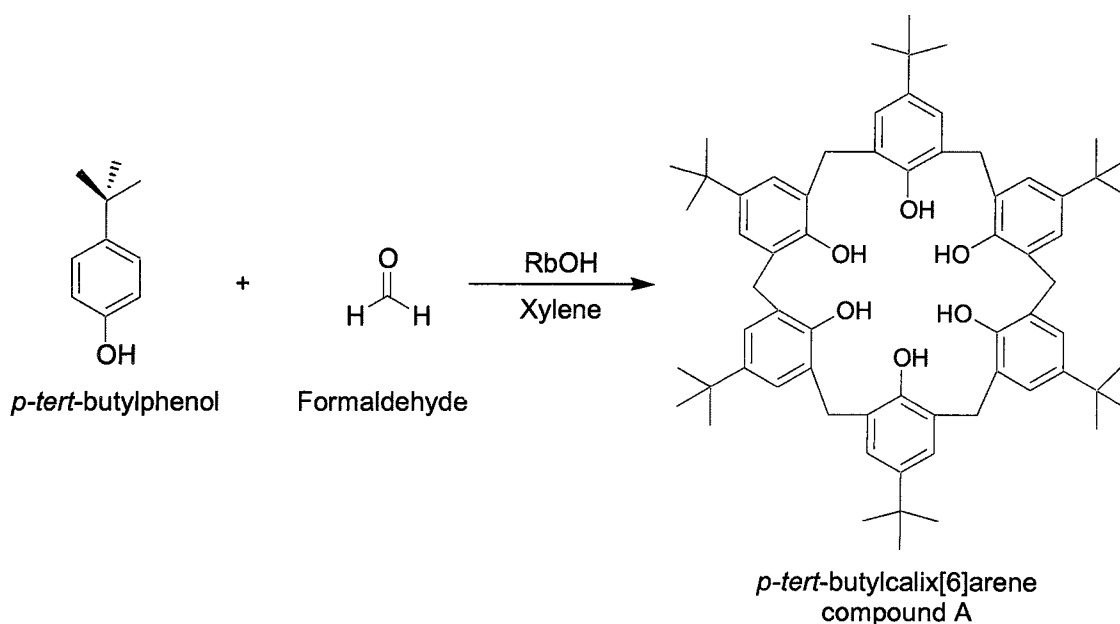


**Figure 2.7.1** Synthesis of *p*-*tert*-butylcalix[6]arene, compound A (5, 11, 17, 23, 29 35-hexa-*p*-*tert*-butyl-37, 38, 39, 40, 41, 42-hexahydroxycalix[6]arene)

The synthesis is a RbOH-induced condensation of *p*-*tert*-butylphenol and paraformaldehyde in refluxing xylene. The rubidium metal cation in the base facilitates the formation of the 24-membered ring of the calix[6]arene annulus by serving as a template for the six phenolic oxygen atoms to organize around.<sup>22</sup>

Calixarenes of various sizes ( $n = 4-8$ ) have been investigated in the calixarene electron beam resist literature, but it has been determined that *calixarenes with a higher number of phenolic residues will have a higher resist sensitivity*.<sup>32,40</sup> Unfortunately, the calix[8]arenes are difficult to dissolve in most organic solvents.<sup>22</sup> This insolubility factor may preclude the efficient use of calix[8]arenes as resists, since they will not easily create the uniform thin films that are absolutely essential to lithography upon spin-casting.<sup>27</sup>

On the other hand, a calix[6]arene offers the advantages of moderate solubility in organic resist solvents and comparatively good sensitivity. Calix[6]arene resist thin films of up to 800 nm can easily be spun onto the wafer surface uniformly and with high film integrity.<sup>30,31</sup> Thus, the end product of the four step synthesis series in this study inherently offers competitive sensitivity with respect to other reported calixarene resist materials.

## 2.8 STEP 2: Synthesis of Dealkylated Calix[6]arene, compound B (37, 38, 39, 40, 41 ,52-hexahydroxycalix[6]arene

Normally, dealkylation of the upper rim of the molecule is a common mode of liberating the *upper rim* of the calixarene for functionalization. This step (Figure 2.8.1) involves a reverse Friedel-Crafts alkylation that uses  $\text{AlCl}_3$  as the Lewis acid catalyst and toluene as the solvent.

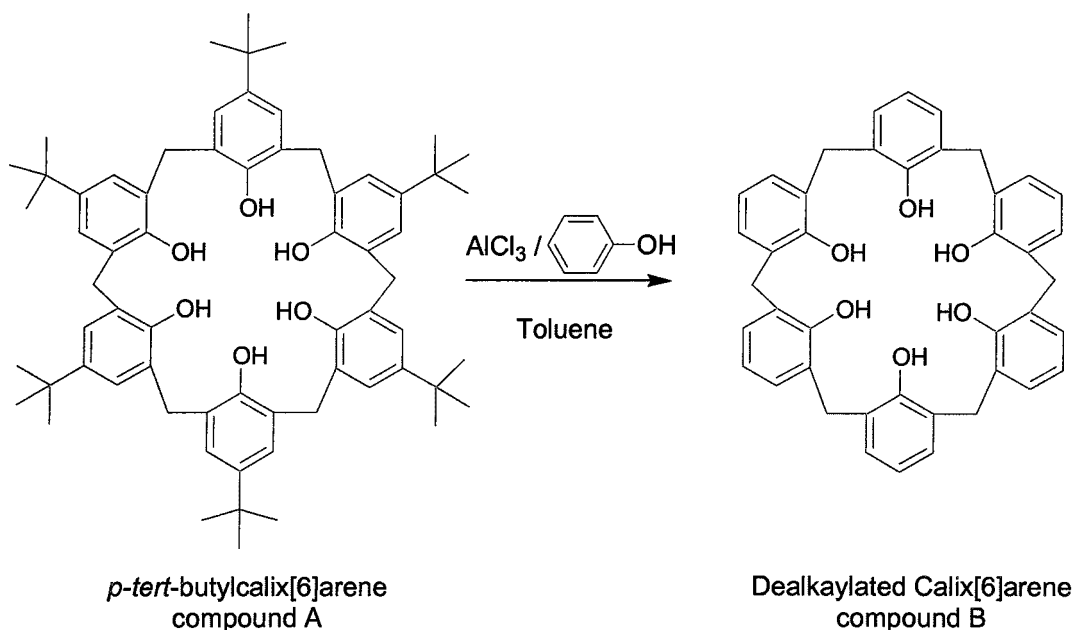


**Figure 2.8.1** Synthesis of Dealkylated Calix[6]arene (37, 38, 39, 40, 41 ,52-hexahydroxycalix[6]arene

This defunctionalization step is done *a priori* to any other step. Upper rim dealkylation affords the liberty and potential to functionalize the upper rim with other groups that may render the molecule more sensitive groups (such as the chloromethyl group,  $-\text{CH}_2\text{Cl}$ ). Dealkylation also gives the molecule a higher degree of flexibility,<sup>22</sup> which will be overcome by bridging.

### 2.9 STEP 3: Synthesis of Diallyloxytetrahydroxycalix[6]arene (37, 40-Diallyloxy-38, 39, 41, 42-tetrahydroxycalix[6]arene)

Preparation of this selectively functionalized compound (C) is achieved in high yields and involves the use of dealkylated calix[6]arene, allyl bromide, and potassium trimethylsilanoate ( $(\text{CH}_3)_3\text{SiOK}$ ) in THF and DMF solvents.<sup>44</sup> The product is shown in Figure 2.9.1 and with the allyl groups on the opposing A and D rings of the molecule.

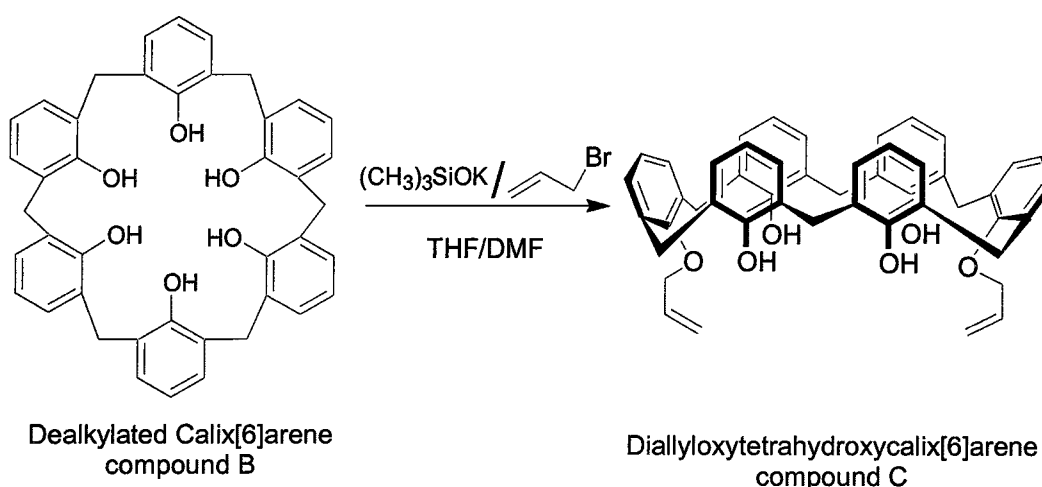


**Figure 2.9.1** Synthesis of Diallyloxytetrahydroxycalix[6]arene, compound C (37, 40-Diallyloxy-38, 39, 41, 42-tetrahydroxycalix[6]arene)

As previously discussed, the selective functionalization of the molecule adds only two photopolymerizable allyl groups, while predisposing the hydroxyl groups of the other four rings (B, C, E, F) to bis-bridging reactions to create semirigid, conformationally immobile compounds. A variety of bis electrophiles may be used to create bridged calix[6]arenes,<sup>25</sup> among them  $\alpha,\alpha'$ -dibromo-*m*-xylene.

**2.10 STEP 4: Stereo-Selective Synthesis of 2 Conformers of Diallyloxy-bis-*m*-xylynyloxy calix[6]arene (37,40-Diallyloxy-(38-42),(39-40)-bis-*m*-xylynyloxy-calix[6]arene)**

It is interesting to note that the creation of the conformers of this molecule is completely dependant upon the reaction conditions. The stereo-selective synthesis of both **1** and **2** are carried out in two independent reactions using diallyloxytetrahydroxycalix[6]arene from step 3 as the starting material. The synthesis of **C1** is accomplished with the use of sodium hydride (NaH) as the base with THF/DMF as the solvent, whereas the synthesis of **C2** involves the use of cesium carbonate (CsCO<sub>3</sub>) as the base with acetonitrile as the solvent (Figure 2.10.1).<sup>34,35</sup>

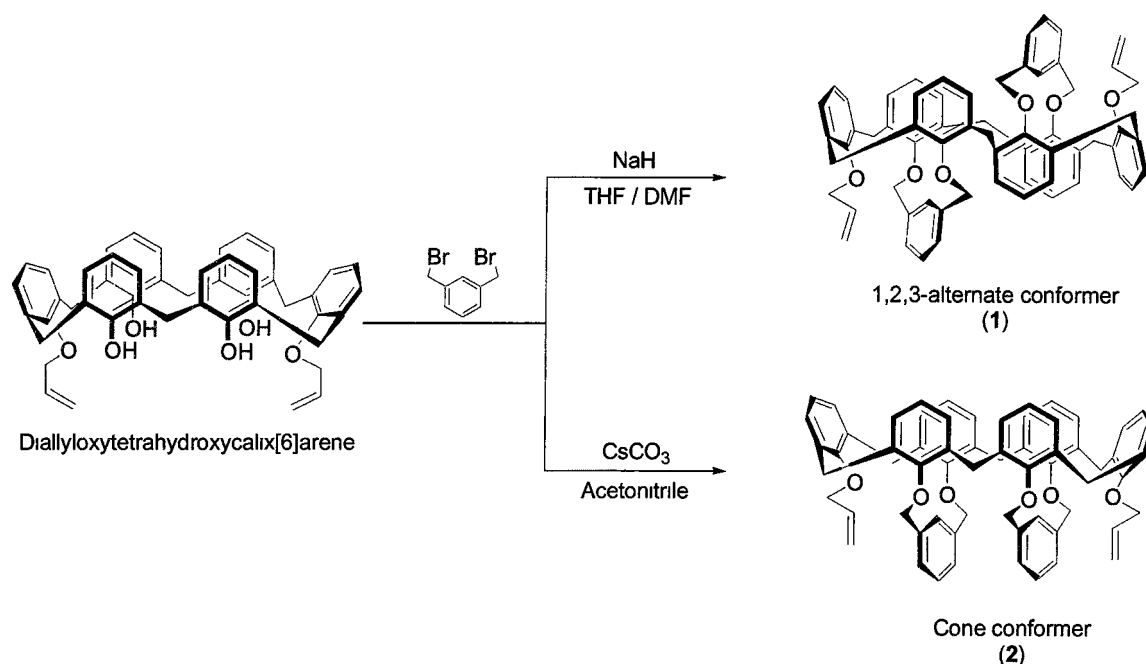


**Figure 2.10.1** Stereo-selective synthesis of **1** and **2**

Each independent synthesis results in a mixture of compounds that necessitate the use of column chromatography to isolate the desired product from the reaction mixtures. Both separations use silica gel with an appropriate solvent eluent mixture, and monitored with thin-layer chromatography (TLC) to determine when the desired product elutes from the column. The cone conformer (C2) is usually obtained from the column in higher yield than the 1,2,3-alternate conformer (C2).

The respective products are then recrystallized and the structures are initially verified using TLC versus a known, pre-isolated **1** or **2** standard.  $^1\text{H}$  and  $^{13}\text{C}$ -nuclear magnetic resonance (NMR) is then used to complete the characterization for each compound. The purified compounds can then be dissolved in chlorobenzene to formulate electron beam resists of various viscosities

Recrystallization of each compound also serves to facilitate the ultrahigh purity that is quintessential for the electron beam-induced polymerization of the calixarenes in the thin film. This phenomenon is fundamental in polymer chemistry and can be expressed with the Carothers Equation (Equation 1).<sup>45,16</sup>

$$\overline{DP} = \frac{1}{1 - p} \quad (1)$$

This equation expresses the relationship of the average degree of polymerization ( $\overline{DP}$ ) to the purity of the monomers used. Here  $p$  is the reaction conversion of the molecules and can be likened to the *purity* of the monomers.

As monomers purity approaches 100 percent, the degree of polymerization approaches infinity, specifically indicating in this case that a high number of calixarenes can actively participate in the aforementioned crosslinking mechanism to create the insoluble polymer matrix. Purity of these calix[6]arenes should thus be considered *absolutely* necessary in order to formulate electron beam resists that are capable of patterning the high resolution, well-defined features that are desired in nanolithography.<sup>51</sup>

## 3.0 EXPERIMENTAL

### 3.1 Materials

All solvents were purchased from EM Scientific and were utilized as received. All reagents were purchased through Aldrich and were used without further purification with the exception of benzoyl peroxide, which was gently recrystallized from a solution of chloroform and CH<sub>3</sub>OH. All reactions were conducted in flame-dried round bottom flasks and under a dry argon atmosphere. For product characterizations, analytical thin layer chromatography (TLC) was performed on precoated silica gel plates, with Silica Gel 1B2-F as the solid phase. For purification purposes, gravity column chromatography was performed with Silica Gel 1B2-F, 60-200 Mesh (75-250 micron). For structural verification, a 400 MHz Varian NMR was used to obtain <sup>1</sup>H-NMR and <sup>13</sup>C-NMR spectra. Chloroform-*d* (CDCl<sub>3</sub>) was the solvent used for NMR samples with tetramethylsilane (TMS) as the internal standard. Chemical shifts (δ) are reported in ppm relative to the internal tetramethylsilane (TMS) standard. All melting points were obtained in unsealed capillary tubes and are uncorrected. The parent compound *p*-*tert*-butyl-calix[6]arene (**A**) was prepared according to known procedures as well as the dealkylated calix[6]arene (**B**) which was obtained by treatment of the parent compound with AlCl<sub>3</sub> and phenol.<sup>30-31</sup>

diallyloxytetrahydroxycalix[6]arene (**C**) was prepared according to known procedures by treating **B** with allyl bromide and potassium trimethylsilanoate.<sup>44</sup>

### 3.2 Semiconductor Processing and Characterization Tools

All lithography experiments were performed on 4" *p*-type silicon wafers obtained from Wacker Siltronic and were used without native oxide strip. These wafers were manufactured by Lucent Technologies and were specified at 10-15  $\Omega$ -cm resistivity with a [1,0,0] crystal orientation. For all resist coating experiments, a WS-400/500 single wafer spin processor (Laurell Technologies) was used. A hotplate (HP30A, Torrey Pines Scientific) was used for all pre-exposure soft bakes. For the determination of the optical properties and pre-exposure film thicknesses of calixarene thin films, a Gaertner L117 3-angle Null Ellipsometer ( $\lambda = 632.8$  nm) was used. A Tencor (Alpha Step 500) Stylus Profilometer was used to obtain additional film thickness data. For all lithographic exposures, a JSM-IC848A (JEOL) Scanning Electron Microscope (SEM) was used. For all sample sputtering, a triode magnetron sputtering system (Hummer X, Anatech Ltd) equipped with a AuPd sputtering target was used. An AutoProbe CP Atomic Force Microscope (AFM, Park Scientific Instruments, APEM-1000) was calibrated to  $\pm 0.001$   $\mu$  accuracy and used to obtain all post-exposure film thicknesses and line widths.

### 3.3 Calix[6]arene Synthesis

#### 3.3.1 Preparation of Compound A

A flame-dried 3 liter three neck, roundbottom flask was equipped with a mechanical overhead stirring unit, Dean-Stark trap, heating mantle, and condenser. 100.0 g (0.666 mol) of 4-*tert*-butylphenol and 40.0 g of paraformaldehyde were added to the roundbottom, along with 1.5 liters of xylene. 26.65 mL of rubidium hydroxide (.2363 mol) in a 50% weight aqueous solution was then added to the mixture using a 25 mL volumetric pipette and adjustable micropipettes. The Dean-Stark trap was then filled with xylene and the system was allowed to reflux for 24 hours under an argon atmosphere. During the reaction, the mixture appeared as a clear yellow liquid and gradually changed to a tan color as the reaction came to completion.

The reaction was allowed to cool and the product was filtered through a large Buchner funnel which left a cake of material that resembled clay. The cake was broken up into two portions and worked up in the following manner. The half cake was transferred to a 2 liter separatory funnel and dissolved in 1 liter of chloroform. This mixture was then washed three times with 1 liter of 2 M HCl. The severe emulsions that were encountered during the washes were stirred with a glass rod and allowed to settle. Back extractions were also performed on the aqueous washes using chloroform. All organic washes and back extractions were recombined and dried with MgSO<sub>4</sub>. The solvent was reduced to 200 mL and the product was precipitated with CH<sub>3</sub>OH. The product was a fine white powder and was filtered, dried, and weighed. The yield was 85 g (79%) and the

melting point was 379-380 °C.  $^1\text{H}$  NMR (400 MHz,  $\text{CDCl}_3$ , 25 °C)  $\delta$ =10.2 (s, ArOH, 12H) 7.10 (s, ArH, 12H), 3.88 (s, ArCH<sub>2</sub>Ar, 12H), 1.25 (s, C(CH<sub>3</sub>)<sub>3</sub>, 54H).  $^{13}\text{C}$  NMR (400 MHz,  $\text{CDCl}_3$ )  $\delta$ =147.2, 144.2, 126.9, 126.1, 34.0, 33.1, 31.4.

### 3.3.2 Preparation of Compound B

A flame-dried 2 L two-neck round bottom was equipped with an overhead stirring apparatus. To this vessel, 51.3 g of compound A (0.053 mol) and 46.4 g of phenol (0.493 mol) were added, along with 1.75 L of toluene. 84.95 g of  $\text{AlCl}_3$  was added in portions as the mixture was allowed to stir. The mixture was then allowed to react for 48 hours under an argon atmosphere.

The mixture was transferred to a 2 L separatory funnel and was quenched with three times with 2 M HCl. Back extractions were performed on the aqueous layer with chloroform. The organic layer was separated and the toluene was removed under reduced pressure. The residue was combined with the chloroform back extract and 1 L of chloroform was added to completely redissolve the product. This organic solution was then dried over  $\text{MgSO}_4$  and filtered. The solvent was then evaporated under reduced pressure to a minimum volume and was precipitated in 500 mL of  $\text{CH}_3\text{OH}$ . The precipitate was filtered, dried, and found to have a mass of 28 g (85%) and mp of 417-418 °C.  $^1\text{H}$  NMR (400 MHz,  $\text{CDCl}_3$ , 25 °C)  $\delta$ = 10.4 (s, ArOH, 6H), 6.7-7.4 (m, ArH, 16H), 4.0 (s, ArCH<sub>2</sub>Ar, 12H).

### 3.3.3 Preparation of Compound C

To a flame-dried 1 L round bottom flask equipped with a magnetic stir bar, 10.0 g of compound B (0.0157 mol) and 14.07 g of potassium trimethylsilanoate (0.110 mol) were placed. To the flask, 450 mL of THF and 50 mL of DMF were added. After the solution was allowed to stir for 15 minutes in a 0 °C ice bath, 4.07 mL of allyl bromide (0.0471 mole) was added and the mixture was allowed to stir for 20 hours. The reaction solvents were removed under reduced pressure, using a water aspirator to draw off most of the THF and then switching to a mechanical pump to remove the remaining DMF solvent. The residue was taken up in 500 mL of chloroform and washed three times with equal volumes of 2 M HCl (500 mL). All aqueous portions were collected and back extracted using 250 mL of chloroform. The organic portions (chloroform) were then collected and dried with MgSO<sub>4</sub> and filtered with a Buchner funnel. The solvent was then reduced to a minimal volume and then added to 500 mL of hexane. The fine white precipitate was collected with a Buchner funnel and was allowed to dry and then weighed to give 10 g of product (88% yield) with a mp of 188-190 °C. <sup>1</sup>H NMR (400 MHz, CDCl<sub>3</sub>, 25 °C) δ= 8.03 (s, -OH, 4H), 7.09-6.89 (m, ArH, 14H), 6.76 (t, ArH, 4H, J= 6.0 Hz), 5.95 (m, -CH=, 2H), 5.40 (d, =CH<sub>2</sub>, 2H, J= 20.0 Hz), 5.08 (d, =CH<sub>2</sub>, 2H, J= 12.0 Hz), 4.46 (d, -OCH<sub>2</sub>-, 4H, J= 6.0 Hz), 3.94 and 3.78 (two s, ArCH<sub>2</sub>Ar, 12H). <sup>13</sup>C NMR (100 MHz, CHCl<sub>3</sub>) δ= 162.5, 152.4, 151.8, 133.2, 131.8, 129.1, 128.9, 128.7, 127.5, 127.1, 125.5, 120.2 and 118.5 (Ar and -CH=CH<sub>2</sub>), 75.9 (-OCH<sub>2</sub>-), 36.4 and 31.5 (ArCH<sub>2</sub>Ar).

### 3.3.4 Preparation of Diallyloxy-bis-*m*-xylenyloxycalix[6]arene (1,2,3-Alternate Isomer, 1)

In a flame-dried 1 L round-bottom flask 3.00 g (4.18 mmol) of (C) was dissolved in 400 mL of dry THF along with 40 mL of DMF. A 60% sodium hydride (NaH) dispersion in mineral oil was added in the amount of 1.53 g and allowed to stir at room temperature for 30 minutes before 4.08 g (15.46 mmol) of  $\alpha,\alpha'$ -dibromo-*m*-xylene was added. The solution was refluxed for 24 hours under an argon atmosphere. The solvent was then removed under reduced pressure. The residue was redissolved in  $\text{CHCl}_3$  (1L) and washed 3 times with 150 mL of 2 M HCl and then dried over  $\text{MgSO}_4$ . The solution was filtered with a Buchner funnel and the solvent was evaporated under reduced pressure. The crude material was then purified by gravity column chromatography on silica gel with a solvent mixture of 86%  $\text{CHCl}_3$ /14% hexane with the  $R_f=0.85$ . The reaction yielded 50% of Compound 1 (1.2 g). mp = 261-263°C  $^1\text{H}$  NMR (400 MHz,  $\text{CDCl}_3$ , 25 °C)  $\delta$ = 7.39 (s, 2H), 7.19 (d of d, 8H), 7.13 (t, J= 7.6 Hz), 7.06 (t, 4H, J= 7.6 Hz), 6.80 (d, 4H, J= 7.6Hz), 6.06 (d, 4H, J= 7.6 Hz), 5.76 (t, 2H, J= 6.4 Hz), 5.73 (m, 2H), 4.45 (m, 4H), 4.39 (d, 4H, J= 12.8 Hz), 4.33 (d, 4H, J= 12.8 Hz), 4.25 (d, 4H, J= 15.2 Hz), 4.01 (s, 4H), 3.99 (d, 4H, J= 2 Hz), 3.21 (d, 4H, J= 15.2 Hz).  $^{13}\text{C}$  NMR (100 MHz,  $\text{CDCl}_3$ )  $\delta$ = 157.22, 153.62, 139.21, 136.32, 135.44, 134.30, 133.52, 130.74, 129.62, 126.46, 126.00, 124.69, 123.39, 123.19, 122.59, 115.54, 74.34, 73.49, 31.38, 30.86.

### 3.3.5 Preparation of Diallyloxy-bis-*m*-xylenyloxycalix[6]arene (Cone Isomer, 2)

In a 1 L round-bottom flask, 5.0 g (5.43 mmol) of compound C was dissolved in 500 mL of CH<sub>3</sub>CN.  $\alpha,\alpha'$ -dibromo-*m*-xylene was added to the solution in the amount of 4.37g (16.6 mmol) along with 13.49 g (41.4 mmol) of Cs<sub>2</sub>CO<sub>3</sub>. The solution was heated to reflux for 12 h under an argon atmosphere. The completed reaction was cooled and the solvent was removed under reduced pressure. The residue was dissolved in CHCl<sub>3</sub> (400mL) and washed 3 X 150 mL of 2M HCl then dried over MgSO<sub>4</sub>. The solution was filtered and the solvent was evaporated under reduced pressure to yield a crude product. The crude product was purified via column chromatography using silica gel. (99% CHCl<sub>3</sub> and 1% Ethyl Acetate) Compound 2 yielded 55%. <sup>1</sup>H NMR (400 MHz, CDCl<sub>3</sub>, 25 °C)  $\delta$ = 7.401 (d of d, 2H, J= 8.8 Hz), 7.396 (d of d, 2H, J= 8.8 Hz), 7.184 (M, 8H), 7.050 (t, 2H, J= 14.8 Hz), 6.948 (d, 4H, J= 7.2 Hz), 6.555 (t, 2H, J= 15.6 Hz), 6.226 (d, 4H, J= 8.0 Hz), 5.853 (M, 2H), 5.465 (s, 2H), 5.139 (d of d, 2 H, J= 14 Hz), 4.215 (d, 8H, J=16 Hz), 4.063 (d of d, 4H, J= 1.2 Hz), 3.566 (d, 2H, J=14.4Hz), 3.443 (d, 4H, J=14.2 Hz). <sup>13</sup>C NMR (100MHz, CDCl<sub>3</sub>, 25 °C)  $\delta$ = 156.4, 155.2, 137.0, 134.6, 134.0, 133.2, 130.2, 130.9, 129.9, 127.4, 125.7, 123.8, 115.5, 75.5, 71.3, 31.4, 28.8.

### 3.4 Formulation of Calixarene Resists

#### 3.4.1 General Formulation Protocol

For the creation of all calixarene resists, HPLC-grade chlorobenzene was used as the solvent, **1** or **2** was used as the monomer, and recrystallized benzoyl peroxide (BPO, if used) was included as the initiator. All formulations were created in tared glass sample vials on an analytical balance by first measuring the amount of **1** or **2** needed to make the desired solution concentration. The BPO (if used) was then measured into the vial containing **1** or **2**. The formulation was completed by weighing in the necessary amount of solvent using a graduated pipette equipped with a three-way bulb.

The solids were dissolved completely with intermittent stirring and heat and then capped, with extra care not to allow the vial to invert. Heating was done with warm water if BPO was in the formulation (to avoid an explosion hazard). If particulate contamination was observed in the solution, the solutions were drawn up into a *glass syringe* and then redispensed into a new vial using a 0.20  $\mu$  PTFE syringe filter. All samples were labeled with the compound, weight percentage, and formulation date.

#### 3.4.2 Calculation of Formulation Masses

All formulations were based on the weight percentage of the monomer to the solvent (w/w). A sample calculation is provided to demonstrate how to determine the amounts of all components that are necessary to formulate a volume of calixarene resist with the desired weight percentage.

Calculation of the mass of calixarene needed to make 18 mL of a 1.0 wt % (1)

resist:

$$\rho_{\text{chlorobenzene}} = 1.107 \text{ g/mL}$$

$$18 \text{ mL} \times 1.107 \text{ g/mL} = 19.93 \text{ g of Chlorobenzene needed}$$

Let  $x$  = the mass of **1** required to make a 1.0 wt % resist:

$$0.01 = x/(x + 19.93)$$

$$x = 0.2013 \text{ g of } \mathbf{1}$$

Thus, in order to make a 1.0 wt % resist of **1**, a 30 mL glass vial was tared, after which 0.2013 g of **1** was quantitatively added. 19.93 g of chlorobenzene was added with a pipette, and the contents were promptly dissolved, capped, and labeled.

### 3.4.3 Formulation of Resists containing BPO

All experiments that involved BPO were formulated at 1.0 wt % of the active monomer (**1** or **2**). Thus, for the preceding calculation, precisely 0.0020 g of BPO was added after **1** was weighed into the mixture (i.e., 1.0% of 0.2013 g of **1**). The solvent was added, the mixture was dissolved and labeled.

## 3.5 Spin-Coating the Calixarene Resists

### 3.5.1 Processing Cleanliness

All work was completed with the utmost care and available methods to achieve process cleanliness in order to avoid *particulate contamination* of the wafers during the coating process. Both the syringe and the coater unit were

pre-rinsed with chlorobenzene. Syringe filters (0.20  $\mu$  PTFE) were utilized in a “point of use” method; that is, the filter is used *each time the resist is being directly applied to the wafer using the syringe*. All resist applications were conducted under a “high efficiency, particulate attenuated” (HEPA filtered) environment and care was taken not to breathe on the samples. In order to prevent contact with the substrate, tweezers were used *each time the wafer was processed or transferred*.

### **3.5.2 Spin-Coating Protocol and Soft Bake Parameters**

For all coating experiments, the resist was dynamically dispensed, with the coater programmed to accelerate rapidly to the final desired spin speed. For all resist applications, a *glass syringe* was utilized to dispense exactly 3.0 mL of formulated resist on a 4” silicon wafer. For each total spin time, the coating unit was programmed to run for 60 seconds. All post-spin (soft) bakes were done immediately following wafer coat on a hotplate at 170 °C for 120 seconds.

### **3.5.3 Dynamic Dispense Procedure**

A clean wafer was centered upon the spin coating unit. In a pre-rinsed 50 mL glass syringe, 3 mL of calixarene resist was drawn up from the glass vial using a large bore syringe needle. The needle was removed and a syringe filter was attached, with care to keep the filtered end of the syringe *up* until the resist was applied. To achieve dynamic dispense of the resist, the spin on the coating unit was initiated and the resist was *immediately* applied, with the syringe

perpendicular to the spinning wafer. The spin speed of the coater was rapidly accelerated to the final desired speed (1000 to 6000 rpm). Color changes were observed on the spinning wafer as the spinner unit ramped to final spin speed and the excess resist was centrifugally removed. The spinner was run for exactly 60 seconds, upon which the coated wafer came to a rest. Immediately following wafer coat, the substrate was transferred to the hotplate using tweezers and baked at 170 °C for 120 seconds. The wafer was allowed to cool and then stored in a covered, dry wafer box.

### **3.6 Characterization of Optical Parameters of 1 and 2 Using 3-Angle Null Ellipsometry**

#### **3.6.1 Determination of Exact Ellipsometric Measurement Angles**

Using an AMD standard (with known Si/SiO<sub>2</sub> thicknesses), the thickness of the native silicon dioxide on a bare wafer (no calixarene coat) was determined as follows. Ellipsometric data was collected on the standard at three approximate angles of incidence (30°, 50°, 70°). The ellipsometric data for all three approximate angles of the Si/SiO<sub>2</sub> standard were analyzed using FilmWizard software from SCl (version 6.4.3). “Best fit” calculations were done using a modified Marquardt-Levenberg computer algorithm<sup>47</sup> to give the *exact angles of incidence*. For all subsequent ellipsometric experiments, the precise incident angles were determined in this manner to collect data for the determination of the optical properties and thicknesses of spin-coated thin films of **1** and **2**.

### 3.6.2 Determination of the Native SiO<sub>2</sub> Thickness of an Uncoated Wafer

In order to determine the native oxide thickness on the wafers, ellipsometric data was collected at three different positions for the Si/SiO<sub>2</sub> standard. A *bare silicon wafer* (unknown) was then measured at three positions and all data for the standard and the unknown were fit using FilmWizard software. The thickness of the native oxide on the bare wafer was determined and a complex, three-layer model was created (Si/SiO<sub>2</sub>/Calixarene) for calixarene samples. For all subsequent ellipsometric measurements of **1** and **2**, the three-layer (best-fit) model was used, and the pre-determined native oxide thickness was assumed.

### 3.6.3 Determination of Indices of Refraction and Extinction Coefficients of **1** and **2**

The following procedure was used to obtain the respective indices of refraction ( $n$ ) and extinction coefficients ( $k$ ) of **1** and **2** at a wavelength of 632.8 nm. For **1**, a 1.0 wt% sample was spun at 3000 rpm and baked for 120 seconds at 170 °C on a bare silicon wafer. Ellipsometric data was then collected about 1 inch from the edge of the sample at three precisely determined angles of incidence. The data was then fit using the FilmWizard SCI software, using the corrected three-layer (Si/SiO<sub>2</sub>/Calixarene) model, and the index of refraction ( $n_1$ ) and extinction coefficient ( $k_1$ ) of **1** were determined. This procedure was repeated using the same coating conditions to find the optical properties of **2** ( $n_2$  and  $k_2$ ).

### 3.6.4 Determination of Resist Film Thickness and Uniformity

The effects of resist concentration of **1** on calixarene film thickness and uniformity of the resist coating *across the wafer* were determined. Four samples (at concentrations of 0.5, 1.0, 1.5, and 5.0 wt%) were formulated and spin coated on separate wafers. For each concentration, 3 mL of resist was dynamically spin coated at 3000 rpm, followed by a 120 second soft bake at 170 °C. At an angle of 69.774°, ellipsometric data was collected at *three* points on the wafer for each respective sample: The wafer center; 1" from the wafer edge; 0.5" from the wafer edge. The SCI program was then used to calculate the thickness of the calixarene films at each measurement point for the respective samples.

### 3.6.5 Stylus Profilometry

Film thickness and uniformity of the 1.5 wt% sample were studied with a stylus profilometer. Using metal tweezers, the coated sample was scratched radially from the wafer center to the wafer edge. For this sample, the step height of the scratch was then measured at ten different positions on the radial scratch.

### 3.6.6 Data Acquisition for Spin Speed Curves

In order to gather data for spin curves, four sets of samples were created and spun (0.5 wt% and a 1.0 wt% formulation of **1** and **2**). Each respective formulation was spun at six different speeds and the resultant thicknesses were measured by ellipsometry. For example, to create a data set for the 0.5 wt% formulation of **1**, the dynamic dispense procedure was performed at six spin

speeds (1000 rpm, 2000 rpm, 3000 rpm, 4000 rpm, 5000 rpm, 6000 rpm) on separate wafers. This yielded six wafers that contained thin films (of 0.5 wt% **1**) with different thicknesses. This procedure was repeated for the other three formulations. The Null Ellipsometer was used to measure the thicknesses of each wafer for each of the four formulation sets in order to gather data for spin speed curves.

### **3.6.7 Remeasurement of Film Thickness of **1****

In addition, the film thickness of the 0.5 and 1.0 wt% formulations of **1** were remeasured with the ellipsometer. The same wafers that had been used to create the spin curves were analyzed a month later to monitor film growth over time. Only the samples spun at higher speeds (thinner films) were remeasured for both weight percent formulations of **1**.

### 3.7 Electron Beam Exposure of the Resists

#### 3.7.1 Sample Preparation

To prepare the samples for all subsequent experiments (exposure and resist sensitivity/contrast), the calixarene-coated wafers were cut into approximately 1X1 inch samples using a wafer cleaving tool. The coated wafer was placed face down on a flat surface on top of a large ChemWipe. A metal ruler was laid on the back of the wafer *at a 45° angle to the major flat of the wafer* (Figure 3.7.1.1). This was done in order to cut *along the crystal axis* of the wafer and create samples with clean, straight edges.

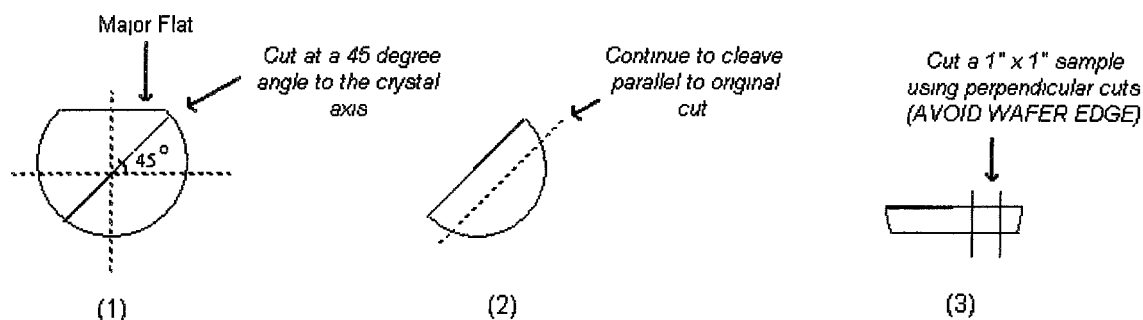


**Figure 3.7.1.1** Sample preparation of a 4" coated wafer (along sample back)

Using the straight edge of the ruler as a guide, the tip of the cleaving tool was then traced repeatedly across the back of the sample until the wafer was cut. This procedure was repeated to shape a wedge, and cuts were then made at a 90° angle to the original cut in order to shape a 1X1" square sample.

A grid was then created on the front (calixarene-coated) part of the wafer by gently laying a metal ruler across the square sample and then scoring two parallel lines. *Care was taken not to touch the active area of the sample with the ruler as the grid was created.* Perpendicular lines were then scored without a ruler. Grids that were created for each sample contained grid boxes that were approximately 1 mm by 2 mm (Figure 3.7.1.2). The sample was then blown of any particulate matter using clean N<sub>2</sub>.

*Scored Grid through Resist  
Into the substrate  
(Boxes are 1 mm x 2 mm)*

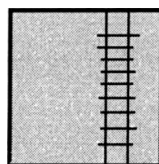


**Figure 3.7.1.2** Creation of grid on the front of a 1"x1" resist-covered wafer

### 3.7.2 Sensitivity/Contrast Exposures

Four samples were created for exposure experiments. For non-BPO experiments, two samples at 7.0 wt% film of **1** and **2** were individually created by dynamically spinning 3 mL of resist onto a bare silicon wafer, followed by a 120 second soft bake at 170 °C on the hotplate. The samples were cleaved and a grid was scored into the sample to mark the active exposure region into *16 boxed (1 mm x 2 mm) areas*. The samples were then exposed with the SEM at a nominal beam current of 6 nA at an acceleration voltage of 20 kV.

In order to generate data for sensitivity and contrast analysis, a *box and a corresponding line* were created in each of the first 15 grid areas. This was done by exposing the resist at 15 different durations for each box and line feature (10 s, 20s, 30 s, 40 s, 50 s, 60 s, 70 s, 80 s, 90 s, 100 s, 110 s, 120 s, 130 s, 140 s, 150 s), as depicted in Figure 3.7.2.

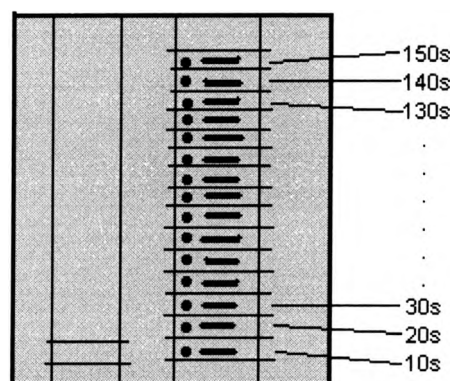


**Figure 3.7.2** Exposure Features (boxes and lines) at their corresponding times

For example, in grid space 1, a *box* was created by exposing the resist for 1 second, and then scanning a 1 second *line* adjacent to the box to complete to “1 second” trial. This procedure was repeated until a series of boxes and lines were created for each of the 15 grid spaces to create the test battery for **1**. This procedure was also repeated for **2**.

In addition, two separate samples were formulated at 7.0 wt% **1** and **2** with BPO initiator (formulated at 1.0 wt% BPO (w/w) of **1** and **2** respectively). These samples were also exposed in the manner described above. For all of the above trials, a picoammeter was used to determine the precise beam current of the exposure tool at the beginning, middle, and end of each exposure trial.

### 3.7.3 High Resolution Exposure and Beam Current Measurement

On all four samples (1, 2, 1 at 1.0 wt% BPO, and 2 at 1.0 wt% BPO), a series of features were created to determine the resolution capabilities of each sample in the sixteenth grid area. For all experiments, the acceleration voltage was left at 20 kV, but the *beam current was lowered and timed* to create lines of various widths for measurement. For example, for sample 1, a marker box was created by exposing the resist at a nominal beam current of 6 nA. Three sets of lines were then exposed at different beam currents in a series, as shown in Figure 3.7.3

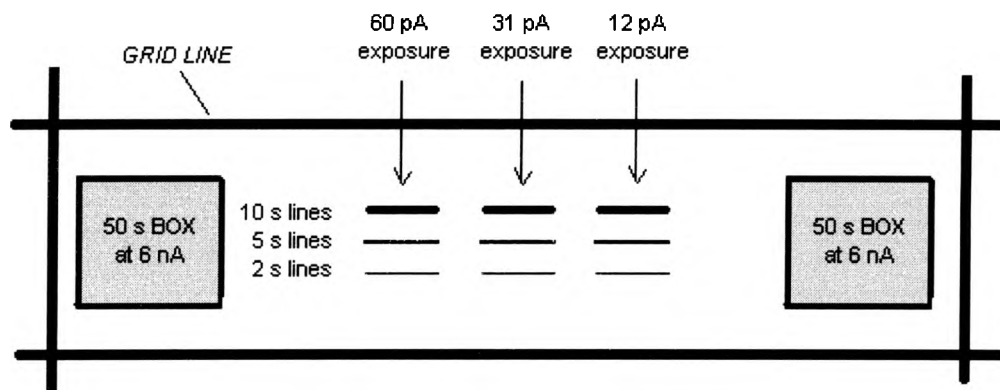


**Figure 3.7.3** Experimental setup for the creation of high resolution lines

For each line set of lines, the beam current was measured before and after the three line series to give average beam currents of 60 pA, 31 pA, and 12 pA. Another marker box was created to complete the experiment for sample 1. This procedure was then repeated for the other three samples (2, 1 at 1.0 wt% BPO, and 2 at 1.0 wt% BPO). Note: only the sample prepared for 2 was analyzed for the high resolution line.

### **3.7.4 Develop and Pattern Inspection**

All samples were developed by dipping in xylene for 30 seconds, followed by a 30 second rinse with isopropyl alcohol (IPA), then a blow dry with clean nitrogen. To assure that the exposures had successfully created features within the grid, the developed samples were visually inspected with an optical microscope. All four samples were labeled accordingly for characterization measurements with the atomic force microscope (AFM).

## **3.8 Characterization of Resist Sensitivity and Contrast using the AFM**

### **3.8.1 Atomic Force Microscopy**

The AutoProbe CP AFM was calibrated to measure  $\pm 0.001 \mu\text{m}$  for all measurements. All four samples were scanned to obtain images of the developed features. All scans were saved in order to measure dimensions of the features.

### **3.8.2 Determination of Post-Exposure Resist Thickness**

To characterize the contrast of each sample as a function of applied electron dose, the *step height of the boxes* in each grid were measured. Snapshots of each feature were used to measure the effective length, width, and height of the boxes.

### **3.8.3 Measurement of High Resolution Linewidths**

Measurement of the high resolution lines was also achieved by the AFM. For sample 2, the high resolution line features (from section 3.7.3) were scanned and saved. The width of each line was then measured at different positions on the line to obtain an average linewidth for each high resolution experiment.

### **3.8.3 Sample Visualization with the SEM**

In order to visualize the samples on the SEM, the samples were sputtered with a 15 nm coat of metal (AuPd coat) using the Hummer X triode magnetron sputtering system. The samples were then loaded and images were obtained for the high resolution lines.

## 4.0 RESULTS

### 4.1 Ellipsometric and Profilometric Characterization of Calix[6]arene Thin Films

#### 4.1.1 Determination of the Native SiO<sub>2</sub> Thickness of an Uncoated Wafer

The thickness of the native oxide coat on a “bare” silicon wafer was measured by using known data ( $n_{\text{SiO}_2}$  and thickness  $t$ ) from the AMD Si/SiO<sub>2</sub> standard. Null ellipsometric measurements were done at three different positions on the wafer to obtain the data shown in Table 4.1.1.1.

Angle (degrees)	P1	A1		P2	A2		$\Delta$	$\Psi$	remarks	#
69.822	48.1	11.2		138.3	169.4		173.6	10.9	1" from center	1
69.6982	48.3	11.5		138.1	169.3		173.6	11.1	0.5" from center	2
69.6973	48	11.5		138.3	169.3		173.7	11.1	Wafer center	3

**Table 4.1.1.1** Raw data for the determination of native oxide thickness

The exact angles of these measurements were determined by using the FilmWizard software, which calculates the best fit of the data using a Marquardt-Levenberg algorithm.<sup>46</sup> The same software was used to calculate the thickness of the oxide at each respective angle to give the results shown in Table 4.1.1.2.

Measurement	Angle of Incidence.	Thickness	RMSE
1	69.822	2.0319 nm	$13 \cdot 10^{-10}$
2	69.6982	2.0788 nm	$30 \cdot 10^{-11}$
3	69.6973	2.0422 nm	$18 \cdot 10^{-13}$

**Table 4.1.1.2** Native oxide thickness for three different positions

These measurements give an average native oxide thickness of 2.05 nm, a parameter that was then fit to analyze the thickness of all calixarene films. Note that *RMSE* is the “root mean square error” and indicates how well data fits to the model; a lower *RMSE* indicates a better fit.

#### 4.1.2 Ellipsometric Determination of $n$ and $k$ of **1** ( $n_1$ and $k_1$ )

In order to determine the optical properties of the calixarene material, a sample of 1.0 wt% **1** was spun at 3000 rpm. The sample was baked on a hotplate for 2 minutes at 170 °C. The sample was then measured on the ellipsometer at three angles, along with the Si/SiO<sub>2</sub> standard. The data for **1** is shown below.

Calculated	P1	A1	I1	P2	A2	I2	$\Delta$	$\Psi$	remarks
Angle (degrees)									
69.8183	57.9	12.0	<20	148.1	168.7	<25	154	11.65	Si/SiO <sub>2</sub>
69.8183	73.0	15.6	22.5	163.6	165.7	<25	123.4	14.95	Calixarene <b>1</b>
49.5228	52.3	32.2	<20	142.5	148.8	<30	165.2	31.7	Calixarene <b>1</b>
49.5228	48.0	32.3	<20	137.8	148.6	25	174.2	31.85	Si/SiO <sub>2</sub>
29.5304	45.5	41.3	<20	135.8	139.6	22.5	178.7	40.85	Si/SiO <sub>2</sub>
29.5304	47.5	41.0	<20	137.2	139.5	24	175.3	40.75	Calixarene <b>1</b>

**Table 4.1.2.1** Raw Ellipsometric Data for the determination of  $n$  and  $k$  of **1**

The Si/SiO<sub>2</sub> standard was used to determine the exact angles of incidence for each measurement using the FilmWizard software. Assuming a native oxide coat of 2.05 nm, the data was fit into the three-layer model and the optical properties of **1** were determined, along with the sample thickness.

Property	Based on measurements at all three angles
$n_f$	$1.56 \pm 0.01$
$k_f$	$62 * 10^{-9}$
thickness (t)	20.9 nm
RMSE	0.39

**Table 4.1.2.2** Optical constants of **1** (assuming 2.05 nm thick native oxide layer)

#### 4.1.3 Comparative Thickness Measurement Using Stylus Profilometry

The thickness of this sample was also measured with the stylus profilometer. By creating a radial scratch and then measuring the step height along the scratch at different locations, a *calixarene film thickness of 14-18 nm was found.*

#### 4.1.4 Measurement on Wt% Series of Films for **1**

The variation in film thickness for the above sample was noted, as well as the slight discrepancy between ellipsometric and profilometric measurements. In order to obtain an idea of how film thickness will vary with the formulation weight percentage of **1**, four samples at different weight percentages were created for measurement, shown in Table 4.1.4.1.

Sample	wt%	Spin speed	Quantity of resist	Hot Plate
Cal-0.5	0.5 %	3000 rpm	3 mL	2 min
Cal-1.0	1.0 %	3000 rpm	3 mL	2 min
Cal-1.5	1.5 %	3000 rpm	3 mL	2 min
Cal-5.0	5.0 %	3000 rpm	3 mL	2 min

**Table 4.1.4.1** Samples of 1 for weight percent

The spin time for all samples was 60 seconds and the bake temperature was 170 °C. The raw ellipsometric data for all weight percent samples is given in the tables below. Each sample was measured at three to four different locations.

Angle	P1	A1	I1	P2	A2	I2	$\Delta$	$\Psi$	location
69.774	62.6	12.7	15	152.9	168.8	20	144.5	11.95	Center
69.774	59.2	112.4	17	150.6	168.2	20	150.2	12.1	0.5" from edge
69.774	60.8	12.8	18	150.6	168	25	148.6	12.4	1" from edge
69.774	60.9	13.0	18	150.6	168.1	22	148.5	12.45	2" from edge

**Table 4.1.4.2** Cal-0.5 (0.5 wt % 1) raw data

Angle	P1	A1	I1	P2	A2	I2	$\Delta$	$\Psi$	location
69.774	70.9	14.9	20	161.3	166.5	23	127.8	14.2	Center
69.774	67.3	14.8	18	160.3	166.7	18	132.4	14.05	1" from edge
69.774	68	14.5	17	159.7	166.9	18	132.3	13.8	0.5" from edge

**Table 4.1.4.3** Cal-1.0 (1.0 wt % 1) raw data

Angle	P1	A1	I1	P2	A2	I2	$\Delta$	$\Psi$	location
69.774	71.2	14.8	18	161.9	161.4	20	126.9	16.7	center
69.774	68.4	14.2	22	159.1	167.3	25	132.5	13.45	1" from edge
69.774	70.3	14.5	21	160.9	167	25	128.8	13.75	0.5" from edge
69.774	70.8	14.9	20	161.15	161.6		128.05	16.65	New Center

**Table 4.1.4.4** Cal-1.5 (1.5 wt %) raw data

Angle	P1	A1	I1	P2	A2	I2	$\Delta$	$\Psi$	remarks
69.774	99	36.3	<25	189.4	146.6	<25	71.6	34.85	See picture for position

**Table 4.1.4.5** Cal-5.0 (5.0 wt %) raw data

The SCI program was used to calculate the thickness of for each sample at each measured location. Calculations were based on the assumption of a 2.05 nm thick native oxide film. The results are summarized below in Table 4.1.4.6.

SAMPLE	POSITION	THICKNESS	RMSE
Cal-0.5 (0.5 wt% 1)	Center	10.58 nm	.312
Cal-0.5	Near Center	8.99 nm	.271
Cal-0.5	1" from edge	8.95 nm	.241
Cal-0.5	0.5" from edge	8.32 nm	.113
Cal-1.0 (1.0 wt% 1)	Center	18.38 nm	.107
Cal-1.0	1" from edge	16.07 nm	.241
Cal-1.0	0.5" from edge	16.10 nm	.057
Cal-1.5 (1.5 wt% 1)	Center	19.06 nm	1.54
Cal-1.5	1" from edge	15.98 nm	.170
Cal-1.5	0.5" from edge	17.85 nm	.318
Cal-5.0 (5.0 wt% 1)	Marked spot	81.11 nm	$16 \times 10^{-7}$

**Table 4.1.4.6** Summary of Ellipsometric Thicknesses of Various Wt% of 1

One can see that films made from higher wt% formulations (higher viscosities) will result in a range of film thicknesses, even when spun at the same conditions. In addition, for any one particular sample, there appeared to be a variation in film thickness (slight non-uniformity). Cal-5.0 (5.0 wt% 1), for example, had the thickest film and made the non-uniformity obvious from its colors. A picture of Cal-5.0 is shown in Figure 4.1.4, with an arrow indicating where the ellipsometric data was taken for this sample.

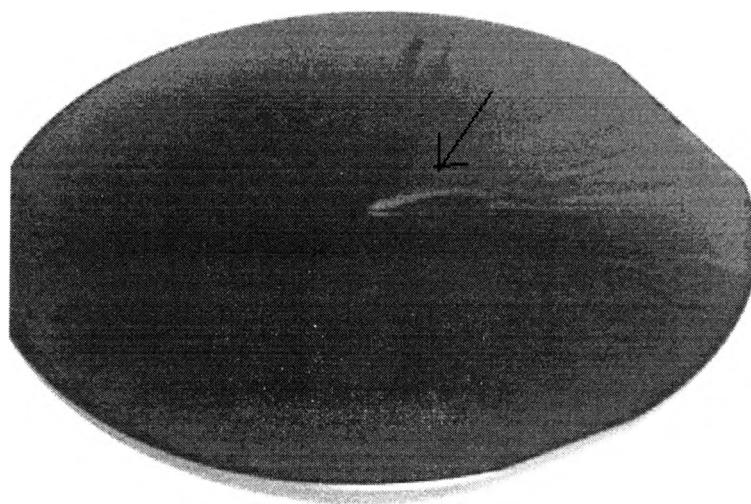


**Figure 4.1.4** Snapshot of Cal-5.0, showing the coloration (film thickness variation) of an 81 nm thick film of 1

#### **4.1.5 Comparative Analysis of Thickness by Profilometry**

In order to test the ellipsometric data from 4.1.4F, the three of the same samples were measured using the stylus profilometer. Scratches were made at several points on Cal-0.5, Cal-1.5, and Cal-5.0 and the step heights were measured at each point. The profilometric results are shown in Table 4.1.5, and

indicate a definite variation in film thickness for all three samples, as shown by the thickness ranges.

SAMPLE	Thickness Range
Cal-5.0	60-70 nm
Cal-1.5	10-16 nm
Cal-0.5	6-8 nm

**Table 4.1.5** Thickness ranges for 3 samples of 1 determined by profilometry

#### 4.1.6 Analysis of Film Thickness Variation for Cal-1.5 by Profilometry

In order to determine the uniformity of the resist, a radial scratch was made into the Cal-1.5 (1.5 wt% 1) sample from the center to the wafer edge. The step height was then measured at ten different positions along the scratch using the stylus profilometer. The results are summarized in Table 4.1.6 and a plot of the profile along the scratch is shown in Figure 4.1.6.

Position	Step Height [nm]
1: Edge	10 nm
2	11 nm
3	9.5 nm
4	11 nm
5	10 nm
6	15 nm
7	12 nm
8	14 nm
9	15 nm
10: Center	11 nm

**Table 4.1.6** Profilometer Results for Resist Thickness Across Cal-1.5 [From wafer edge (1) to wafer center (10)]

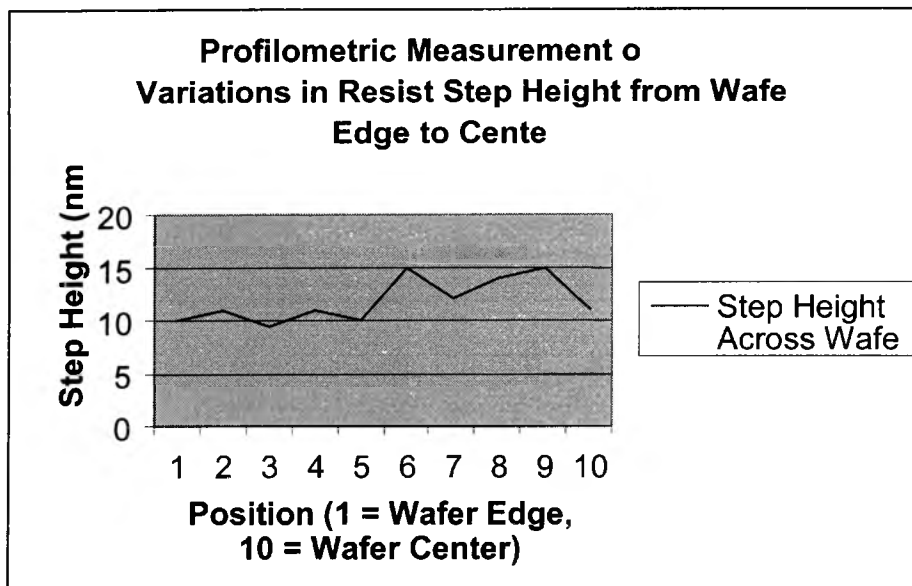


**Figure 4.1.6** Profilometric Cross-section of Resist Step Height for the edge of the wafer to the wafer center

As a brief summary, the optical properties of **1** were determined using ellipsometry. The index of refraction ( $n_1$ ) was determined to be  $1.56 \pm 0.01$ , while the extinction coefficient ( $k_1$ ) was  $62 \cdot 10^{-9}$ . These established optical constants allow the thickness of different films of **1** to be readily determined by ellipsometry. In addition, stylus profilometric analysis of resist thickness (step heights) showed fair agreement with the ellipsometric data for samples with different weight percentage formulations (0.5, 1.0, 1.5, and 5.0 wt%). Both stylus and ellipsometric analysis indicate a fair degree of non-uniformity of the resist film, with the thinner films (spun from lower weight percentages) having more uniform resist profiles.

## 4.2 Creation of Spin Speed Curves of 1 (at 0.5 and 1.0 wt%)

### 4.2.1 Preparation and Ellipsometric Measurement of Samples (0.5 wt% 1)

18 mL of a 0.5 wt % 1 was formulated. This sample was spun on different wafers, with each wafer having a spin speed ranging from 1000 to 6000 rpm (intervals differing by 1000 rpm). For each of the six trials, 3 mL of resist was applied and standard post-spin bake time and temperatures were used. Each of the six wafers of 1 were then analyzed with the null ellipsometer. In order to determine the average film thickness on the respective wafer, each wafer was measured at two points. The raw data for each wafer is shown in Table 4.2.1.

0.5 wt % 1 Series									
SPIN SPEED: 1000rpm									
Angle	P1	A1	I1	P2	A2	I2	$\Delta$	$\Psi$	Remarks
69.774	66.1	13.9	18	156.6	167.1	20	137.7	13.4	1" from wafer edge
69.774	66.8	14	15	158.4	168.5	16	134.8	12.75	1" from opposite edge
SPIN SPEED: 2000 pm									
Angle	P1	A1	I1	P2	A2	I2	$\Delta$	$\Psi$	Remarks
69.774	63.5	13.5	14	154.3	167.8	17	142.2	12.85	1" from wafer edge
69.774	63	13	15	153.8	168.1	16	143.2	12.45	1" from opposite edge
SPIN SPEED: 3000 pm									
Angle	P1	A1	I1	P2	A2	I2	$\Delta$	$\Psi$	Remarks
69.774	60.3	13.2	16	150.6	168.3	17	149.1	12.45	1" from wafer edge
69.774	60.2	12.7	16	150.8	168.2	16	149	12.25	1" from opposite edge

**Table 4.2.1** Raw Ellipsometric Data for Spin Curve Series of 0.5 wt% 1

SPIN SPEED: 4000 rpm									
Angle	P1	A1	I1	P2	A2	I2	$\Delta$	$\Psi$	Remarks
69.774	59.8	13.2	16	148.8	168.6	17	151.4	12.3	1" from wafer edge
69.774	59.3	13	15	149.6	168.5	16	151.1	12.25	1" from opposite edge
SPIN SPEED: 5000 rpm									
Angle	P1	A1	I1	P2	A2	I2	$\Delta$	$\Psi$	Remarks
69.774	58.1	12.4	15	149.2	168.8	16	152.7	11.8	1" from wafer edge
69.774	58	12.1	15	148.6	168.7	16	153.4	11.7	1" from opposite edge
SPIN SPEED: 6000 rpm									
Angle	P1	A1	I1	P2	A2	I2	$\Delta$	$\Psi$	Remarks
69.774	57.9	12.8	15	149.4	168.9	17	152.7	11.95	1" from wafer edge
69.774	58.6	12.7	16	149.1	168.9	18	152.3	11.9	1" from opposite edge

**Table 4.2.1** Ellipsometric Data for Spin Curve Series of 0.5 wt% 1 (Continued)

#### 4.2.2 Results and Spin Speed Curve for 0.5 wt% 1 (from 1000-6000 rpm)

For each wafer, the data was used to determine an average thickness of resist coating on each wafer using the SCI software from each combination of delta ( $\Delta$ ) and psi ( $\Psi$ ). The calculation of  $\Delta$  and  $\Psi$  and their physical significances was discussed in 4.0. For each wafer, the two calculated thickness values from opposite sides of the wafer were averaged. These calculations assumed a native oxide thickness of 2.05 nm. The numerical results, including the root mean square error (RMSE), are shown in Table 4.2.2. The resultant spin speed curve for 0.5 wt% 1 at six different speeds is shown in Figure 4.2.2

0.5 wt% 1 (Spun with 3 mL for 1 minute, baked 2 minutes on hotplate at 170 °C)					
Spin Speed [rpm]	Minimum Value [nm]	Maximum Value [nm]	Delta Thickness [nm]	RMSE	Average Thickness [nm]
1000	13.6009	14.6909	1.09	0.56	14.1459
2000	11.02455	11.45205	0.4275	0.44	11.2383
3000	8.67765	8.71115	0.0335	0.35	8.6944
4000	7.79605	7.90835	0.1123	0.4	7.8522
5000	7.0352	7.2974	0.2622	0.27	7.1663
6000	7.3006	7.449	0.1484	0.241	7.3748

**Table 4.2.2** Calculated average thicknesses for 0.5 wt%1 at 6 spin speeds

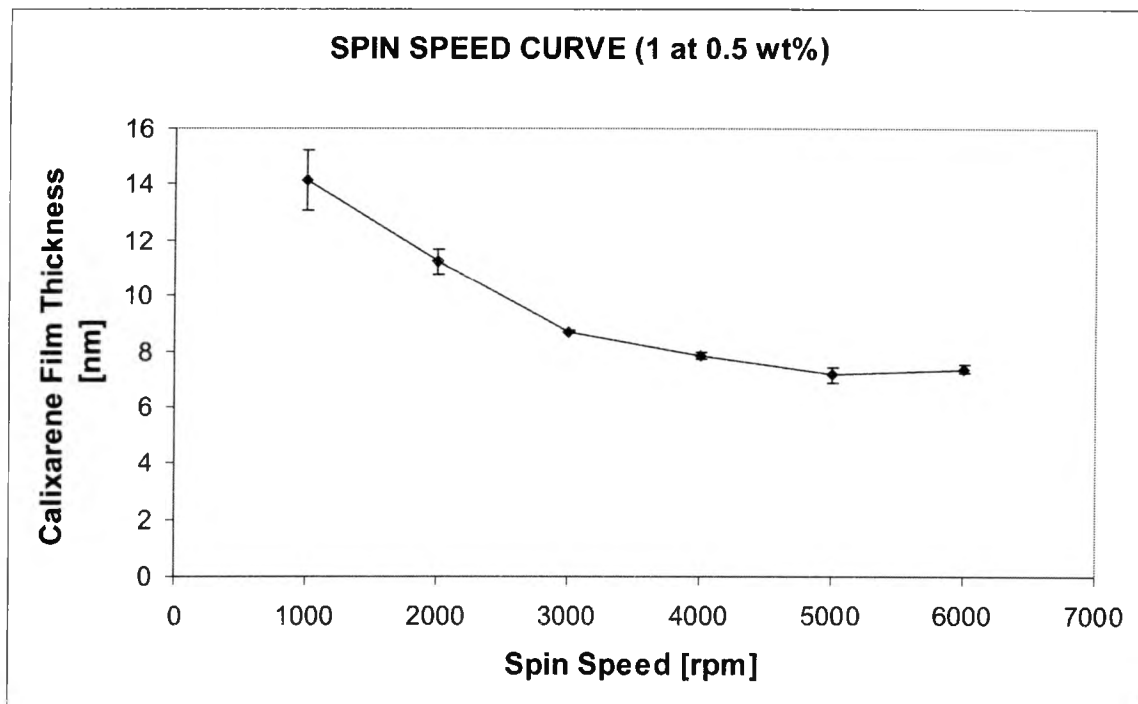


**Figure 4.2.2** Spin Speed Curve of 0.5 wt% Calixarene (1) Resist

#### 4.2.3 Preparation and Ellipsometric Measurement of Samples (1.0 wt% 1)

In precisely the same manner as for the 0.5 wt% 1 series, another series of wafer samples were created for an 18 mL volume of 1.0 wt% 1. All conditions for the 1.0 wt% series of spin speed experiments were performed as described for the 0.5 wt% series, as described in 4.2.1. Table 4.2.3 show the raw data.

1.0 wt % 1 Series									
SPIN SPEED: 1000rpm									
Angle	P1	A1	I1	P2	A2	I2	$\Delta$	$\Psi$	Remarks
69.774	81.9	19.8	16	173.1	162.6	14	105	18.6	1" from wafer edge
69.774	81	19.7	16	173.3	163	15	105.7	18.35	1" from opposite edge
SPIN SPEED: 2000 rpm									
Angle	P1	A1	I1	P2	A2	I2	$\Delta$	$\Psi$	Remarks
69.774	74.2	16.6	17	165.3	165	17	120.5	15.8	1" from wafer edge
69.774	74.3	15.9	17	165.6	165	16	120.1	15.45	1" from opposite edge
SPIN SPEED: 3000 rpm									
Angle	P1	A1	I1	P2	A2	I2	$\Delta$	$\Psi$	Remarks
69.774	68.3	14.6	15	160.3	166.4	16	131.4	14.1	1" from wafer edge
69.774	68.2	14.3	14	158.7	166.9	16	133.1	13.7	1" from opposite edge
SPIN SPEED: 4000 rpm									
Angle	P1	A1	I1	P2	A2	I2	$\Delta$	$\Psi$	Remarks
69.774	67.3	14.3	16	158.1	167.1	16	134.6	13.6	1" from wafer edge
69.774	68.5	13.9	16	158.2	167.8	16	133.3	13.05	1" from opposite edge

**Table 4.2.3** Raw Ellipsometric Data for Spin Curve Series of 1.0 wt% 1

SPIN SPEED: 5000 rpm									
Angle	P1	A1	I1	P2	A2	I2	$\Delta$	$\Psi$	Remarks
69.774	68.7	14	17	159.9	167.2	17	131.4	13.4	1" from wafer edge
69.774	68.8	14.1	16	159.6	166.8	16	131.6	13.65	1" from opposite edge
SPIN SPEED: 6000 rpm									
Angle	P1	A1	I1	P2	A2	I2	$\Delta$	$\Psi$	Remarks
69.774	69.1	14.7	16	160.8	166.9	16	130.1	13.9	1" from wafer edge
69.774	69	14.4	16	159.7	166.8	16	131.3	13.8	1" from opposite edge

**Table 4.2.3** Ellipsometric Data for Spin Curve Series of *1.0 wt% 1* (Continued)

#### 4.2.4 Results and Spin Speed Curve for *1.0 wt% 1* (from 1000-6000 rpm)

The average thickness of the resist coating for each wafer in the *1.0 wt% 1* series was also calculated from each combination of delta ( $\Delta$ ) and psi ( $\Psi$ ) with the SCI FilmWizard software. In the same manner as for the *0.5 wt% 1* series, the two calculated thickness values from opposite sides of the wafer were averaged. The numerical results, including the root mean square error (RMSE), are shown in Table 4.2.4. The resultant spin speed curve for *1.0 wt% 1* at six different speeds is shown in Figure 4.2.4

1.0 wt% 1 (Spun with 3 mL for 1 minute, baked 2 minutes on hotplate at 170 °C)					
Spin Speed [rpm]	Minimum Value [nm]	Maximum Value [nm]	Delta Thickness [nm]	RMSE	Average Thickness [nm]
1000	32.49695	33.08925	0.5923		32.7931
2000	22.2409	22.4385	0.1976	0.39	22.3397
3000	15.5607	16.3939	0.8332	0.6232	15.9773
4000	14.81215	15.38605	0.5739	0.4614	15.0991
5000	16.2223	16.3037	0.0814	0.0814	16.263
6000	16.38102	16.97198	0.59096	0.591	16.6765

**Table 4.2.4** Calculated average thicknesses for 1.0 wt% 1 at 6 spin speeds

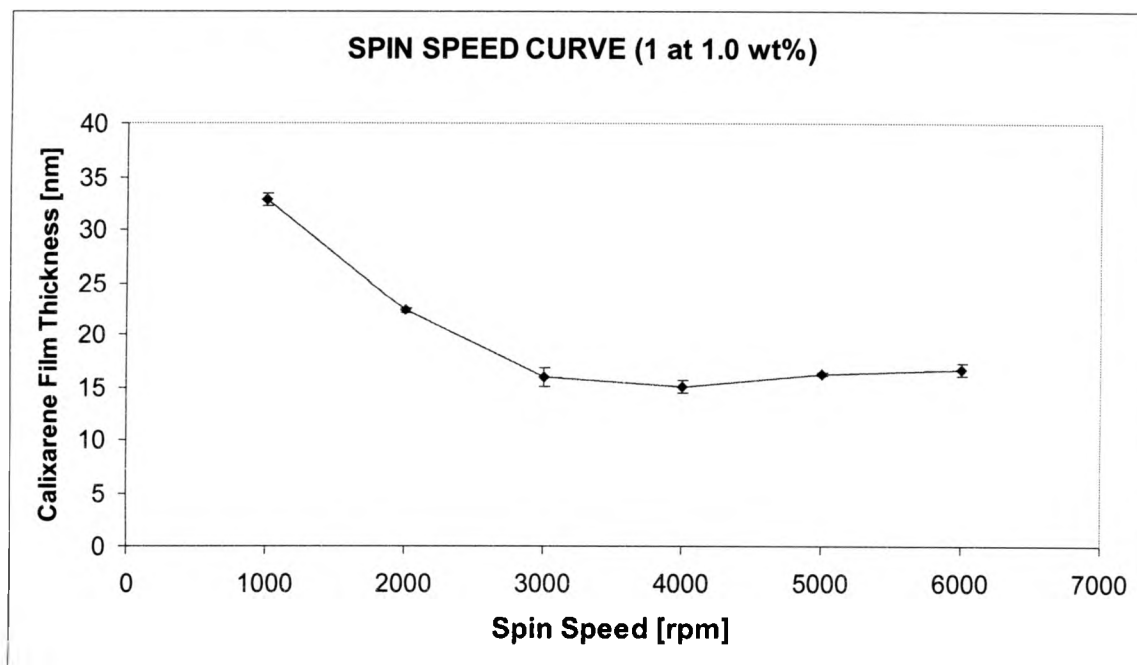


**Figure 4.2.4** Spin Speed Curve of 1.0 wt% Calixarene (1) Resist

#### 4.2.5 Summary of Spin Speed Curves for 1

Spin speed curves of 1 at 0.5 and 1.0 wt% formulations were created. These curves ascertain that indeed the thickness of a resist layer is dependant upon the volume of resist applied, the final spin speed, and the viscosity of the resist (which is determined by the weight percentage of the formulation).<sup>3</sup> For a given volume of resist and a given final spin speed, a *lower viscosity (lower weight percentage) will create a thinner resist coat*. These results are summarized in Figure 4.2.5 with a superimposed spin speed curve of 0.5 and 1.0 wt% 1.

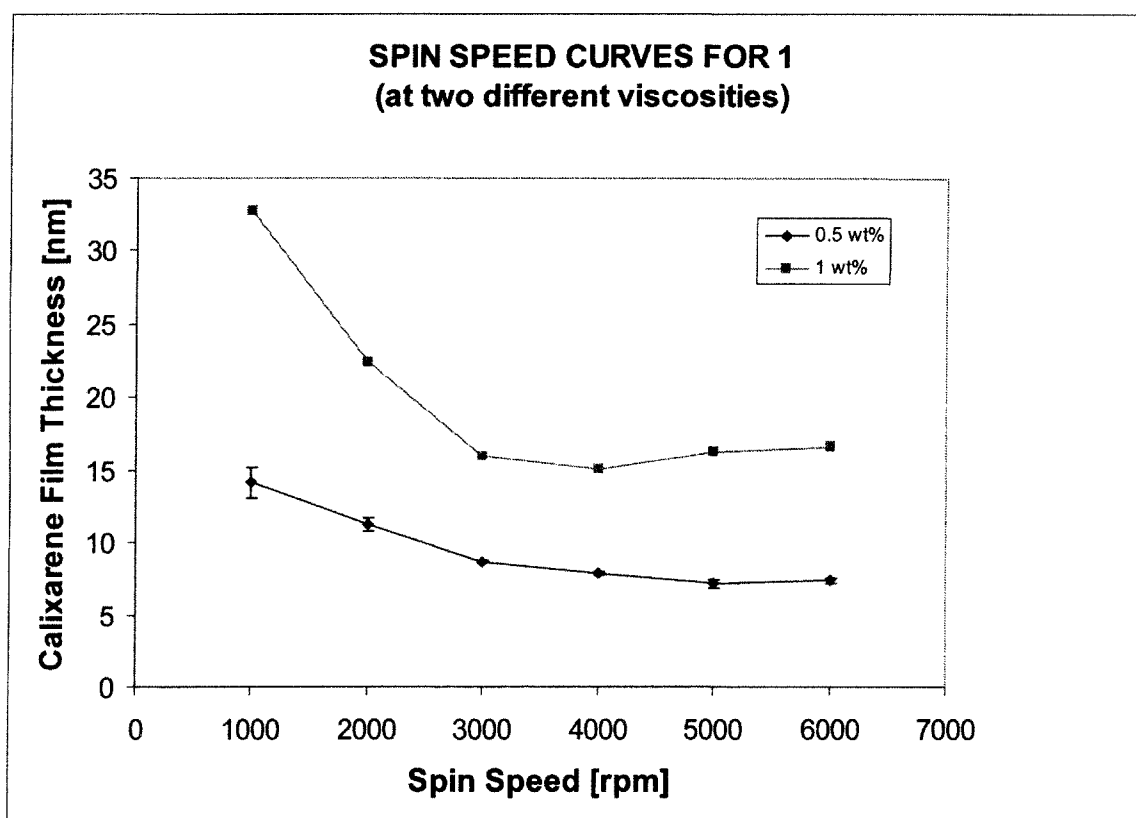


Figure 4.2.5 Combined Spin Speed Curves of 1 at 0.5 and 1.0 wt%

### 4.3 Ellipsometric Determination of $n$ and $k$ of **2** ( $n_2$ and $k_2$ )

#### 4.3.1 Sample Preparation and Raw Data for Determination of $n_2$ and $k_2$

In order to determine the optical properties of **2**, the complete experimental procedure for **1** was replicated. 3 mL of a 1.0 wt% **2** was spun at 3000 rpm. The sample was baked on a hotplate for 2 minutes at 170 °C. The sample was then measured on the ellipsometer at three angles, along with the Si/SiO<sub>2</sub> standard. The data for **2** is shown below.

Calculated Angle (degrees)	P1	A1	I1	P2	A2	I2	$\Delta$	$\Psi$	Remarks
69.8183	57.9	12	<20	148.1	168.7	<25	154	11.65	Si/SiO <sub>2</sub>
69.8183	73	15.6	22.5	163.6	165.7	<25	123.4	14.95	Calixarene <b>2</b>
49.5228	52.3	32.2	22.5	142.5	148.8	<30	165.2	31.7	Calixarene <b>2</b>
49.5228	48	32.3	<20	137.8	148.6	25	174.2	31.85	Si/SiO <sub>2</sub>
29.5304	45.5	41.3	<20	135.8	139.6	22.5	178.7	40.85	Si/SiO <sub>2</sub>
29.5304	47.5	41	<20	137.2	139.5	24	175.3	40.75	Calixarene <b>2</b>

**Table 4.3.1** Raw Ellipsometric Data for the determination of  $n$  and  $k$  of **1**

#### 4.3.2 Determination of $n_2$ and $k_2$

The FilmWizard software was used to determine the exact value for all three incident angles, using the Si/SiO<sub>2</sub> standard as a reference. A native oxide layer of 2.05 nm was assumed, and the data was fit into the three-layer model to

determine the optical properties of **2**, as well as the sample thickness. These constants are given in Table 4.3.2.

Property	Based on measurements at all three angles
$n_2$	$1.56 \pm 0.01$
$k_2$	$81 * 10^{-16}$
thickness (t)	22.9 nm
RMSE	0.31

**Table 4.3.2** Optical Constants of **2** (assuming 2.05 nm thick native oxide layer)

#### 4.4 Creation of Spin Speed Curves for **2** (at 0.5 and 1.0 wt%)

##### 4.4.1 Preparation and Ellipsometric Measurement of Samples (0.5 wt% **2**)

This procedure was slightly different from that used to create spin speed curves for **1**. 18 mL of a 0.5 wt % **2** was formulated. This sample was spun on different wafers, with each wafer having a spin speed ranging from 1000 to 4000 rpm (intervals differing by 1000 rpm). *Due to experimental error, it was necessary to prepare a new sample of resist.* An additional 6 mL sample of 0.5 wt% **2** was formulated to complete the trial at the 5000 and 6000 rpm part of the curve. In addition, due to a shortage of 4" wafers, *two 1"x1" silicon wafer samples were cut out of one wafer and used for the 5000 and 6000 rpm trials.*

Nevertheless, for each of the six trials, 3 mL of resist was applied and standard post-spin bake time and temperatures were used. Each of the six samples of **2** were then analyzed with the null ellipsometer. In order to determine the average film thickness on the respective sample, all were measured at two different points. The raw data for each sample is shown in Table 4.4.1.

0.5 wt % 2 Series									
SPIN SPEED: 1000 rpm									
Angle	P1	A1	M	P2	A2	I2	$\Delta$	$\Psi$	Remarks
69.774	69.3	14.8	20	158.9	167.3	19	131.8	13.75	1" from wafer edge
69.774	69.6	14.5	19	159.3	166.8	19	131.1	13.85	1" from opposite edge
SPIN SPEED: 2000 rpm									
Angle	P1	A1	I1	P2	A2	I2	$\Delta$	$\Psi$	Remarks
69.774	66	13.9	19	157.1	167.9	19	136.9	13	1" from wafer edge
69.774	66.1	13.7	18	157.3	167.5	19	136.6	13.1	1" from opposite edge
SPIN SPEED: 3000 rpm									
Angle	P1	A1	I1	P2	A2	I2	$\Delta$	$\Psi$	Remarks
69.774	62.4	13.5	17	153.8	168	17	143.8	12.75	1" from wafer edge
69.774	62.8	13.2	17	154	168.1	18	143.2	12.55	1" from opposite edge
SPIN SPEED: 4000 rpm									
Angle	P1	A1	I1	P2	A2	I2	$\Delta$	$\Psi$	Remarks
69.774	61.8	12.9	16	151.9	168.2	20	146.3	12.35	1" from wafer edge
69.774	61.7	12.9	17	151.8	168.1	20	146.5	12.4	1" from opposite edge
SPIN SPEED: 5000 rpm NOTE: used DIFFERENT experimental conditions here									
Angle	P1	A1	I1	P2	A2	I2	$\Delta$	$\Psi$	Remarks
69.774	63.4	13.2	16	153.8	168.3	20	142.8	12.45	1"x1" Sample--1 cm from edge
69.774	63.8	13.2	17	153.8	168.2	19	142.4	12.5	1"x1" Sample--1 cm from edge
SPIN SPEED: 6000 rpm NOTE: used DIFFERENT experimental conditions here									
Angle	P1	A1	I1	P2	A2	I2	$\Delta$	$\Psi$	Remarks
69.774	62.9	13	16	152.3	168.2	19	144.8	12.4	1"x1" Sample--1 cm from edge
69.774	62.2	12.6	19	152.6	168.2	19	145.2	12.2	1"x1" Sample--1 cm from edge

**Table 4.4.1** Raw Ellipsometric Data for Spin Curve Series of 0.5 wt% 2

#### 4.4.2 Results and Spin Speed Curve for 0.5 wt% 2 (from 1000-6000 rpm)

For each wafer (or square sample), the data was used to determine an average thickness of resist coating on each wafer using the SCI software from each combination of delta ( $\Delta$ ) and psi ( $\Psi$ ). For each wafer (or square sample), the two calculated thickness values from opposite sides of the spin sample were averaged. These calculations assumed a native oxide thickness of 2.05 nm. The numerical results, including the root mean square error (RMSE), are shown in Table 4.4.2.

0.5 wt% 1 (Spun with 3 mL for 1 minute, baked 2 minutes on hotplate at 170 °C)					
Spin Speed [rpm]	Minimum Value [nm]	Maximum Value [nm]	Delta Thickness [nm]	RMSE	Average Thickness [nm]
1000	16.4918	16.8456	0.3538	0.0804	16.6687
2000	14.0269	14.1697	0.1428	0.201	14.0983
3000	10.9991	11.2434	0.2443	0.2156	11.1213
4000	9.874	9.9535	0.0795	0.1843	9.9138
**5000	11.4083	11.58	0.1717	0.1489	11.4942
**6000	10.398	10.5701	0.1721	0.1164	10.4841

**Table 4.4.2** Calculated average thicknesses for 0.5 wt% 2 at 6 spin speeds

The different experimental conditions for the 5000 and 6000 rpm trials leads to a *loss of continuity* in the spin curve trend. The reasons behind this behavior are rationalized in the “Discussion” section. The trend loss is evident in the resultant spin speed curve for 0.5 wt% 2, which is shown in Figure 4.4.2

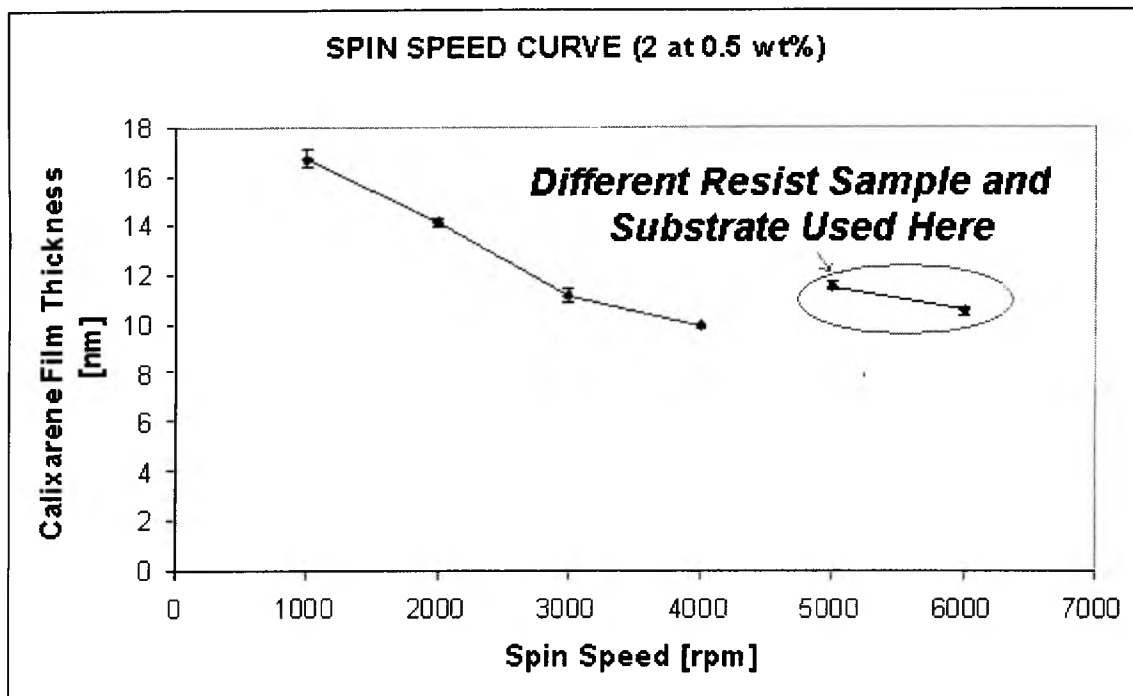


**Figure 4.4.2** Spin speed curve of 0.5 wt% calixarene (2) resist

#### 4.4.3 Preparation and Ellipsometric Measurement of Samples (1.0 wt% 2)

For this series, *all resist films were once again made on 4" wafers*, a factor that led to more consistent data and spin curves. Samples were prepared as for the 1.0 wt% 1 and analyzed on the null ellipsometer. Raw ellipsometric data is provided in Table 4.4.3.

1.0 wt % 2 Series									
SPIN SPEED: 1000rpm									
Angle	P1	A1	I1	P2	A2	I2	$\Delta$	$\Psi$	Remarks
69.774	82.8	20.2	20	174	162.2	19	103.2	19	1" from wafer edge
69.774	83	20.1	19	173.3	162.1	17	103.7	19	1" from opposite edge

**Table 4.4.3** Raw Ellipsometric Data for Spin Curve Series of 1.0 wt% 2

1.0 wt % 2 Series									
SPIN SPEED: 2000 rpm									
Angle	P1	A1	I1	P2	A2	I2	$\Delta$	$\Psi$	Remarks
69.774	79	18.2	21	169	164.1	19	112	17.05	1" from wafer edge
69.774	78.3	18	19	168.4	164.3	18	113.3	16.85	1" from opposite edge
SPIN SPEED: 3000 rpm									
Angle	P1	A1	I1	P2	A2	I2	$\Delta$	$\Psi$	Remarks
69.774	74.6	16.3	17	164.5	165.2	19	120.9	15.55	1" from wafer edge
69.774	74	16.2	18	164.2	165.4	19	121.8	15.4	1" from opposite edge
SPIN SPEED: 4000 rpm									
Angle	P1	A1	I1	P2	A2	I2	$\Delta$	$\Psi$	Remarks
69.774	72.3	15.3	18	162.4	166.4	19	125.3	14.45	1" from wafer edge
69.774	72	15.6	19	162.8	166.3	18	125.2	14.65	1" from opposite edge
SPIN SPEED: 5000 rpm									
Angle	P1	A1	I1	P2	A2	I2	$\Delta$	$\Psi$	Remarks
69.774	70.9	14.9	17	160.8	166.3	20	128.3	14.3	1" from wafer edge
69.774	70.2	14.9	19	160.7	166.38	19	129.1	14.05	1" from opposite edge
SPIN SPEED: 6000 rpm									
Angle	P1	A1	I1	P2	A2	I2	$\Delta$	$\Psi$	Remarks
69.774	68.1	14.7	19	158.7	167.2	19	133.2	13.75	1" from wafer edge
69.774	68.2	14.2	19	159	167.3	19	132.8	13.45	1" from opposite edge

**Table 4.4.3** Ellipsometric Data for Spin Curve Series of 1.0 wt% 2 (Continued)

#### 4.4.4 Results and Spin Speed Curve for 1.0 wt% 2 (from 1000-6000 rpm)

The numerical results from the SCI program calculations are presented in Table 4.4.4. The spin curve for 2 at 1.0 wt% is shown in Figure 4.4.4, and shows a more ideal spin curve. The obvious repercussions that were noted in the 0.5 wt% curve are not seen here, indicating that *in a real processing environment, the same source of resist should be used when processing a series of wafers.*

1.0 wt% 2 (Spun with 3 mL for 1 minute, baked 2 minutes on hotplate at 170 °C)					
Spin Speed [rpm]	Minimum Value	Maximum Value	Delta Thickness [nm]	RMSE	Average Thickness [nm]
1000	35.1635	35.5779	0.414	0.9455	35.3703
2000	27.536	28.4651	0.9291	0.4303	28.0006
3000	21.9894	22.5344	0.545	0.0219	22.2619
4000	19.9208	19.9935	0.0727	0.326	19.9572
5000	17.8726	18.306	0.4334	0.0972	18.0893
6000	15.8085	15.9833	0.1748	0.2468	15.9169

**Table 4.4.4** Calculated average thicknesses for 1.0 wt% 2 at 6 spin speeds

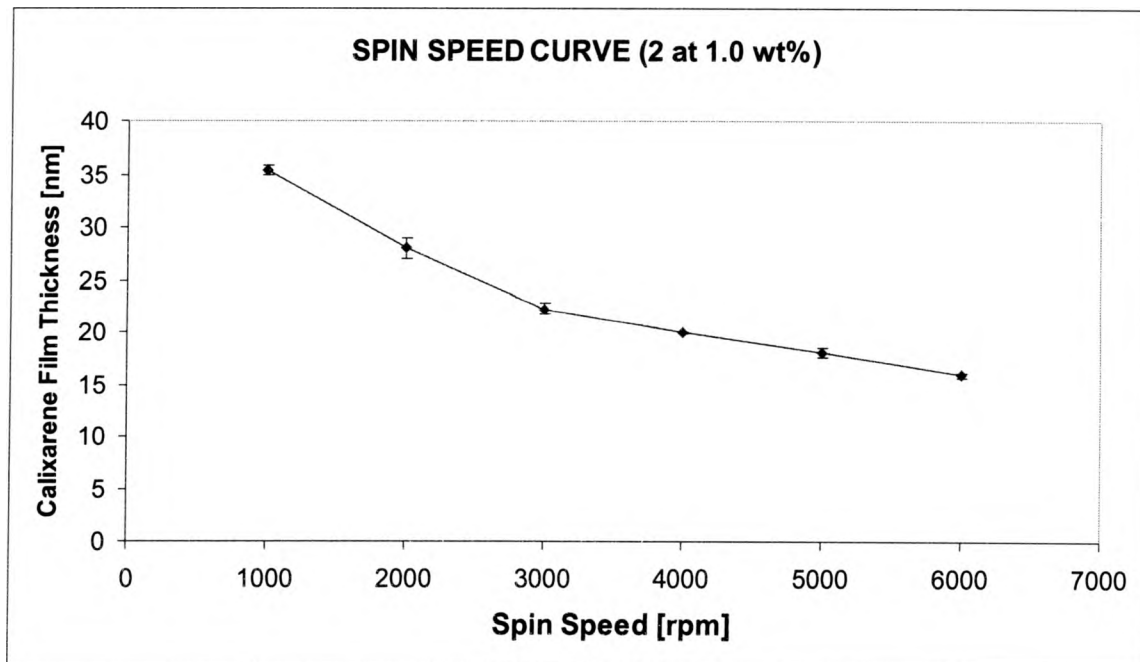


**Figure 4.4.4** Spin Speed Curve of 1.0 wt% Calixarene (2) Resist

#### 4.5 Remeasurement of Film Thickness of 1 (0.5 and 1.0 wt%)

In order to monitor if the coated calixarene films would change over time, the thickness of the films formed at higher spin speeds (3000-6000 rpm) was remeasured for both wt% formulations of 1. *Ellipsometric analysis was performed on the same wafers used to do the initial thickness analysis (from section 4.2) one month after the initial ellipsometric analysis.*

##### 4.5.1 Ellipsometric Data

Raw ellipsometric data is shown below in Table 4.5.1. This analysis was performed in the same manner described before. Two points on opposite sides of each wafer were measured in order to create two values for  $\Delta$  and  $\Psi$ .

REMEASUREMENT of 1.0 wt % 1 Series (at spin speeds of 3000-6000 rpm)									
SPIN SPEED: 3000 rpm									
Angle	P1	A1	I1	P2	A2	I2	$\Delta$	$\Psi$	Remarks
69.774	69.8	14.7	21	159.6	166.8	20	130.6	13.95	1" from wafer edge
69.774	68.5	14.3	19	159.1	166.9	19	132.4	13.7	1" from opposite edge
SPIN SPEED: 4000 rpm									
Angle	P1	A1	I1	P2	A2	I2	$\Delta$	$\Psi$	Remarks
69.774	69.1	14.6	18	159	166.3	19	131.9	14.15	1" from wafer edge
69.774	68.5	14.6	19	159.5	167	19	132	13.65	1" from opposite edge
SPIN SPEED: 5000 rpm									
Angle	P1	A1	I1	P2	A2	I2	$\Delta$	$\Psi$	Remarks
69.774	69.3	14.1	19	159.7	166.9	20	131	13.6	1" from wafer edge
69.774	69.7	14.5	19	160.1	167	19	130.2	13.75	1" from opposite edge
SPIN SPEED: 6000 rpm									
Angle	P1	A1	I1	P2	A2	I2	$\Delta$	$\Psi$	Remarks
69.774	70.9	15.1	27	162	166.1	31	127.1	14.6	1" from wafer edge
69.774	70.9	14.8	21	160.1	167	21	129	13.9	1" from opposite edge

**Table 4.5.1** Raw data for remeasurement of film thickness of 1 after one month

REMEASUREMENT of 0.5 wt % 1 Series (at spin speeds of 3000-6000 rpm)									
SPIN SPEED: 3000 rpm									
Angle	P1	A1	I1	P2	A2	I2	$\Delta$	$\Psi$	Remarks
69.774	60.6	12.8	30	151.8	168.2	31	147.6	12.6	1" from wafer edge
69.774	60.8	13	28	151.7	168.2	31	147.4	12.4	1" from opposite edge
SPIN SPEED: 4000 rpm									
Angle	P1	A1	I1	P2	A2	I2	$\Delta$	$\Psi$	Remarks
69.774	59.6	12.3	26	149.2	168.3	28	151.2	12	1" from wafer edge
69.774	59.3	12.5	23	149.3	168.7	26	151.4	11.9	1" from opposite edge
SPIN SPEED: 5000 rpm									
Angle	P1	A1	I1	P2	A2	I2	$\Delta$	$\Psi$	Remarks
69.774	59.6	12.4	18	149.4	168.5	22	151	11.5	1" from wafer edge
69.774	58.9	12.4	19	149.3	168.3	22	151.8	12.05	1" from opposite edge
SPIN SPEED: 6000 rpm									
Angle	P1	A1	I1	P2	A2	I2	$\Delta$	$\Psi$	Remarks
69.774	59.5	12.3	18	148.9	169	24	151.6	11.65	1" from wafer edge
69.774	60	12.3	20	148.8	168.7	21	151.2	11.8	1" from opposite edge

**Table 4.5.1** Remeasurement of film thickness of 1 after one month (continued)

#### 4.5.2 Results and Spin Curves of Remeasured Films

Both films (0.5 and 1.0 wt%) showed an increase in film thickness over time. Factors which may have contributed to this phenomenon will be presented in the discussion section.

REMEASUREMENT RESULTS for 1.0 wt% 1			
Spin Speed (rpm)	Initial Thickness (nm)	Remeasured Thickness in nm (1 month later)	GROWTH $\Delta t$ (nm)
3000	15.9773	16.493	0.516
4000	15.0991	16.2731	1.174
5000	16.263	16.924	0.661
6000	16.6765	18.258	1.583

**Table 4.5.2** Thickness Growth of Calixarene Films over 1 month

REMEASUREMENT RESULTS for 0.5 wt% 1			
Spin Speed (rpm)	Initial Thickness (nm)	Remeasured Thickness in nm (1 month later)	GROWTH $\Delta l$ (nm)
3000	8.6944	9.386	0.6916
4000	7.8522	7.894	0.0418
5000	7.1663	7.858	0.6917
6000	7.3748	7.85	0.4752

**Table 4.5.2** Thickness Growth of Calixarene Films over 1 month (continued)

Resultant film increases over time were determined to be as large as 1.5 nm, which indicates that wafers with a spin-coated calixarene film should be exposed as soon as possible. Possible reasons for film growth are discussed later. Comparative spin curves which graphically display the film growth over time are shown in Figure 4.5.2 (1.0 wt% 1) and 4.5.3 (0.5 wt% 1).

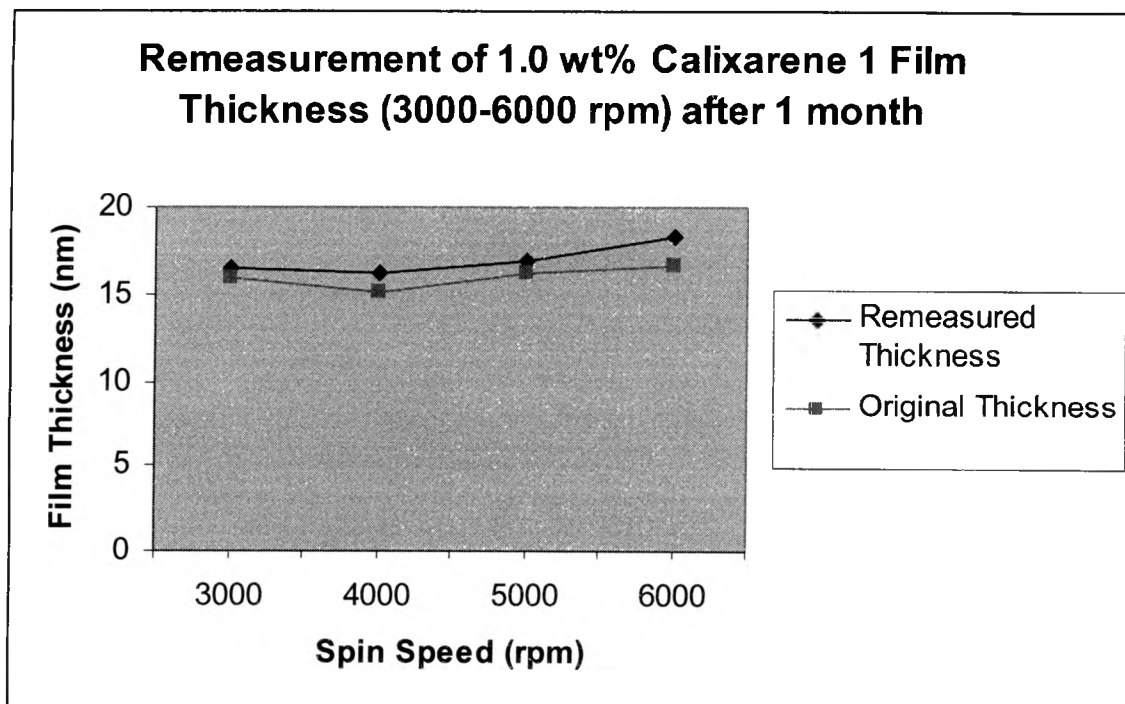


**Figure 4.5.2** Spin curve showing film growth of a thin film of 1.0 wt% 1 over time

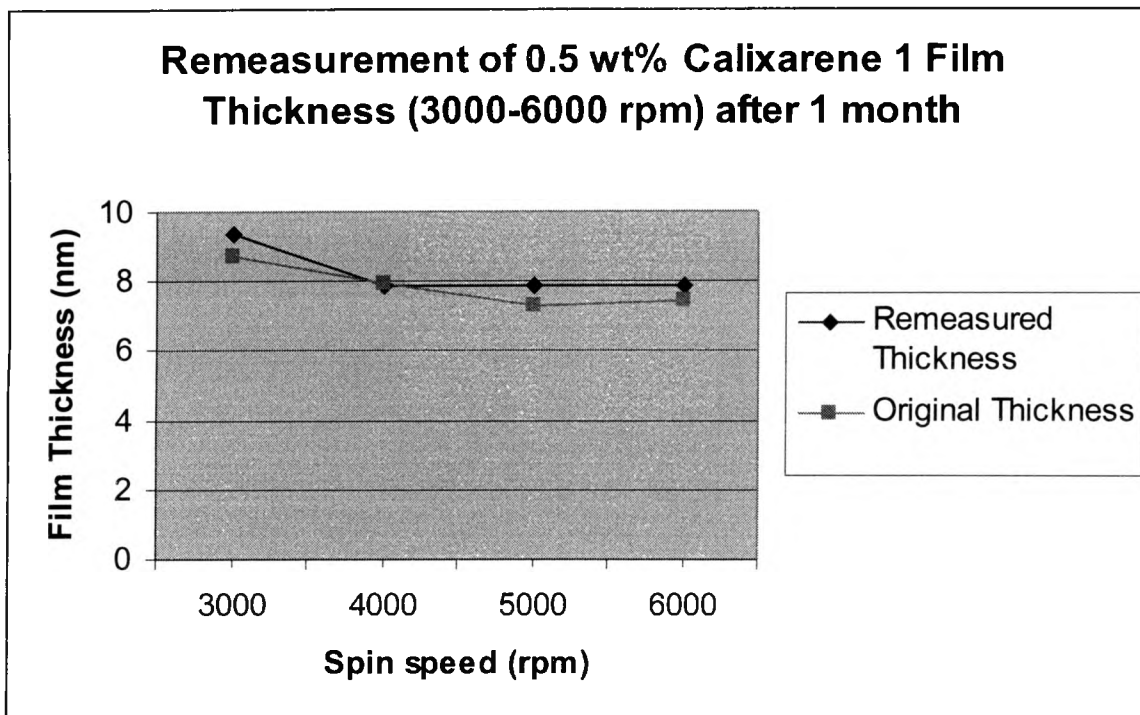


**Figure 4.5.3** Spin curve showing film growth of a thin film of 0.5 wt% **1** over time

## 4.6 Initial Measurement of Calixarene Line Widths Using Atomic Force Microscopy

### 4.6.1 Examination of Preliminary Samples of **1** and **2**

Qualitatively, *all exposed samples of calixarene 1 and 2 formulations (including those with benzoyl peroxide) showed boxes and lines after development.* For these trials, each (box and line) feature was created by exposing each sample formulation at timed iterations of 1, 2, 5, 10, 20, 50, and 100 seconds (refer to 3.7.2 for procedure and spinning conditions).

Using the optical microscope, lines were observed for each iteration. In contrast, the *boxes* began to appear at the 20 second iteration (as a thin scum) and become visually thicker as the iterations approached 100 s. Representative AFM scans of **2** (non-benzoyl peroxide formulation) can be seen in Figure 4.6.1.

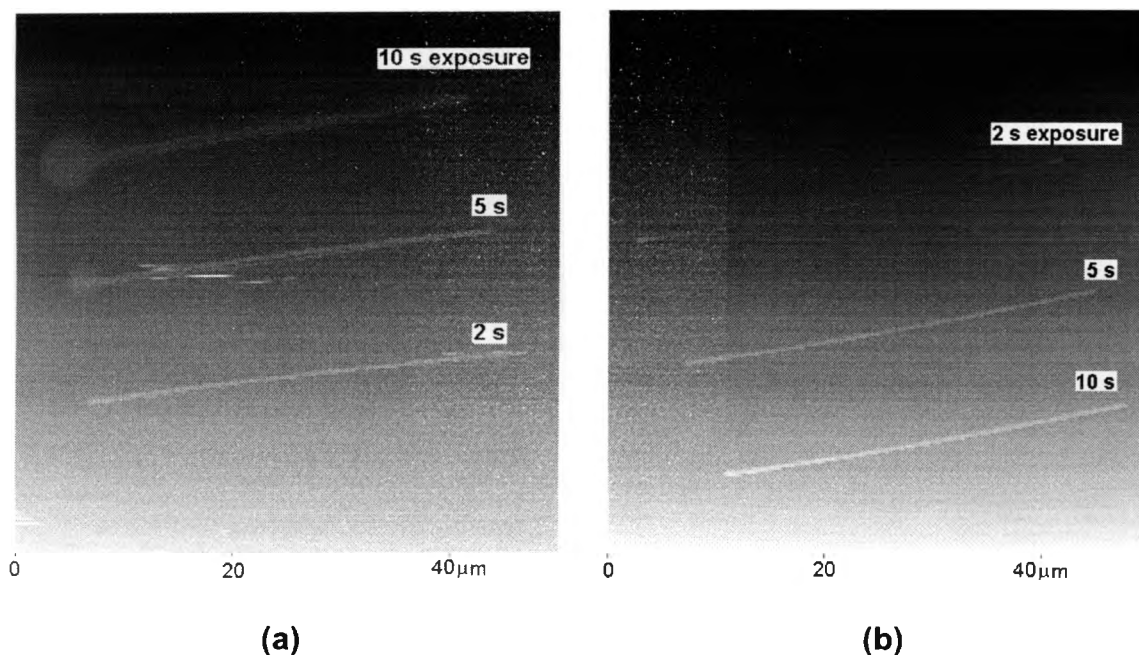


**Figure 4.6.1** AFM scans of (a) **2** at beam current of 107 pA and (b) **2** at 84 pA. Note the visual differences in line widths at different beam currents (dosages).

All features were exposed at a 20 kV acceleration voltage. In order to monitor the actual beam current at the sample during exposure, a probe current detector (PCD) was used during these experiments. The average beam current for these lines was 107 and 84 pA respectively. Line widths range from 2.4  $\mu\text{m}$  to 0.8  $\mu\text{m}$  (respective measurements for (a) at 10 s and (b) at the 2 s exposure).

#### 4.6.2 Changes in Line Width as a Result of Exposure Dosage

There was an obvious change in line width *at different exposure times* (due to different exposure dosages) for all samples, an effect that is easily visualized in 4.6.1. This effect can be attributed to a higher amount of calixarene polymerization (and resultant increase in the matrix and pattern size) as the dosage is increased. Thus lines that are exposed at higher beam currents

become *overexposed*. This phenomenon is explained in more detail in the discussion section.

In order to illustrate the dramatic increase of line width with applied electron dosage (*i.e.*, exposure time), the line width of the 1 s and 100 s lines from a sample of **2** was measured. Three-dimensional AFM scans of these lines are shown in Figure 4.6.2.1 and Figure 4.6.2.2.

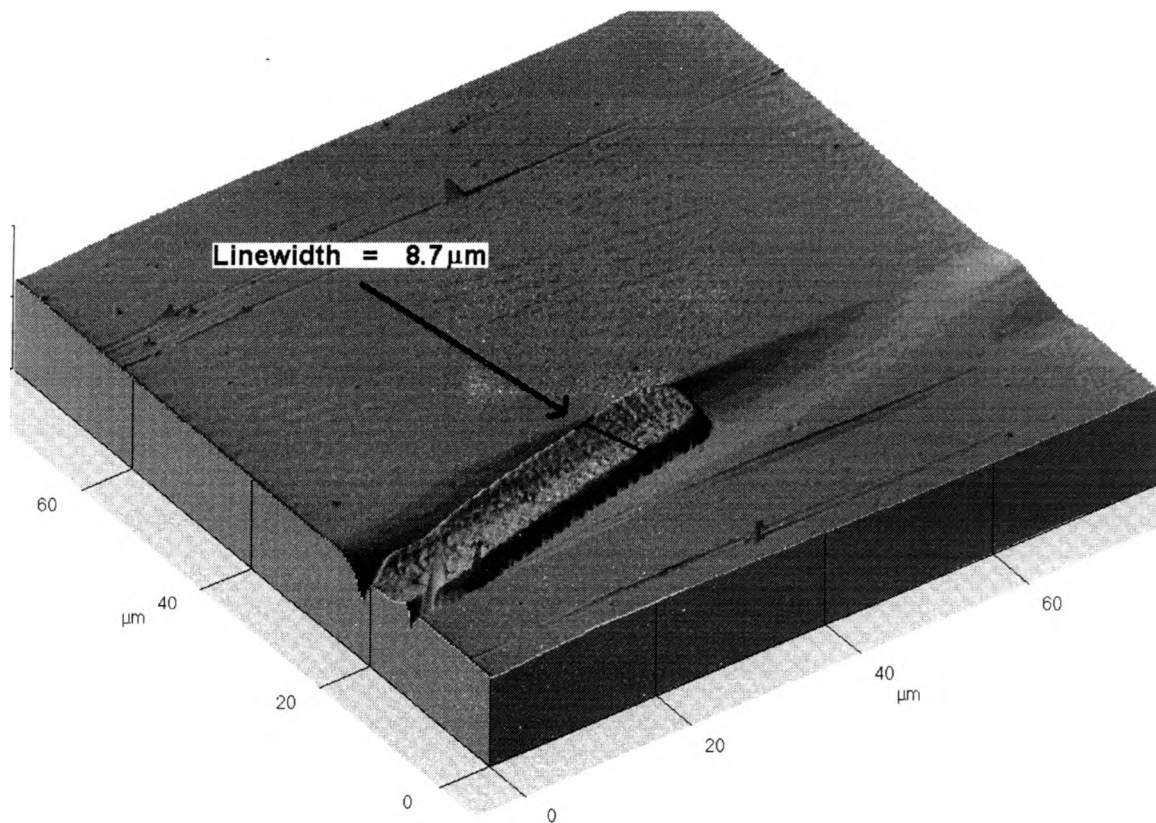


**Figure 4.6.2.1** Line width of **2** as a result of exposure time (dose). Line width of this *overexposed* feature is 8.7  $\mu\text{m}$  (100 s exposure)—compare with Figure 4.6.2.2

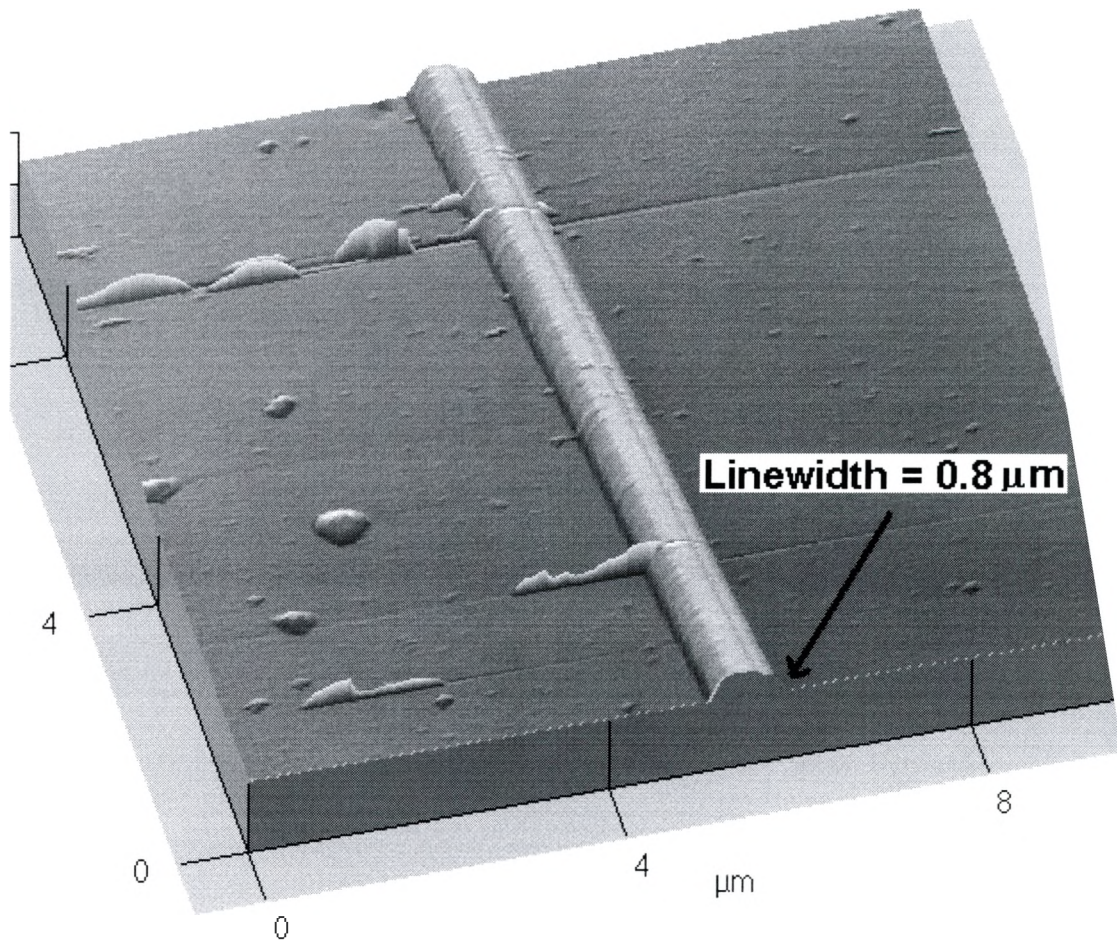


**Figure 4.6.2.2** Line width 2 as a result of exposure time (dose). Line width of this feature is  $0.8 \mu\text{m}$  (2 s exposure)

Both lines were created at a 20 kV acceleration voltage with an average beam current of 1.3 nA (as measured by the PCD). Both lines were  $40 \mu\text{m}$  long. However, the width of the 1 second line was  $0.8 \mu\text{m}$ , while that of the overexposed 100 second line was  $8.7 \mu\text{m}$ .

#### 4.6.3 Determination of the Width of the Highest Resolution Line

To obtain an accurate reading of the thinnest feature achieved in these experiments, measurements were taken of a 2 second line that was created at a beam current of 45 pA. This was also from a sample of **2**, created as described in 3.7.3. Six cross-sectional measurements were taken at different points across the line. *The average linewidth was 0.474  $\mu\text{m}$ , and was the thinnest of the high resolution experiments for **2**.* The line also showed moderate uniformity with a variation of 0.016  $\mu\text{m}$ . The raw data for this measurement is shown below in Table 4.6.2. The actual line is shown in Figure 4.6.2.

Measured Linewidths ( $\mu\text{m}$ )	Average Width ( $\mu\text{m}$ )	$\Delta\text{width}$
0.472, 0.472, 0.467, 0.483, 0.473, .476	0.474	0.016

**Table 4.6.3** Measurements of a line created at 45 pA (2 s, 20 kV) exposure

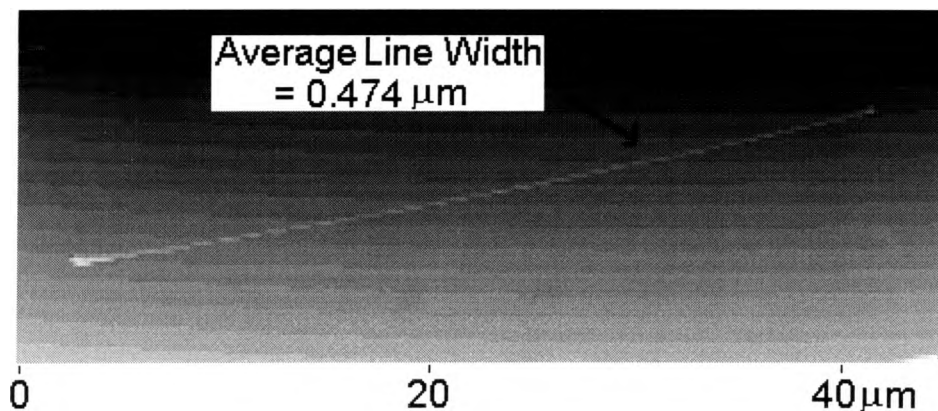


**Figure 4.6.3** Highest Resolution Line, created at 20kV acceleration voltage with a beam current of 45 pA (2 s exposure)

#### 4.7 Examination of Line Widths of Calixarene 1 and 2 Formulations With BPO Using the Scanning Electron Microscope (SEM)

In order to begin to evaluate the resolution capabilities of **1** and **2**, samples containing benzoyl peroxide (radical initiator) were prepared as described in section 3.8.3. Two samples containing a 7.0 wt% coat of **1** and **2** (formulated with 1% benzoyl peroxide and spun at 1000 rpm) were examined. In order to prevent the charging of the resist under the SEM, a 15 nm layer of AuPd was sputtered on top of developed features.

The samples were then visualized under the SEM at a 20 kV acceleration voltage and a magnification ranging from 25,000 to 27,000X. These features had dimensions comparable to those obtained from the AFM for non-BPO formulations. Line widths of these BPO-containing features were approximately 0.5 to 0.6  $\mu\text{m}$ , as seen in Figure 4.7.



**Figure 4.7** SEM micrographs of: (a) **1** with 1% BPO and (b) **2** with 1% BPO exposed by using a 20 kV electron beam at an average beam current of 1.2 nA

## 4.8 AFM Analysis of Box Features

### 4.8.1 Dose-Dependant Appearance of Boxes

For the aforementioned timed iterations, boxes were also exposed using the same conditions as the lines (at iterations of 1, 2, 5, 10, 20, 50, and 100 seconds). These boxes were exposed at 20 kV and an average beam current of 1.3 nA. Unlike the lines (which appeared for all iterations upon development), the boxes began to appear *at the 20 second iteration*.

The thickness of these boxes was observed under the optical microscope to gradually increase, as the coloration of the boxes increased from an almost transparent color to a rich pink color. Like the corresponding linear features, the boxes were also dose dependant. AFM scans of a representative 100 second box are seen in Figures 4.8.1 and 4.8.2.

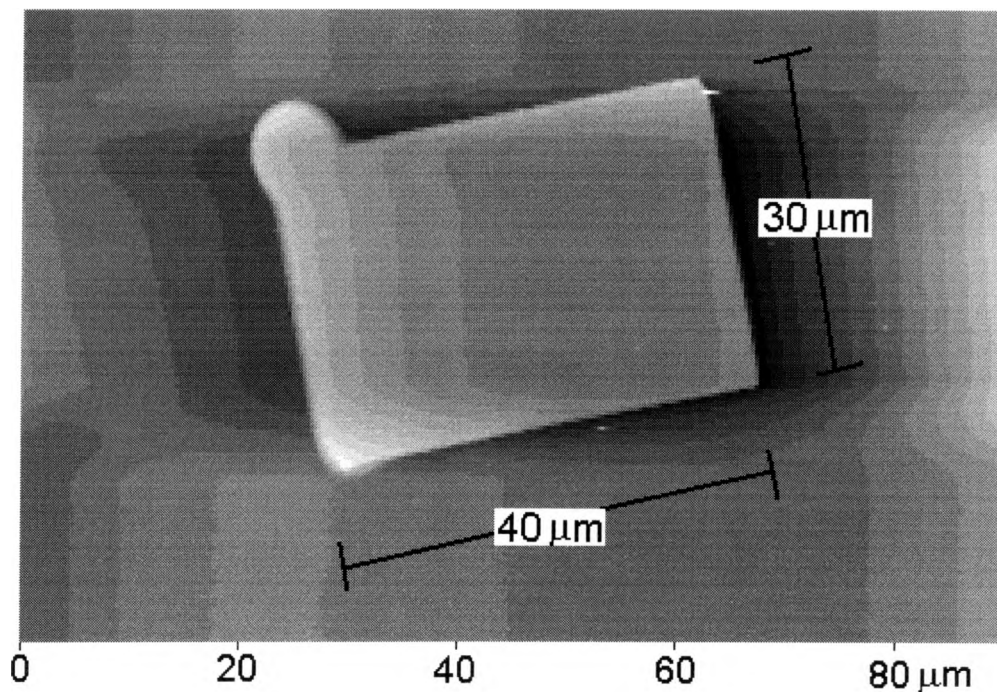


**Figure 4.8.1** AFM scan of a 100 second box made from 2

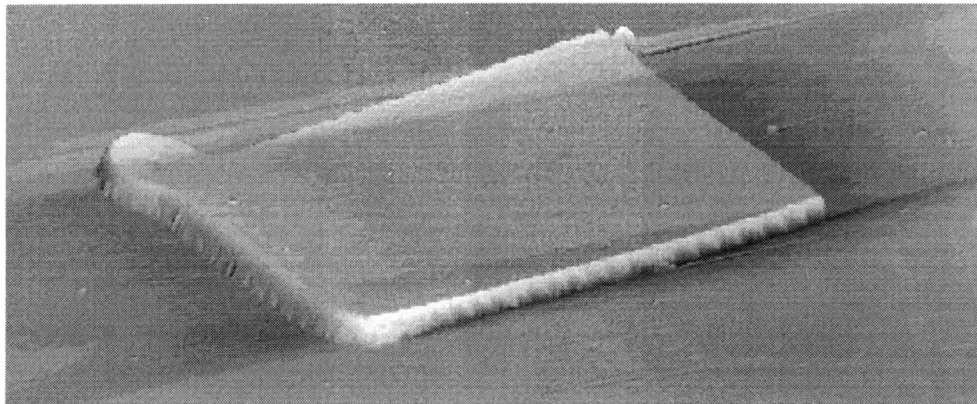


**Figure 4.8.2** 3-Dimensional scan of the 40X30  $\mu\text{m}$  (100 s) box made from 2

#### **4.8.2 Measurement of Box dimensions**

Using the AFM, all boxes were measured to have dimensions of approximately 40  $\mu\text{m}$  by 30  $\mu\text{m}$ . A small notch at the upper left corner of each box was observed. The boxes also had a slight variation in height, ranging from 0.193 nm to 0.198 nm. To determine the average height of the 100 second box, a series of six measurements were taken. These measurements gave an average height of 0.195  $\mu\text{m}$ .

It was demonstrated that at a 100 s exposure, the boxes had reached the height of the original, unexposed calixarene thin film. To ascertain this fact, other experiments (using samples of 1 and 2) were conducted at times of 110, 120, 130, 140, and 150 seconds. The corresponding average step heights for these boxes gave about the same height as that of the 100 second thickness, indicating that full thickness had been reached.

## 4.9 Creation of a Contrast Curve for 1

### 4.9.1 Resist Sensitivity and Contrast

The sensitivity of a negative resist can be defined as the incident dose of radiation that is necessary to produce a given amount of insolubilization.<sup>5</sup> For an negative electron beam resist, this is the amount of electrons (or charge) per unit area that is required to create a certain amount of cross-linking. The contrast ( $\gamma$ ) of a negative electron beam resist is a function of the rate of the formation of a cross-linked matrix at a constant input dose. Contrast will determine the lithographically useful dosages of a given electron beam resist.<sup>4,6</sup>

In order to determine the sensitivity and contrast of a resist, areas of resist of a known size are exposed to varying amounts of electron beam doses. The features are developed and the film thickness remaining after development is measured for each exposed feature. The data is then used to create a contrast curve, such as one seen in Figure 1.11.6 for literature calixarenes.

### 4.9.2 Gel Dose ( $D_g$ ) and Insolubilization Dose ( $D_i$ )

In negative resists, the resist will not begin to respond to the electron beam until a critical dosage has been reached. This parameter is called the *gel dose* ( $D_g$ ) and indicates the minimum dosage that is necessary to produce an insoluble residue.<sup>6</sup> On the other hand, there is a dosage at which the film thickness will be equal to the original (unexposed) film thickness. This parameter is the *insolubilization dose* ( $D_i$ ), and will indicate the minimum dosage required to produce an insoluble matrix whose film thickness is the same as the initial film.<sup>5</sup>

### 4.9.3 Attenuation of the Beam Current

In order to create an accurate contrast curve, it is necessary to have a stable beam current. In order to monitor the actual beam current at the sample during the exposure of **1**, a probe current detector (PCD) was used during these experiments. *Previous experiments showed a slow downward drift of beam current in between exposure experiments.* Therefore, In order to stabilize this drift for the contrast curve experiment, the beam current was manually attenuated to about 0.50 nA before each exposure iteration. For all exposures used to gather data for the contrast curve, the actual beam current was measured (to an accuracy of  $\pm 0.001$  nA).

### 4.9.4 Data for the Contrast Curve of **1**

A 1.0 wt% film of **1** was exposed as described in section 3.7.2. The results of the contrast curve experiment are shown in Table 4.9.4.

Iteration Time (sec)	PCD (nA)	Exposure Dose ( $\mu\text{C}/\text{cm}^2$ )	$\log_{10}$ Dose	Average Thickness (nm)	Normalized Thickness
95	0.511	4045	3.61	195	1
90	0.502	3765	3.58	182	0.92
85	0.499	3535	3.55	183	0.92
80	0.509	3393	3.53	172	0.85
75	0.494	3088	3.5	147	0.69
70	0.503	2934	3.47	117	0.49
60	0.506	2530	3.4	96	0.35
55	0.498	2283	3.36	77	0.23
50	0.506	2108	3.32	51	0.06
40	0.509	1697	3.23	43	0.01
30	0.501	1253	3.1	42	0

**Table 4.9.4** Data collected for the determination of sensitivity and contrast of **1**

A sample calculation is provided in Figure 4.9.4 to demonstrate the determination of the actual dosage for the 55 s box from the contrast experiments. Dosages for 1 was reported in the units of  $\mu\text{C}/\text{cm}^2$  in order to draw a comparison to the dosage of literature calixarenes.

$$\text{Dosage} = \frac{\text{Charge}}{\text{Unit Area}} = \frac{it}{A}$$

For the 55 s box,  $i = 0.498 \text{ nA}$

$$\begin{aligned} \text{Box area} &= 30 \mu\text{m} \times 40 \mu\text{m} \\ &= 1200 \mu\text{m}^2 \\ &= 1.2 \times 10^{-5} \text{ cm}^2 \end{aligned}$$

$$\text{Dosage} = \frac{(0.498 \text{ nA})(55 \text{ s})}{1.2 \times 10^{-5} \text{ cm}^2} = 2.29 \times 10^6 \frac{\text{nC}}{\text{cm}^2}$$

$$= \boxed{2290 \frac{\mu\text{C}}{\text{cm}^2}}$$

**Figure 4.9.4** Calculation for the Dosage of the 55 s contrast curve box

#### 4.9.5 Contrast Curve for 1

The data was plotted by using the base 10 logarithm of the applied dosage of each box as the x-axis and using the normalized film thickness as the y-axis. Normalized film thickness at each iteration was determined by dividing each measured box thickness by the largest thickness value. The plot of the curve is shown in Figure 4.9.5.

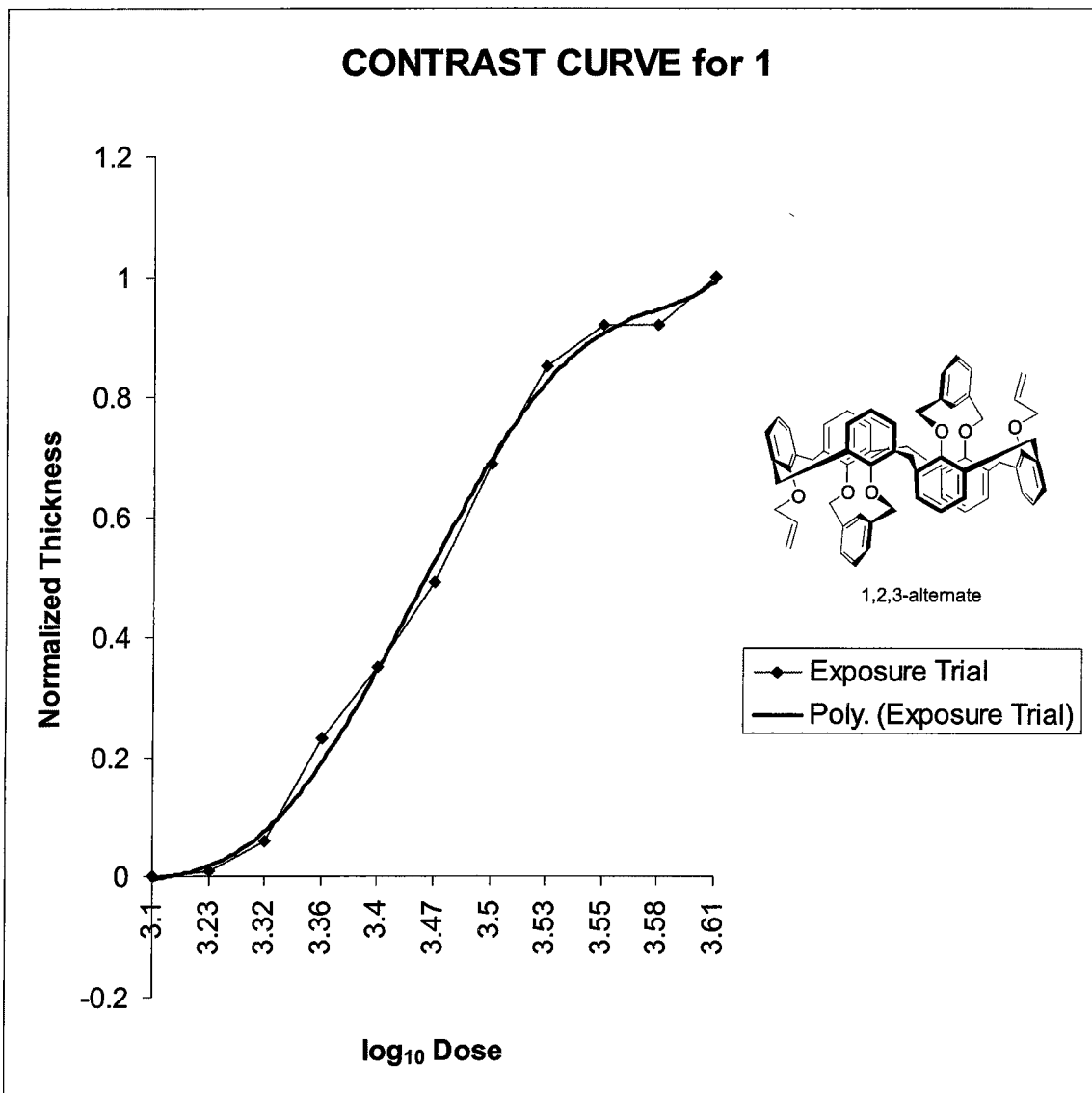


**Figure 4.9.5** Contrast curve for 1

#### 4.9.6 Determination of the Contrast of 1 Using an Extrapolated Line

The contrast ( $\gamma$ ) of a resist was determined by extrapolating a line along the linear portion of the contrast curve and determining the slope of the line. This analysis is the standard method for determining the contrast of negative resists.<sup>6</sup> The contrast curve of 1 shows the extrapolated line as well as the points on the plot that determine the gel dose ( $D_g$ ) and the insolubilization dose ( $D_i$ ) of 1.

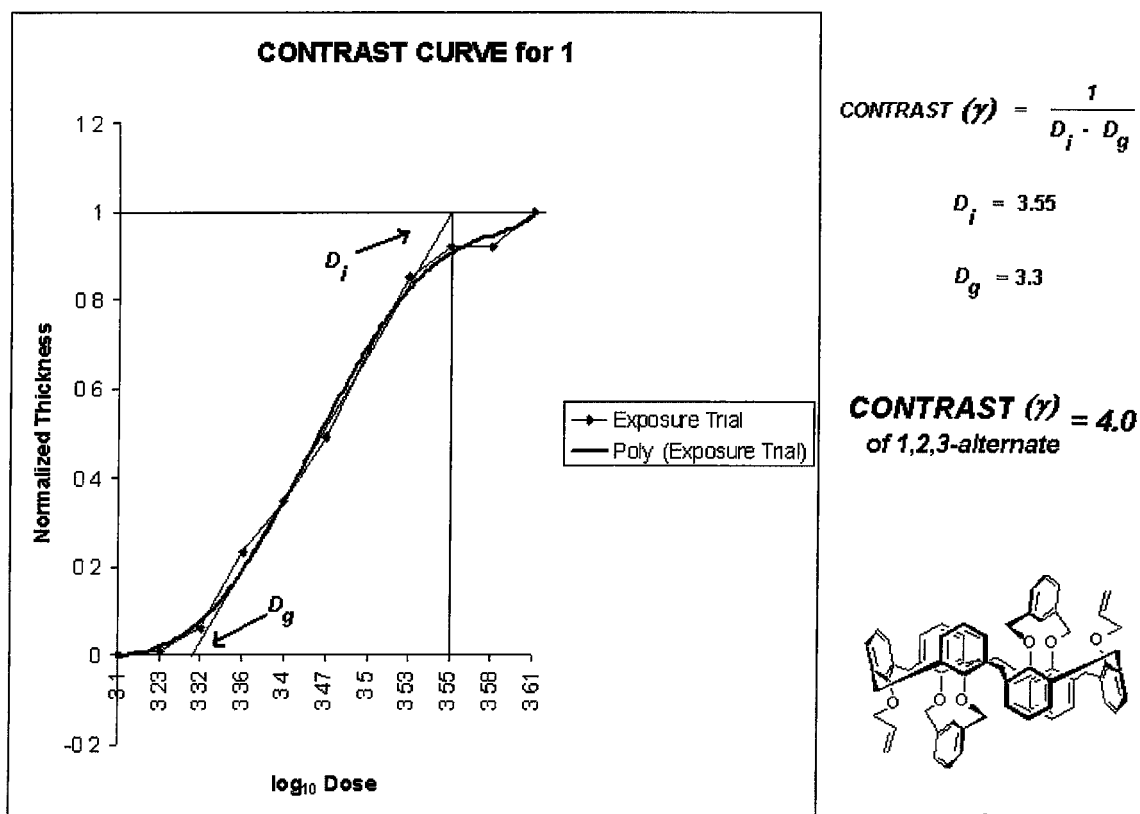


**Figure 4.9.6** Determination of the contrast of **1** using an extrapolated line

The contrast of **1** was 4.0, a value that was determined using the contrast equation (shown in the Figure above). This equation utilizes  $D_i$  and  $D_g$  and is the established parameter used to calculate the contrast of negative resists.<sup>5,6</sup> The apparent threshold of sensitivity of **1** is given by  $D_g$  (which was  $2.0 \mu\text{C}/\text{cm}^2$ ).  $D_i$  for **1** was  $3.6 \mu\text{C}/\text{cm}^2$ . A comparison is drawn between the sensitivity and contrast of **1** versus literature calixarene resists in the discussion section.

## 5.0 DISCUSSION

### 5.1 Overview

The capacity of any resist to print submicron and nanometer-scale features can be limited by a variety of physical and chemical phenomena.<sup>7</sup> In order to investigate the ability of a resist to facilitate the accurate pattern transfer of resist features onto a substrate, a number of factors must be considered. Even with a clean processing environment and reliable processing tools, a great deal of time must be invested in the evaluation of new resists in order to optimize their performance as robust semiconductor fabrication materials.

During the synthesis, formulation, and processing of the negative electron beam resists made from **1** and **2**, a great deal of experiments were conducted in order to begin to determine their potential as prospective, high-performance materials for lithography. The lithography results, while limited due to the lack of a purpose-built electron-beam lithography system, do clearly demonstrate the great potential of these calix[6]arenes as electron beam resists for nanolithography.

This discussion describes solutions to some of the problems encountered during these experiments. Some possible factors that attributed to discrepancies in data (as well as non-ideal results) are presented. In addition, the sensitivity,

contrast, and resolution that were determined for **1** and **2** during these experiments are compared to those of literature calixarenes.

## **5.2 Considerations for the Spin Coating Process**

### **5.2.1 Non-Uniform Calixarene Thin Films**

It was noted during initial experiments that the films spun from **1** and **2** were not uniform in thickness. This problem was visually observed by the radial streaks and color variations that were prominent on many areas of the wafer after the coating process, seen in Figure 5.2.1. Examination of the coated wafer with an optical microscope showed particulate contamination to be a primary culprit that led to the apparent streaking problem.

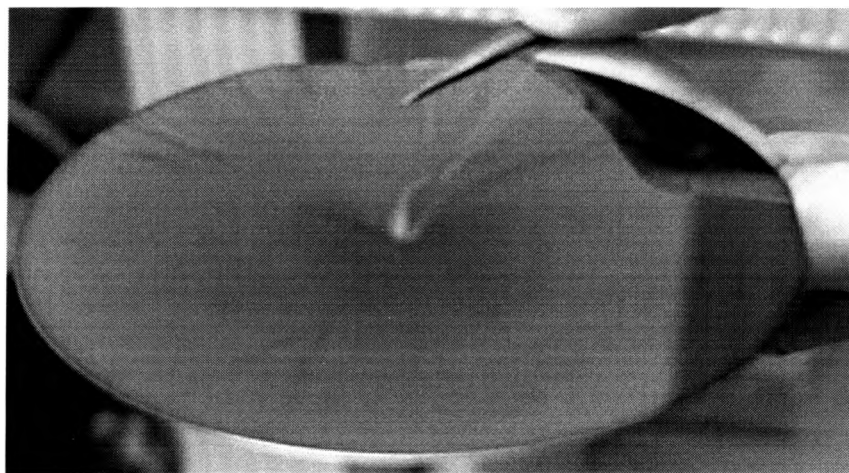


**Figure 5.2.1** Non-uniform film observed on a wafer coated with **1**

A resist coat such as this is not suitable for the fabrication of semiconductor devices with submicron features. This is because film uniformity across a single substrate (and from substrate to substrate) must vary by no more

than  $\pm 5.0$  nm in order to ensure reproducible line widths, development times, and etch rates.<sup>48,7</sup>

### 5.2.2 Creation of Uniform Films

It is well-known in resist technology that the formation of films with satisfactory adhesion and uniformity must be free of particulate contamination.<sup>6</sup> Both the substrate and the resist itself must be void of matter that is large enough to create a problem during the coating process. The aforementioned streaking problem was eventually resolved by attaching 0.20  $\mu\text{m}$  PTFE filter to the syringe during the coating procedure.

To prevent further contamination problems, the use of plastic syringes during the application of resist was avoided. The liquid used to suspend the calixarenes was chlorobenzene, an organic solvent that can potentially dissolve the polypropylene walls of plastic syringes over time. Instead, chemically inert glass syringes were fitted with syringe filters to create a "point-of-use" filtration method.

Calixarenes in general are renowned for their lack of solubility in common organic solvents.<sup>22</sup> This phenomenon became apparent during the formulation of resists with higher weight percentages of **1** and **2**. It was therefore necessary to assure that the solid was completely dissolved in the chlorobenzene solvent during resist formulation in order to circumvent uniformity problems due to calixarene precipitates.

### 5.2.3 Uniformity Problems attributed to Humidity

Another factor that contributed to adhesion problems was ambient moisture. The humidity of the processing area used for the coating procedure was determined to be quite high. It is reasonable to assume that moisture may collect on the bare wafer, since the surface of the wafer is a native  $\text{SiO}_2$ , a polar substrate. This phenomenon would certainly present an adhesion problem when spinning with chlorobenzene. Since the humidity of the processing room could not be controlled, all wafer samples were processed briskly during wafer coat, and the boxes that stored unprocessed, bare wafers were covered immediately when not used. This protocol could only protect the bare wafers from particulate contamination and not the excessive ambient humidity of the processing area.

### 5.2.4 Possible Reasons for Thickness Variation of Resist Across the Wafer

The film thickness was measured for a 1.5 wt% coat of 1 (spun at 3000 rpm) was measured with a stylus profilometer, as described in section 3.6.5. Measured thickness ranged from 9.5 to 15 nm at different points along the wafer (shown in Figure 4.1.6). Comparative thickness analysis of the same sample also demonstrated changes in film thickness from the wafer center to the edge.

Factors that may have led to variations in step height (along with humidity and particulates) may actually be attributed to the *spin coating unit* itself. The spin of the unit was assumed to be constant when it reached full speed. However, it may be possible that the wafer may not have been centered on the vacuum chuck, since the placing of the wafer on the chuck is done manually

(using tweezers). Inprecise wafer centering due to human error would then lead to variations in angular velocity of the resist along the wafer plane during the spin, a factor that may have caused irregularities in film uniformity.

### **5.3 Considerations Concerning Ellipsometric Measurements of 1 and 2**

Due to the sensitivity of the technique, ellipsometry can be a highly accurate method to determine optical properties and thickness of a film.<sup>46</sup> Nevertheless, there were a number of significant considerations during the measurement, modeling, and fitting of the data for **1** and **2** that merit discussion. In addition, non-ideal spin curve trends (such as increase in film thickness of a given resist at higher speeds) were observed and are explained in this section.

#### **5.3.1 Determination of the Native SiO<sub>2</sub> Thickness of an Uncoated Wafer**

All samples of calixarene coats were made on wafers which were not stripped of their native oxide coat. Thus, in order to make accurate resist film measurements, the thickness of the native oxide on a blank wafer was determined to be 2.05 nm. A three-layer ellipsometric model was then used to determine the thickness of **1** and **2**. Figure 5.3.1 shows a representation of the three layer “sandwich,” and respective optical constants.

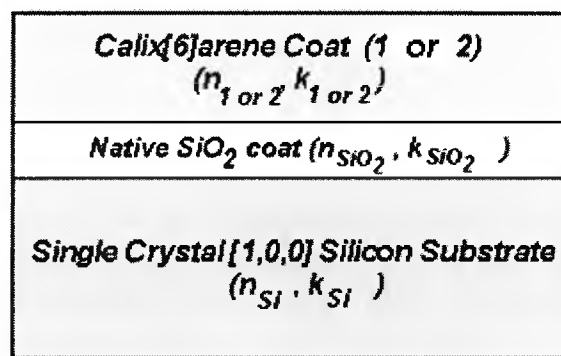


**Figure 5.3.1** Three layer “sandwich” used to create modeling and fit of the optical constants of **1** and **2**

The physical data obtained from the model yielded indices of refraction of the calixarenes ( $n_1$  and  $n_2$ ) that had a consistent fit, since they had small RMSE (root mean squared error) values.<sup>46,47</sup> In addition, the resultant thickness calculated for films of **1** and **2** were reasonably close to values obtained by profilometry. It should be noted, however, that the profilometric results are less accurate than the ellipsometric results (due to the scratching of the resist that was necessary to prepare the sample for the profilometer).

### 5.3.2 Ellipsometric Conditioning of $k_1$ and $k_2$

The ellipsometric values obtained for the extinction coefficients of **1** and **2** were quite different. The value of  $k_1$  was  $62 \times 10^{-9}$ , while that of  $k_2$  was  $81 \times 10^{-16}$ . The *extinction coefficient* is a measure of how much of the energy from the incident light is absorbed in the film or material.<sup>47</sup> This can be related to the penetration depth of light into a given material. The film thicknesses of **1** and **2**

(20.9 and 22.9 nm respectively) were *too thin* to determine accurate  $k$  values, given the observed variation in  $k_1$  and  $k_2$ .

### 5.3.3 Reasons for Discrepancies Between Ellipsometric and Profilometric Thickness Values

In order to create an accurate ellipsometric model for **1** and **2**, the profilometric thickness of a 1.5 wt% formulation of **1** (spun at 3000 rpm) was measured to range between 10-16 nm (see Table 4.1.5). A close approximation of film thickness is essential to ellipsometry, as the RMSE for the model must rely on a true approximation of the film thickness and not a local minima.<sup>47,49</sup> This effect is seen in Figure 5.3.3.1.

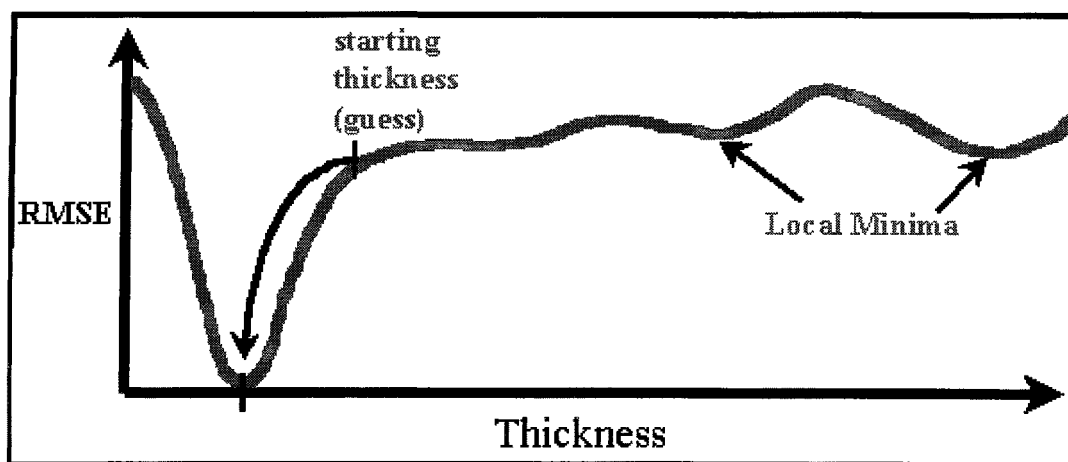


**Figure 5.3.3.1** Estimation of true film thickness with the lowest RMSE<sup>49</sup>

The ellipsometric values that were determined at different points on the same sample ranged from 16 to 18 nm. This differed from the profilometric values by up to 6 nm. Initially, this discrepancy in calixarene film thickness may

seem distressing, but the variation but can be justified with a variety of reasons. The rationale for variation between techniques depends upon considerations of the sample, the ellipsometer, and the profilometer.

The sample itself was not quite uniform, as determined by both measurement techniques. In addition, the points at which measurements were taken by each method were not the same. Non-uniformity can be seen on the sample due to the scattering of light at the ellipsometric examination point. This effect is seen in Figure 5.3.3.2, which is an enlargement of the scattering at an ellipsometric measurement point.



**Figure 5.3.3.2** Microscopic view of scattered light from a contamination-free ellipsometric measurement point of a sample.

*If the calixarene film was completely flat, a specular beam would be reflected.*<sup>47</sup>

Thus highly sensitive ellipsometric measurements may vary from those

determined by profilometry since the measurement point and film uniformity of the sample were not the same.

The ellipsometer itself may also have contributed to a degree of instrumental error, as it was known that the arm that holds compensator was not completely aligned. Even a small misalignment in the compensator element of a null ellipsometer can possibly create a skew of the reflected beam at the analyzer.<sup>47</sup> This error during thickness measurement could conceivably give different readings at the analyzer element, which would give inaccurate measurements of  $\Delta$  and  $\Psi$ . Hence, resultant thicknesses may vary slightly from the true thickness value.

Nevertheless, due to the accuracy of ellipsometric techniques, it is more conceivable that the profilometric measurements were not as accurate. Since the force of the stylus during measurement was not recorded, it is plausible that the tip of the profilometer tool may have penetrated into the soft resist film of the sample. This possible error may be confounded when measuring at non-uniform points of the calixarene film.

#### **5.4 Non-Ideal Spin Curves**

The determination of a spin curve for resist is a crucial part of process development. The coat thickness and spinning characteristics of a given resist must be known to evaluate the efficiency of the resist during lithographic and etch-related applications.<sup>1, 4</sup> Curves were created for **1** and **2** during these experiments. The reasons contributing to non-ideal curves are discussed here.

### 5.4.1 The Necessity For Identical Spin Conditions During Processing

During the creation of the spin curve for 0.5 wt% **2**, the experimental conditions had drastically changed at the 5000 and 6000 rpm speeds. The resultant curve is re-depicted below.

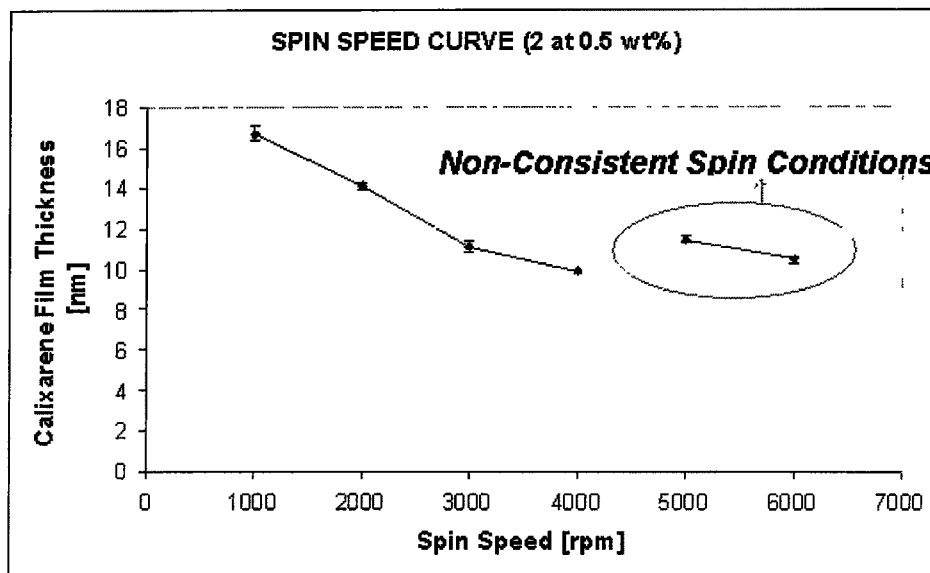


**Figure 5.4.1** Non-ideal spin curve of 0.5 wt% **2**

The thickness of a given viscosity of resist should normally decrease with increasing spin speed.<sup>6</sup> There are *three* reasons for the abnormality of this curve. For the creation of films between 1000 to 4000 rpm, the same sample of formulated resist was used. However, due to a shortage of resist during these trials, it was necessary to create an additional sample of the same concentration of **2**. Obviously, the resist may not have been precisely the same viscosity, which would have led to thicker values at 5000 and 6000 rpm.

In addition, due to a shortage of 4" substrates, two 1x1 inch samples were cleaved from a bare wafer to complete the trial. The volume of resist applied during coat was 3 mL (the same volume as for an entire 4" wafer), which affected the thickness. Lastly, the resultant tangential velocity across the square 1X1" sample was not the same size and dimensions as the 4" substrates used for all other spin curve trials. The results of this curve at 5000 and 6000 rpm demonstrate that, if possible, the same resist batch and the same substrates should be used during the processing of integrated circuits.

#### **5.4.2 Importance of Precision in Resist Application**

During the preliminary trials of resist coating, a pump was used to dispense the resist at a constant speed and with a uniform volume of resist. When uniform coats began to be achieved, the pump was no longer used and the resist was manually dispensed. During the creation of the spin curve for 1 at 1.0 wt%, there was another noticeable lack of consistency with resist behavior at 5000 and 6000 rpm. The problem is shown in Figure 5.4.2.

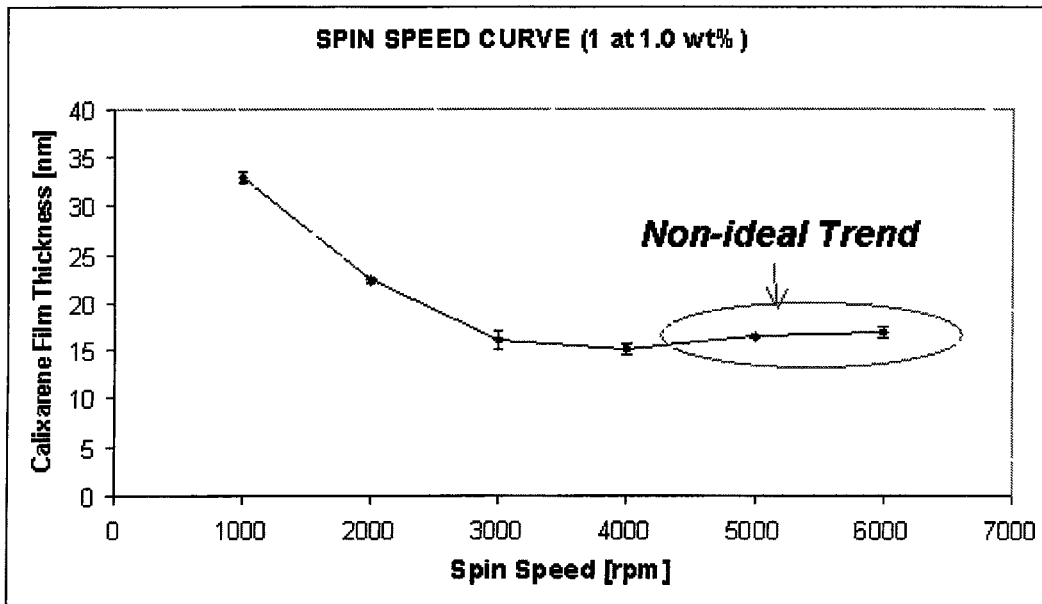


**Figure 5.4.2** Non-Ideal spin curve for 1.0 wt% 1

The lack of consistency to this curve was due to human error, as 4 mL of resist was applied to the 5000 and 6000 rpm samples. Since final film thickness is dependent upon volume, the amount of resist applied during the coating process must be consistent. A proactive solution to this problem may be to use a pump once again in future experiments in order to obtain precise spin curves.

### 5.4.3 Shelf Life of Resist Coats

Section 4.5 describes the re-measurement of the thinner films of the 0.5 wt% and 1.0 wt% 1 formulations. The results demonstrated an increase in film thickness of up to 1.2 nm over a period of a month. Attempts to expose and develop box *and* line features for samples prepared from these substrates yielded no pattern formation. This was an indication that a shelf life problem of the calixarene resist was present.

A possible reason that may have contributed to the problem was that the coated wafers were not stored in a moisture-free environment. The ambient moisture may have been absorbed into the matrix over time to cause a mild degree of swelling and resultant increase in film thickness. Also, wafers were not handled in clean room conditions; particulate matter was visible to the naked eye on the substrates.

Thus, airborne particulates and chemical contamination may have caused problems during exposure, since the calixarene monomers in the film were no longer pure. Impurities would plausibly cause the degree of polymerization to decrease drastically.<sup>16</sup> Thus, the dosage used in attempted exposure of the aged and contaminated calixarene films may have been lower than the threshold dosage for gel formation.

## **5.5 Exposure Considerations**

The preliminary exposure and development experiments of **1** and **2** were not always successful. The lack of good results may have been attributed to the usage of aged samples. Over time, it was eventually determined that a 20 kV acceleration voltage and a beam current of 1.3 nA or less was necessary in order to consistently pattern features on freshly coated substrates.

### **5.5.1 Creation of the Grid**

Even when successful results were achieved, the features were difficult to find on the sample. It became necessary to create a coordinate “grid” on the

substrate in order to readily find the features for all microscopic methods (*i.e.*, AFM, SEM, and optical microscope). This grid was scored into samples as described in section 3.7.2. Creation of a grid *before* coating the wafer was intentionally avoided in order to maintain consistent resist flow characteristics over the wafer. Figure 5.5.1 is a snapshot of a grid with a box feature as seen under an optical scope, and illustrates the difficulty of seeing even the larger features.

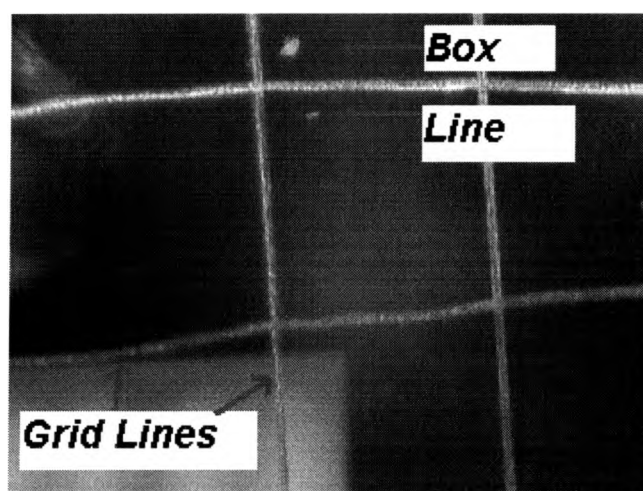


**Figure 5.5.1** Microscope picture of the grid with patterned features inside

### **5.5.2 Use of a Thicker Calixarene Resist Film For SEM Visualization**

In order to prevent charging of the sample during SEM visualization of the patterned features, all SEM samples were sputtered with a 15 nm coat of a conformal AuPd alloy. However, the sputtered SEM samples that contained features created from thin calixarene coats (ranging from 7.4 to 35.6 nm) were *not* seen using the SEM. This may have been due to problems with resolution

settings, or possibly with the difficulty of *detecting the edges of the feature* well enough to provide data for an image.<sup>7</sup>

Nevertheless, the visualization problem was overcome by spinning samples of **1** and **2** that had higher viscosities. For these samples, 7.0 wt% concentrations of **1** and **2** resulted in films with an approximate pre-exposure thickness of 200 nm. These samples were then processed and inspected with the optical scope to assure the creation of patterned features. The samples were sputtered with AuPd alloy and were then successfully viewed on the SEM.

### **5.5.3 Charging Effect of Thick Films During Exposure**

*The exposure process for the thick films was done briskly, as a marked charging affect was observed.* An implication of this effect is that the substrate could be exposed in unintended areas due to charging when moving from one exposure area to another. This should be considered in the future if thick films are to be manually exposed with the SEM.

### **5.5.4 Importance of Well-defined Side Walls of Submicron Lines**

During the lithography process, it is imperative to create features with smooth side walls, since the successful performance of most devices will depend upon control of the size of critical features (such as the gate).<sup>7</sup> The amount of variance that is allowed (along a single feature and from one feature to another) is called the tolerance.<sup>6</sup> As critical dimensions (CD) decrease from one generation of ICs to the next, the tolerance along critical features becomes more

constrained. For example, the tolerance for a feature with a CD of  $0.50\ \mu\text{m}$  is  $\pm 0.5\ \mu\text{m}$ , whereas a  $0.25\ \mu\text{m}$  feature has a tolerance of  $\pm 0.05\ \mu\text{m}$ .

The importance of uniform line edges is then especially important in nanolithography, since smaller critical features will be packed together in a high density array. The pitch for features is the distance that the features are from each other. A bridging effect was noted during an experiment to create lines with a small pitch. This bridging is seen in Figure 5.5.4 (at the left end of the lines).

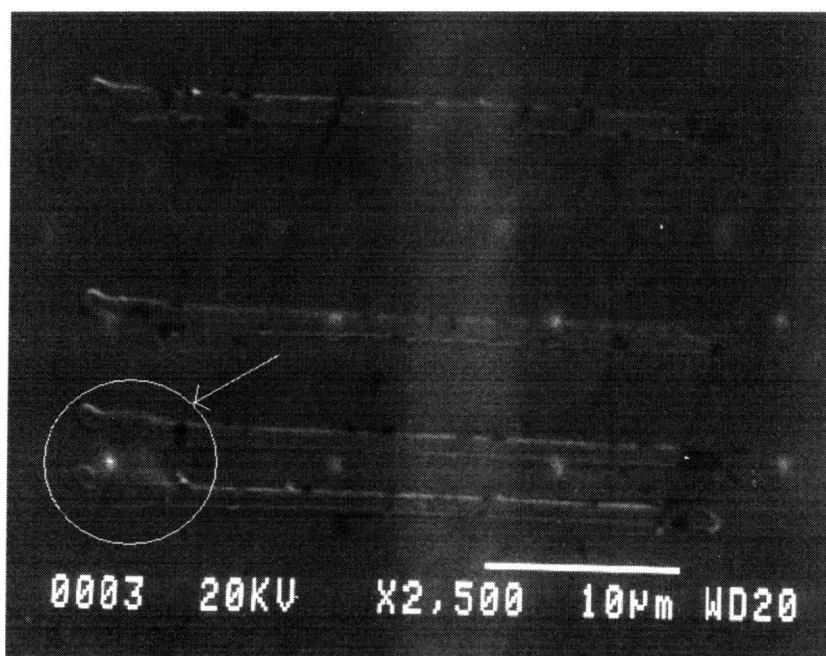


**Figure 5.5.4** Bridging between lines of **2** during a pitch experiment

This sample was made from an approximately 200 nm thick sample of 7.0 wt% **2** that was formulated with benzoyl peroxide (BPO). Since the contrast of the formulations was not evaluated in these experiments, an assumption that the BPO initiator played a part in the bridging problem would be uncertain at best. A

better explanation is the observation of thicker points on the left sides of most of the patterns created from by the SEM. In any event, lithographic processing errors (such as non-uniformity of the side walls of features) should be controlled in the fabrication of functional integrated circuits, since the pattern will be transferred to the substrate during the etch process. In addition, incomplete development or a proximity effect (due to back-scattered) electrons could also be a cause of bridging.

### 5.5.5 Consistent AFM Measurement Points For Step Height

During the analysis of the step heights of the patterned boxes, it was noted that the boxes were not completely flat. AFM measurements across different points on the box features showed a variation across step height from the left edge to the right edge, illustrated in Figure 5.5.5.

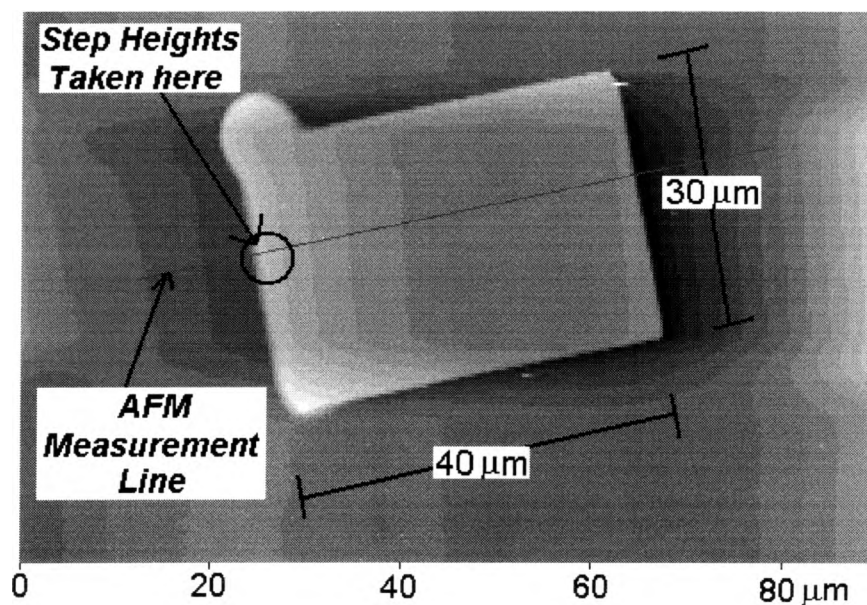


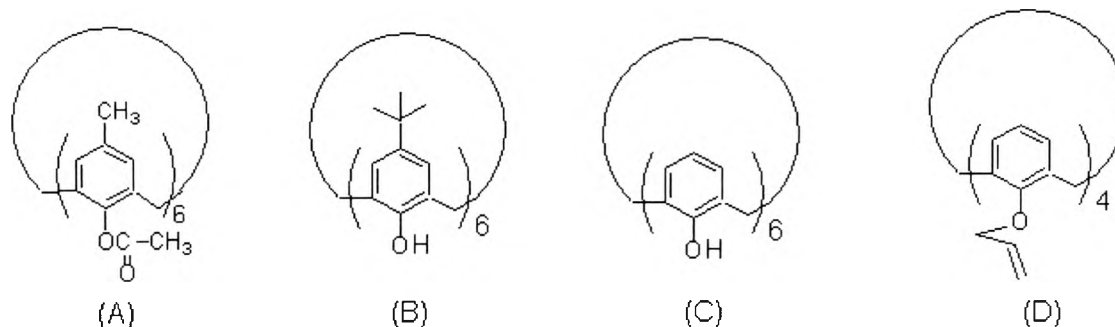
**Figure 5.5.5** Consistent measurement point of step height of a box with AFM

The step height variation may be attributed to the manner in which the electron beam scans across the surface of the calixarene resist as the feature is being exposed. There was an obvious dwell time on the left side of the boxes, as this part of the box feature had step heights that were consistently larger than the rest of the box. In order to create consistent data for the contrast curve, *it was necessary to measure each feature at the same points*. The normalized heights of the boxes at these measurement points would then present a precise estimation of the resist contrast for **1**.

### **5.6 Comparison of Resolution, Sensitivity, and Contrast of 1 and 2 with Calixarenes From the Literature**

In order to effectively compare the results determined for **1** and **2**, one must consider all experimental conditions used to create features from which the results were determined. The acceleration voltage and beam current are two important examples, since exposing a given resist at a higher voltage means that more energy is being used to deliver the electrons. Another consideration for comparison is the hardware and software used to pattern the resist.

High acceleration voltages are problematic since the underlying substrate can be potentially be damaged, while backscattered electrons can cause unwanted areas of resist to be exposed.<sup>50</sup> For this reason, experiments done for **1** and **2** were done at the relatively low acceleration voltage of 20 kV. A comparison table is shown below with corresponding structures.



Calixarene	Exposure Conditions	Film Thickness	CONTRAST	SENSITIVITY (mC/cm <sup>2</sup> )	RESOLUTION (nm)
A	50 kV	40 nm	1.7-4.7	D <sub>g</sub> = 6	10 nm
	I = 1 nA			D <sub>i</sub> = 20	
B	25 kV	not homegeous	Not reported	D <sub>g</sub> = 2.3	Not reported
	I = ?	25-500 nm	-	D <sub>i</sub> = 6	
C	25 kV	better film quality	Not Reported	D <sub>g</sub> = 3.5	Not Reported
	I = ?	25-500 nm	-	D <sub>i</sub> > 7	
D	25 kV		Not Reported	D <sub>g</sub> about 0.6	18 nm
	I = ?		-	D <sub>i</sub> > 2.5	
1	20 kV	35 nm	4	2	474 nm
	I = 0.5 nA			3.5	
2	20 kV	35 nm	Not determined	Not determined	same
	I = 0.5 nA				

**Table 5.6** Comparison table for literature calixarenes with **1** and **2**

Values that are not presented in this table were unavailable, since they were not reported in the literature for the respective compounds. The contrast of **1** (which was 4.0) can be compared to calixarene A, whose value varied from 1.7 to 4.7 in different reports.<sup>30,36,51</sup> When considering contrast, the conditions of all

experiments should be known. Note that exposure of **1** was done at a lower beam energy, and that **1** had a contrast comparable to A.

Considering the sensitivity, a dose *in between*  $D_g$  and  $D_i$  would be most useful in electron beam lithography, since this would be somewhere *on the steepest point of the contrast curve*.<sup>5</sup> Note that in all reported cases except for calixarene C, the sensitivity of **1** is greater. C is a tetraallyloxy-calix[4]arene and the high number of allyl groups may contribute to the sensitivity.

Finally, the resolution of **1** and **2** was about the same in these experiments, with the highest resolution of the line being 474 nm. This value is 40 times higher than the resolution reported for the literature calixarenes. Nevertheless, a valid comparison of the resolution capabilities of **1** and **2** is not possible at this time: *the JEOL 848 SEM used to create features for **1** and **2** is not currently equipped with a lithography system that would make the creation of ultrahigh resolution patterns possible*. Future experiments (in which the exposure SEM is equipped with writing software) will be necessary in order to unveil the true resolution capabilities of the conformationally immobile calix[6]arenes in this study.

## 6.0 CONCLUSION

### 6.1 Summary of Results

Compound **1** and **2** were synthesized via a pre-elaborated pathway<sup>34,35</sup> and formulated into negative electron beam resists. The index of refraction (at 632.8 nm) was determined to be 1.56 for both compounds. Spin speed curves of 1.0 and 0.5 wt% **1** and **2** were created, and **1** was found to have better film-forming characteristics at higher concentrations (up to 7.0 wt%).

During lithographic evaluation, *all formulations (including those with benzoyl peroxide) gave qualitative results*, as patterns were observed under an optical microscope after development. The sensitivity of **1** was found to be relatively good with respect to known literature calix[6]arenes and PMMA. A high contrast of 4.0 was determined for **1** by constructing a contrast curve. The gel dose for **1** was determined to be 2.0 mC/cm<sup>2</sup>, while the insolubilization dose was 3.5 mC/cm<sup>2</sup>.

In addition, formulations using 1.0 wt% benzoyl peroxide (w/w of **1** or **2**) were made (to test how the resists would respond with the presence of a radical initiator), with no real difference in lithographic capability noted. SEM images were obtained for both initiator-containing compounds (at a formulation of 7.0 wt% and spin speed of 1000 rpm). A shelf life issue was noted for all samples,

as the calixarene films that were spun and unprocessed for a period of 1 month were difficult to pattern.

The dimensions of the line with the highest resolution were 40  $\mu\text{m}$  long by 0.474  $\mu\text{m}$  wide, as determined by the AFM. This feature was created using from a 7.0 wt% sample of **2** that was spun at 1000 rpm. The pre-exposure thickness of this line was not determined. The line was exposed at an acceleration voltage of 20 kV and a PCD beam current of 45 pA.

## 6.2 Future Experiments

*A full evaluation of sensitivity, contrast, and resolution experiments for **1** and **2** is indicated* in order to truly measure how well the conformationally immobile calix[6]arenes perform lithographically, with respect to literature calix[n]arenes. Obviously, it will be necessary to pattern ultra-thin lines by using an electron beam system equipped with software that will enable the creation of high resolution features. In addition, more contrast curves of **1** and **2** will be necessary to determine repeatability of sensitivity and contrast.

Once ultrahigh resolution features are patterned, it may be necessary to use an ultrasonically-assisted development process, in order to avoid the swelling of the resist.<sup>15,5</sup> A spectroscopic analysis of the indices of refraction for both compounds is advised. To complete the lithographic evaluation of **1** and **2**, the features *must be dry etched* in order to determine whether the additional aryl (xylenyloxy) groups actually do confer a new level of protection to the substrate.<sup>5</sup>

Future experiments with different types of chemical functionalization will provide new insight to the study of calix[6]arene electron beam resist candidates. If possible, these future experiments should be performed with a native oxide strip. Chloromethylation of the upper calix[6]arene rim is indicated, in order to increase the sensitivity of all calixarene compounds.<sup>5,33</sup> The lithographic evaluation of compounds of diallyloxycalix[6]arene<sup>44,52</sup> (a conformationally mobile calixarene) versus **1** and **2** may provide determine the role that allyl groups play in the lithographic performance of calixarene resists.<sup>36</sup>

## REFERENCES

1. Zant, P. Microchip Fabrication, McGraw Hill: New York, **1997**.
2. Willson, C. G.; Bowden, M. J. In Electronic and Photonic Applications of Polymers. Eds. Bowden, M. H.; Turner, S. R. American Chemical Society: Washington, D. C., *Advances in Chemistry Series 218*, **1988**.
3. Ohring, M. Reliability and Failure of Electronic Materials and Devices, Academic Press Limited: San Diego, **1998**.
4. Dammel, R. R., Diazonaphthoquinone-based Resists, Bellingham, WA: SPIE Optical Engineering Press, *Vol. TT-11*, 1993.
5. Wilson, C. G., in Thompson, L. F.; Willson, C. G.; Bowden, M. J. Introduction to Microlithography, Second Edition, American Chemical Society: Washington, D. C., **1994**.
6. Thompson, L. F., in Thompson, L. F.; Willson, C. G.; Bowden, M. J. Introduction to Microlithography, Second Edition, American Chemical Society: Washington, D. C., **1994**.
7. Bowden, M. J., in Thompson, L. F.; Willson, C. G.; Bowden, M. J. Introduction to Microlithography, Second Edition, American Chemical Society: Washington, D. C., **1994**.
8. Reiser, A., Photoreactive Polymers-The Science and Technology of Resists, J. Wiley & Sons: New York, **1989**.
9. Knop, A., Scheib, W., Chemistry and Application of Phenolic Resins, Springer, New York, **1979**.
10. Furuta, A.; Hanabata, M.; Uemura, Y. "High Performance Positive Resists," *J. Vac. Sci. Technol. B.*, **1986**, 4, 430.
11. Furuta, A.; Hanabata, M. *J. Photopolymer Sci. Tech.*, **1989**, 2, 383.

12. Kuller, A.; Eck, W.; Stadler, V.; Geyer, W.; Golzhauser, A., "Nanostructuring of Silicon by Electron-Beam Lithography of Self-Assembled Hydroxybiphenyl Monolayers", *J. Appl. Phys.*, **2003**, 82(21), 3776.
13. Lide, D., ed. CRC Handbook of Chemistry and Physics, 78<sup>th</sup> ed. CRC Press: Boca Raton, **1998**.
14. Atkins, P.; de Paula, J. Physical Chemistry, Seventh Edition, New York: W. H. Freeman and Company, **2002**.
15. Yasin, S.; Hasko, D. G. "Nanolithography using ultrasonically assisted development of calixarene negative electron beam resist" *J. Vac. Sci. Technol. B.*, **2001**, 19(1), 311-313.
16. Allcock, H.R., Lampe, F.W. Contemporary Polymer Chemistry, Second Edition, ed. Lafferty, K. M.; Prentice-Hall, Inc.: Englewood Cliffs, New Jersey, **1990**.
17. Plastics World, April, **1996**, 41-46.
18. "International Technology Roadmap for Semiconductors", 2001 edition. International SEMATECH. [http:// public.itrs.org](http://public.itrs.org)
19. Brewer, G. R. In Electron-Beam Technology in Microelectronic Circuit Fabrication, Ed. Brewer, G. R. Academic Press: Orlando, FL, **1980**.
20. Herriot, D. R.; Brewer, G. R. In Electron-Beam Technology In Microelectronic Circuit Fabrication, Ed. Brewer, G. R. Academic Press: Orlando, FL, **1981**.
21. Born, M.; Wolf, E. In Principles of Electron Optics, 4<sup>th</sup> ed. Pergamon Press: New York, 1970.
22. Gutsche, C. D. Calixarenes Revisited In Monographs in Supramolecular Chemistry, ed. Stoddart, J. F. The Royal Society of Chemistry: Cambridge, England, **1998**.
23. Gutsche, C. D. Calixarenes In Monographs in Supramolecular Chemistry, ed. Stoddart, J. F. Royal Society of Chemistry: Cambridge, England, **1989**.
24. Arduini, A.; Casnati, A. "Calixarenes" in Macrocyclic Synthesis: a Practical Approach, ed. Parker, D. Oxford University Press: Oxford, **1996**.

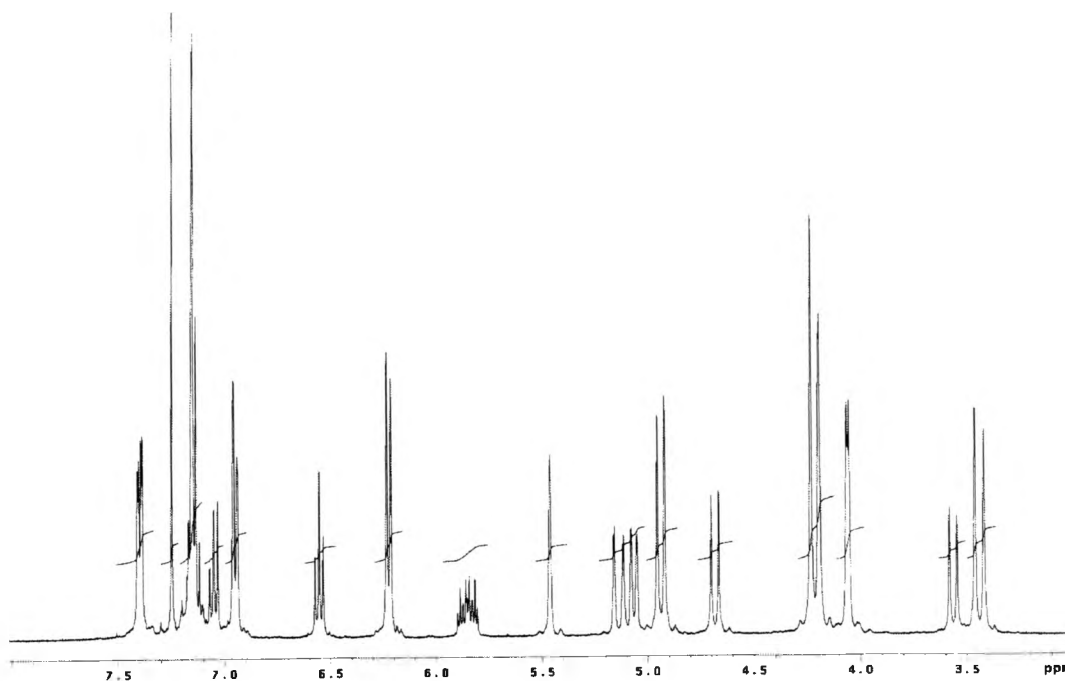
25. Mandolini, L.; Ungaro, R. *Calixarenes In Action*, ed. Mandolini, L.; Ungaro, R. Imperial College Press: London, **2000**.
26. Wamme, N.; Ohnishi, Y. "Film properties and applications of hexaacetate *p*-methylcalix[6]arene" *Polym. Mater. Sci. Eng.* **1992**, *67*, 451-452.
27. Fujita, J.; Ohnishi, Y.; Ochiai, Y.; Matsui, S. "Ultrahigh resolution of calixarene resist in electron beam lithography" *Appl. Phys. Lett.*, **1996**, *68(9)*, 1297-1299.
28. Gokan, H.; Esho, S.; Ohnishi, Y. "Dry etch resistance of organic materials" *J. Electrochem. Soc.* **1983**, *130(1)*, 143.
29. Ohnishi, Y.; Fujita, J.; Ochiai, Y.; Matsui, S. "Calixarenes-Prospective Materials For Nanofabrication" *Microelectronic Eng.*, **1997**, *35*, 117-120.
30. Fujita, J.; Ohnishi, Y.; Ochiai, Y.; Nomura, E.; Matsui, S. "Nanometer-scale resolution of calixarene negative resist in electron beam lithography" *J. Vac. Sci. Technol. B.*, **1996**, *14(6)*, 4272-4276.
31. Almi, M.; Arduini, A.; Casnati, A.; Pochini, A.; Ungaro, R. *Tetrahedron*, **1989**, *45*, 2177.
32. Fujita, J.; Ohnishi, Y.; Manako, Y.; Ochiai, Y.; Nomura, E.; Matsui, S. "Resolution of calixarene resist under low energy electron irradiation" *Microelectron. Eng.*, **1998**, *41/42*, 323-326.
33. Sakamoto, T.; Manako, S.; Fujita, J.; Ochiai, Y.; Baba, T.; Yamamoto, H.; Teshima, T. "Nanometer-scale resolution of a chloromethylated calixarene negative resist in electron-beam lithography: Dependence on the number of phenolic residues" *Appl. Phys. Lett.*, **2000**, *77(2)*, 301-303.
34. Farmer, D. B. "Synthesis And Cation Binding Properties of Bis-Bridged Calix[6]arenes" M.S. Thesis, Southwest Texas State University, 1999.
35. Staggs, S. "Stereo-Selective Synthesis of Bis-bridged Calix[6]arenes" M.S. Thesis, Southwest Texas State University, 2003.
36. Sailer, H.; Rudersich, A.; Kern, D. P.; Schurig, V. "Evaluation of calixarene-derivatives as high-resolution negative tone electron-beam resists" *J. Vac. Sci. Technol. B.* **2002**, *20(6)*, 2958-2961.
37. Ohnishi, Y.; Wamme, N.; Fujita, J. "Calixarene Resists For Nanolithography" *Polym. Mater. Sci. Eng.*, **1992**, *67*, 451-452.

38. Sakamoto, T.; Kawaura, H.; Baba, T.; Fujita, J.; Ochiai, Y. "Fabrication of 30 nm gate length electrically variable shallow-junction metal-oxide-semiconductor field effect transistors using a calixarene resist" *J. Vac. Sci. Technol. B.*, **1997**, *15*(6), 2806-2808.
39. Gutsche, C.D.; Dhawan, B.; No, K. H.; Muthukrishnan, R. *J. Am. Chem. Soc.* **1981**, *103*, 3782.
40. Prins, F. E.; Pfeiffer, J.; Raible, S.; Kern, D. P.; Schurig, V. "Systematic studies of functionalized calixarenes as negative tone electron beam resist" *Microelectron. Eng.* **1998**, *41/42*, 359-362.
41. Yasin, S.; Hasko, G.; Carecanac, Jr., F. "Nanolithography using ultrasonically assisted development of calixarene negative electron beam resist" *J. Vac. Sci. Technol. B.*, **2001**, *19*(1), 311-313.
42. Garrat, P.G., "Radiation-Induced Solid State Polymerization" *Polymer*, **1962**, *3*, 323.
43. Okamura, S.; Hayashi, K.; Kitanishi, Y. "Radiation-Induced Solid State Polymerization of Ring Compounds," *J. Polymer. Sci.*, **1962**, *58*, 925.
44. Nam, K. C.; Park, K. S. "Selective Functionalization of Calix[6]arene" *Bull. Korean Chem. Soc.* **1995**, *16*(2), 153-157.
45. Cassidy, P. E. CHE 5351, *Polymer Chemistry Notes*, Southwest Texas State University, Spring **2002**.
46. Tompkins, H. G.; McGahan, W. A. *Spectroscopic Ellipsometry and Reflectometry*, John Wiley and Sons: New York, **1999**.
47. Tompkins, H. G., *A User's Guide to Ellipsometry*, Academic Press: San Diego, **1993**.
48. Skidmore, K. *Semicond. Int.*, **1988**, *11*(2), 57.
49. [http://www.jawoollam.com/Tutorial/Tutorial\\_6.html](http://www.jawoollam.com/Tutorial/Tutorial_6.html)
50. Tilke, A.; Vogel, F.; Simmel, A.; Kriele, R.; Blick, H.; Lorenz, H.; Wharam, D. A.; Kothaus, J. P. "Low-energy electron-beam lithography using calixarene" *J. Vac. Sci. Technol. B.*, **1999**, *17*(4), 1594-1597.
51. Manako, S.; Ochiai, Y.; Yamamoto, H.; Teshima, T.; Fujita, J.; Nomura, E. "High-purity, ultra-high resolution calixarene electron-beam negative resist" *J. Vac. Sci. Technol. B.*, **2000**, *18*(6), 3434-3427.

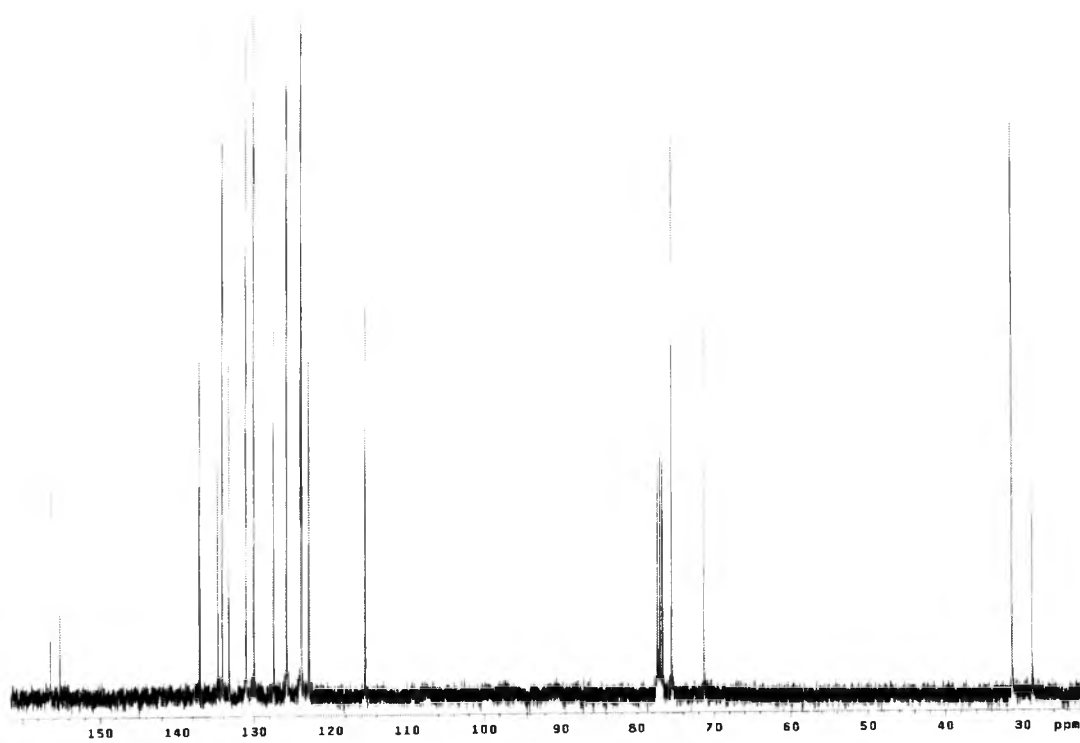
52. Blanda, M. T.; Farmer, D. B.; Brodbelt, J. S.; Goolsby, B. J. "Synthesis and Alkali Metal Ion Binding Properties of Two Rigid Stereochemical Isomers of Calix[6]arene Bis-crown-4" *J. Am. Chem. Soc.*, **2000**, *122*, 1486-1491.

## **APPENDIX: NMR SPECTRA OF 1 AND 2**





**SPECTRUM 3**  $^1\text{H}$  NMR of Compound 2.



**SPECTRUM 4**  $^{13}\text{C}$  NMR of Compound 2.

## **VITA**

Gabriel Hernandez Monreal was born on September 25, 1970, the son of Rafael Perez Monreal and Berta Hernandez. In 1989, after graduating from Theodore Roosevelt High School, San Antonio, Texas, he entered Baylor University in Waco, Texas. In 1993, he earned the degree of Bachelor of Arts in Chemistry with a Minor in Biology. He worked at Sony Semiconductor of America, San Antonio, Texas, as a Manufacturing Associate for a year, and then at Philips Semiconductors, Inc., as a Manufacturing Technician in the Photolithography Division for over two years. In January, 2001, he entered the Graduate School of Southwest Texas State University in San Marcos, Texas. There, he earned the degree of Master of Science in Chemistry with a Minor in Physics, on August 9, 2003.

This thesis was typed by Gabriel Hernandez Monreal.

